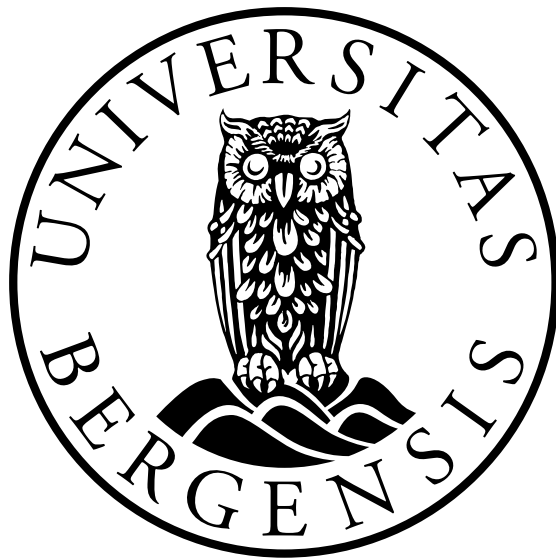


Geological Storage of CO₂: Sensitivity and Risk Analysis

Meisam Ashraf



Dissertation for the degree of Philosophiae Doctor (PhD)

Department of Mathematics
University of Bergen

November 2012

Scientific environment

This dissertation is submitted as a partial fulfillment of the requirements for the degree Doctor of Philosophy (PhD) at the University of Bergen. It is part of the project Mathematical Modeling and Risk Assessment of CO₂ storage, MatMoRA, which is funded by the Norwegian Research Council, Statoil and Norske Shell under grant no. 178013/I30 and lead by Professor Helge Dahle at the Department of Mathematics, University of Bergen (UiB).

The working environment have been SINTEF-ICT in Oslo, and CIPR in Bergen, and SIMTECH in Stuttgart. The chief scientist at SINTEF-ICT, professor Knut-Andreas Lie, has been the main adviser and Professor Jan M. Nordbotten at the Department of Mathematics, UiB, along with the research scientist at SINTEF, Halvor M. Nilsen, have been the co-advisers. With warm supports from professor Rainer Helmig, head of department of hydromechanics and modelling of hydrosystems at Stuttgart university, last parts of the work is benefited from advices of professor Wolfgang Nowak, head of Stochastic modelling of hydrosystems, Dr. Sergey Oladyshkin, postdoctoral fellow at SIMTECH, and professor Holger Class at Stuttgart university.

Acknowledgements

I dedicate this to my father, who wished to do a PhD, but the situation did not help him.

I would like to appreciate my decision to do a PhD after years of being in the industry . My first motivation was to experience the educations in a mathematical environment. I was very pleased and lucky to work with the best mathematicians in Norway on the topic of CO₂ storage.

First and foremost, Knut-Andreas Lie was more than an adviser for me, whom I had the chance and honor to work with closely and in a daily-based manner. I learned a lot from discussions with Halvor M. Nilsen, initially my only friend in Norway, when I left my family and friends and moved to start the program. Jan M. Nordbotten always inspired me and made me to love mathematics even more. Helge Dahle warmly helped me with every aspect of my studies. Maria Elenius gave me the enthusiasm as a colleague to enjoy my research. I enjoyed being an office-mate at SINTEF with Christian Schulz. Arne Skorstad is among those whom I was proud to work with. I was lucky to work with Princeton people, Michael Celia and Sarah Gasda. I enjoyed learning from Ivar Aavatsmark, Hans Munthe-Kaas, and Anette Stephansen. And many friends in Bergen Math. department that I always enjoyed discussing interesting topics with them.

During this program I had the chance to spend one semester in Stuttgart to work with mathematicians on stochastic analysis. I was proud to be sitting in the group of Rainer Helmig, to enjoy time with such a live and friendly research group. Thanks to Stuttgart people, one by one, for such a nice social time that I had over there. I had very constructive scientific discussions with Segrey Oladyshkin and Wolfgang Nowak, Holger Class, and Anozie Ebigboe. I extremely enjoyed working with them.

I would like to thank my manager at my new employer, Ed Leung, for supporting me to finish my thesis.

And thanks to the coffee machine and printer at SINTEF-ICT, for helping me a lot in writing this report.

Abstract

In the context of geological CO₂ storage, one main uncertainty that makes the prediction of operational success more complicated, is the geological heterogeneity in the system. The CO₂ storage capacity and risk of leakage from the storage location are highly sensitive to the geological modeling of the problem. The main motivation of our works is to address the importance of proper geological modeling and to provide a practical work-flow for assessing the geological uncertainty consequences in the operations.

We choose the shallow-marine depositional system for our studies, but the same method could be implemented for any other types. The study is based on large number of geological realizations with different levels of heterogeneity. The heterogeneity is modeled by the main geological parameters and used to discuss the flow responses that are important in the storage of CO₂. Among those parameters are the aggradational angle, levels of barriers in the system, faults, lobosity, and progradation direction.

We describe the flow behavior in terms of flow responses that can be used to evaluate the performance of geological storage of CO₂ in the aquifers and abandoned oilfields. The injected plumes of CO₂ are analyzed for their volumes and numbers and their dynamics in the system. Detailed sensitivity analysis and risk assessment are performed on the designed injection and early migration study. The geological parameters are ranked based on their influence on the flow response variations. No general conclusion for uncertainty assessment is expected from our studies, since this may change in different geological regions. However, we demonstrate a practical work-flow that can be used in any uncertainty assessment project.

We mainly consider the injection and early migration of CO₂ as this work is part of a project that covers the long-term CO₂ migrations. Nevertheless, the discussions and results here can be used with some modifications (such as extending the model spatial extent) in the long-term migrations.

The work is presented and published in many scientific conferences in the form of proceedings, posters, and seminars. Some parts are submitted to the literature and are in their way to be published in the literature.

List of papers

1. M. Ashraf, K.A. Lie, H.M. Nilsen, J.M. Nordbotten & A. Skorstad, *Impact of geological heterogeneity on early-stage CO₂ plume migration*, XVIII International Conference on Water Resources (CMWR 2010), J. Carrera (Ed), CIMNE, Barcelona, 2010.
2. M. Ashraf, K.A. Lie, H.M. Nilsen & A. Skorstad, *Impact of geological heterogeneity on early-stage CO₂ plume migration: sensitivity study*, Proceedings of the 12th European Conference on the Mathematics of Oil Recovery (ECMOR XII), Oxford, UK, 6-9 September 2010.
<http://www.earthdoc.org/publication/publicationdetails/?publication=41331>
3. M. Ashraf, K.A. Lie, H.M. Nilsen & A. Skorstad, *Impact of geological heterogeneity on early-stage co₂ plume migration: CO₂ distribution sensitivity study*, submitted to the International Journal of Greenhouse Gas Control(IJGGC).
4. M. Ashraf, *Impact of geological heterogeneity on early-stage co₂ plume migration: pressure sensitivity study*, submitted to the International Journal of Greenhouse Gas Control(IJGGC).
5. M. Ashraf, S. Oladyshkin, W. Novak, *Geological storage of CO₂: global sensitivity analysis and risk assessment using the arbitrary polynomial chaos expansion*, Proceedings of the European Geosciences Union (EGU) General Assembly 2012, April, Vienna, Austria, Geophysical Research Abstracts., Vol. 14, EGU2012-9243. Submitted to special issue of the International Journal of Greenhouse Gas Control(IJGGC), in second review.

Contents

Scientific environment	i
Acknowledgements	iii
Abstract	v
List of papers	vii
1 Introduction	1
1.1 Introduction	2
1.2 Carbon storage	3
1.3 Modeling procedure	4
1.4 Geological description	6
1.4.1 Uncertainty	6
1.4.2 Geological parameters	7
1.5 Flow equations	9
1.5.1 Single phase flow	9
1.5.2 Two-phase flow	11
1.6 Flow regimes	15
1.6.1 Injection and early migration	16
1.6.2 Long term migration	18
1.7 Vertical averaging	19
1.8 Flow modeling	21
1.8.1 Numerical scheme	21
1.8.2 Flow scenarios	23
1.8.3 Flow responses	25
1.9 Sensitivity and risk analysis	27
1.9.1 Stochastic analysis	27
1.9.2 Arbitrary polynomial chaos expansion	28
1.9.3 Sensitivity analysis	31
1.9.4 Risk analysis	33
1.10 Implementation of work-flow	33
2 Introduction to the papers	35
2.1 Introduction	36
2.2 Summary of papers	36

3 Scientific results	41
3.1 Impact of geological heterogeneity on early-stage CO ₂ plume migration	43
3.2 Impact of geological heterogeneity on early-stage CO ₂ plume migration: sensitivity study	53
3.3 Impact of geological heterogeneity on early-stage CO ₂ plume migration: sensitivity study	69
3.4 Geological storage of CO ₂ : heterogeneity impact on pressure behavior	85
3.5 Geological storage of CO ₂ : global sensitivity analysis and risk assessment using the arbitrary polynomial chaos expansion	105

List of Figures

1.1	Green-house gases act like a blanket trapping the heat received from the sun.	3
1.2	Geological sequestration is a proposed solution for mitigating the industrial CO ₂ emissions.	4
1.3	Modeling procedure diagram.	5
1.4	Lobosity levels are defined based on the shoreline shape, which is caused by the interplay between fluvial and wave forces.	8
1.5	Barrier levels caused by periodic floods.	8
1.6	Aggradation angle levels.	9
1.7	Progradation levels.	9
1.8	Flow domain and boundaries.	10
1.9	Permeability is an idication of how easy it is for the fluids to flow trough the medium.	10
1.10	Wettability and interfacial tension in water-CO ₂ system.	11
1.11	Multi-phase flow in the pore scale.	12
1.12	Two-phase flow and relative permeability.	12
1.13	Capillary pressure can be expressed as a function of wetting saturation. The plot is a typical curve of capillary pressure function with a maximum of P_{cmax}	13
1.14	Capillary pressure distribution in the transition zone.	14
1.15	Saturation distribution in the capillary transition zone.	14
1.16	Flow regimes in geological CO ₂ storage.	19
1.17	Hydrostatic equilibrium condition results in three zones: the CO ₂ zone with thickness h_{co_2} , the water table with thickness h_w , and the capillary transition zone h_{pc}	21
1.18	Transmissibility calculation for two cells a and b.	22
1.19	Well modeling inside a simulation cell.	23
1.20	Top, bottom, and upper side boundaries are closed and the rest are open to the flow.	24
1.21	External pressure drive.	25
1.22	Mobile and residual CO ₂ volume.	25
1.23	We use a 2D Gaussian distribution for leakage probability on the cap-rock.	26
1.24	Marker codes used to plot the simulation results of all cases together.	27
1.25	Collocation points are combined in different uncertainty directions such that the total probability in all directions is maximized.	30
1.26	Flow-chart of work process implemented in an automated procedure.	34

Chapter 1

Introduction

1.1 Introduction

“We won’t have a society if we destroy the environment”

– Margaret Mead, American cultural anthropologist, 1901-1978

The commencement of industrial revolutions in the last centuries is closely related to the outbreak of environmental damages and harmful manipulation of ecosystems. Environmental issues are actual and can lead to serious consequences for human beings and ecosystems.

The contribution of human CO₂ emissions as green-house gas in the climate change has been shown by studies such as [37]. The underground sequestration of the CO₂ produced from localized sources like power-plants and oil and gas recovery sites is proposed as a possible solution to reduce the rate of CO₂ emission into the atmosphere [13, 36]. The required technology for this solution is close to what is in use in the oil, gas, and mining industry. However, there are some challenges that are specific to carbon storage operations. Primary, the time and space scales in these problems are larger. Secondary, the risk of leakage of stored CO₂ up to the surface via conductive features like fractures and faults and man-made features such as leakage through ill-plugged wells and broken cap-rock due to high pressure imposed to the system during the injection operations is a major concern.

The main objectives of carbon storage operations are to maximize the storage size and the volumetric injection rate, and to minimize the risk of leakage of the stored CO₂. The CO₂ storage operations require a multidisciplinary collaborations. The work-flow from initial phases of a project until end of storage operations are divided between government and private section, research organizations and industry. It is the task of research community to investigate the safety of CO₂ sequestration and provide the methodology for CO₂ fate prediction [7].

Bachu [7] discusses the road-map of site selection for geological CO₂ sequestration. He defines the process in three steps: to assess the general suitability of the site, to perform the inventory study on the source point and storage location and the operational transport issues, and finally to investigate the safety and assess the capacity of the storage. Issues about safety and storage capacity are looked at differently from the perspective of immediate and ultimate results. For example, when talking about the risk of leakage, we might consider the leakage through ill-plugged wells or fractures during the injection time as the immediate risk. On the other hand, leakage caused by plume migration long time after the injection and contamination to other aquifer systems are considered as ultimated risks.

To predict the CO₂ injection fate, it is crucial to study the dynamics of flow in the medium. Dynamical study of flow includes quantification of acting forces in a geological heterogeneous medium that can end up in solving a complicated system of mathematical equations. It seems convenient to replace the geological heterogeneous medium with an equivalent homogeneous medium. However, proper modeling of geological heterogeneity is a major control on reservoir assessment and carbon storage studies [8, 21, 50, 51].

In this thesis, we report a series of works performed within a PhD program framework under MatMora project. MatMora is a strategic project that is defined to address the needs of mathematical tools to model the geological storage of CO₂ and to assess the uncertainty and risk in the modeling work-flow. The work in this thesis is focusing on the fundamental uncertainty in geological description used in modeling of CO₂ storage problems. The work is reported in a series of papers, and the objective is to perform a sensitivity analysis on variational geological parameters used to describe the geology of shallow-marine depositional systems. Although the focus is on a particular depositional system, the procedure can be implemented for any other systems of interest.

We start the introduction section by discussing the global warming and its causes, and the carbon storage as an interim proposed solution to mitigate the increasing level of industrial CO₂ emission to the

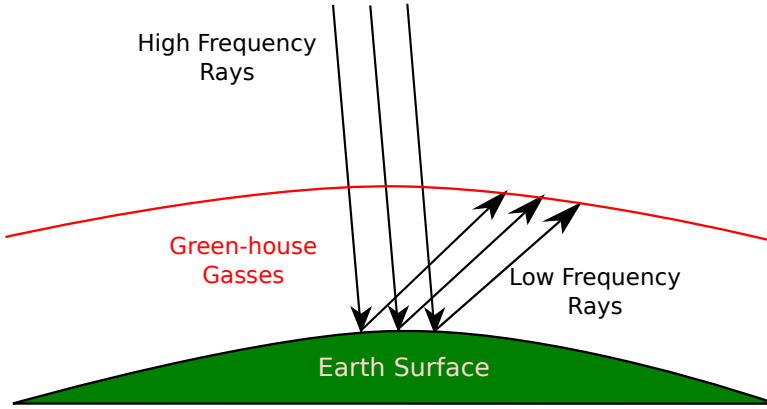


Figure 1.1: Green-house gases act like a blanket trapping the heat received from the sun.

atmosphere. Section 1.3 provides the work-flow of the works reported in the thesis. A brief overview of the literature is given and the work is discussed in that section.

In Section 1.4, we review a systematic definition for uncertainty from the literature and after that, the geological uncertainty and parameters are described. Flow equations for single-phase and two-phase flow problems are discussed in Section 1.5. In section 1.6, various flow regimes occurring during geological storage of CO₂ are described briefly by discussing the force balance within the medium at different times. Next we discuss the vertical averaging method which can be used in large aquifers to enhance the speed of simulation.

The introduction to the thesis continues by a discussion on flow simulation scenario and assumptions taken in the work in Section 1.8. We use a set of flow responses that monitor the performance of the operation and requirements to achieve the objectives of a typical carbon storage problem, with a special emphasis on the injection and early migration of CO₂ in the medium. Flow dynamics and a linear sensitivity analysis performed on the simulation results are discussed in this section.

Section 1.9 provides an overview on the fast flow solution techniques that can be used for rapid flow simulation. We use a response surface method to simulate the flow responses. This proxy model is then used in global sensitivity analysis and Monte-Carlo risk assessment process. The introduction section ends by introducing the Matlab functions used in the calculation work-flow.

1.2 Carbon storage

There are a number of theories that explain the causes of climate change. Milankovich theory [29] relates the energy received from the sun to the cyclical variation of earth orbit around the sun, and earth rotation around its axis. The earth orbit changes eccentricity between circular and elliptical. This influences the difference between earth and sun, and on its maximum influence can lead to about 20% difference in the energy received from the sun. The second variation occurs in the rotation of earth around its plane axis. This rotation wobbles approximately every 13600 years and the summer solstice switches from June to January. Also, a tilt variation of earth rotational axis happens approximately after every 41000 years. This can cause warmer winters and colder summers in high latitudes [29].

The solar radiation changes by a small amount of 0.1% over a 11 year cycle. Also on the scales of tens to thousands of years variations in the earth orbit result in seasonal changes and that in the past caused glacial and inter-glacial cycles.

The theory of green house effect relates the earth climatic change to the fact that the long wave radiation from earth back to atmosphere is absorbed by the green-house gases, mainly carbon dioxide, water vapor, and methane existing in the atmosphere. This results in trapping of heat energy and an increase in atmosphere temperature level (Figure 1.1) [29].

Human manipulations in the nature has led to about 100 ppm increase in carbon dioxide level in

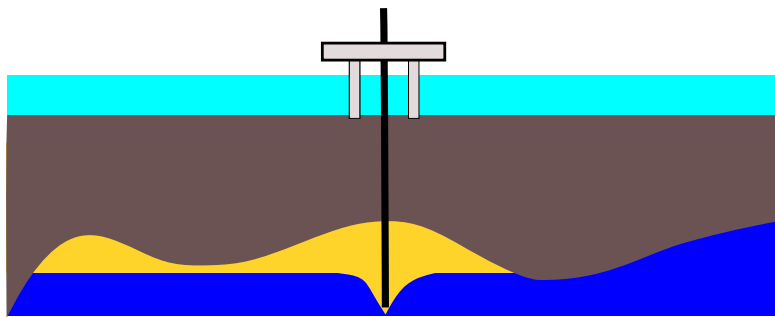


Figure 1.2: Geological sequestration is a proposed solution for mitigating the industrial CO₂ emissions.

the atmosphere. Most scientists believe that we are already experiencing the global warming due to green house effects. The IPCC Second Assessment report states that the climate change in the late 19th century is most likely due to anthropogenic causes.

Carbon capture and storage (CCS) has got a major attention in the industry and the scientific communities. According to the International Energy Agency (IEA), the cost of mitigating climate change by 2050 is estimated to be 70% higher without implementing CCS.

CCS is considered as an interim solution, because it is valid due to fossil fuel consumption, and the long term strategy of replacing fossil fuel with renewable energy will terminate the validity CCS. Therefore, initiating the CCS topic has to be done in a reasonable fashion such that it does not slow down the research for renewable energy. Another concern regarding the CCS is the acceleration of coal and fossil fuel consumption with the excuse of availability of CCS technology.

Sequestration of CO₂ at the ocean floor and also in deep underground aquifers are the options available for permanent storage of CO₂. Large availability of storage places and potential for almost permanent storage makes the geological sequestration the most practical option (Figure 1.2). Nevertheless, this alternative is not free from economical, social and industrial concerns.

In the last decades, the scientific community has been putting efforts into convincing the public about feasibility of these operations. A fair public acceptance must be based on social awareness. Any plan to increase the acceptance level in a society starts by measuring the current knowledge level of that society.

The EU has conducted a survey to assess the public awareness in 12 European states. This survey is published in the recent Eurobarometer report in May 2011. People's awareness and acceptance of climate change and its causes, and the methods to avoid or mitigate the problems, in particular the CCS technology, was examined in the survey. The majority of European participants are either fairly or very well informed about causes and consequences of climate change. However, the awareness of CCS in between the European respondents was low. Two third of the participants in the survey have had not heard at all about CCS.

The same survey suggests that the overall trust in Europe in the sources of information regarding CCS is best in universities and other scientific institutions. Governments are investing in research, not only to move toward industrialization of CCS, but also to make it well received by public. This highlights the importance of researching the storage of CO₂ and the way it is needed both for industrial demands and social concerns.

1.3 Modeling procedure

Predicting the fate of CO₂ storage involves identification and quantification of the relevant uncertainties and risk assessment process. The procedure starts with a geological description and continues with modeling of flow in geological formations. After constructing a deterministic flow model, the stochastic

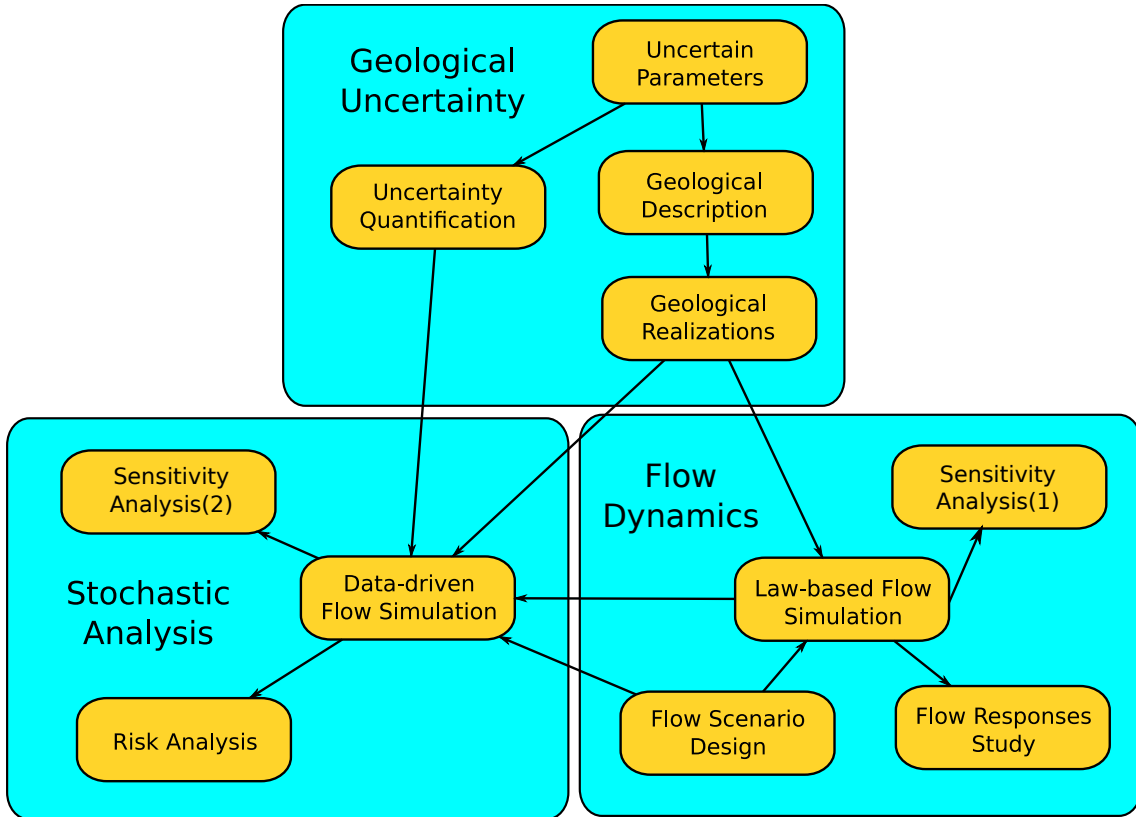


Figure 1.3: Modeling procedure diagram.

nature of the problem is analyzed by studying the variation in the model outcome due to uncertainties in the system.

Figure 1.3 shows the modeling work-flow implemented in the work of this thesis. The steps are categorized in three parts: geological uncertainty, flow dynamics, and stochastic analysis. The relations between steps are plotted by arrows in the flow-chart. In this section, we briefly describe each step. More details will follow in the next sections.

Uncertain parameters: In the first step, we identify the uncertain parameters of the model to study their influence in the modeling outcome. It is possible that our knowledge of model sensitivity to the parameters is limited. Then, in a conservative approach we choose larger number of parameters and by doing a primary sensitivity analysis with a fast technique, we filter out the important parameters. Herein, the focus is on the geological parameters. In addition, we use most of the influential parameters modeled in the SAIGUP study.

Uncertainty quantification: After identification of the uncertain geological parameters, we assign a likelihood to each of the parameters. It is hardly possible to have a unique likelihood template that applies to every geological location. Thus, we note that probabilities of existence for an uncertain geological feature can change from place to place. The uncertainty enters the modeling in the form of parameter frequency histograms. The conventional practice is to consider an analytical distribution function to be assigned to the parameters. However, the sampling procedure normally ends in scarce frequency histograms that are difficult to fit into a unique analytical distribution function.

Geological description: Geological uncertainty study is normally done by series of runs to measure the sensitivity of the model to the parameter variations. Results are valid, only if the geology used in the work-flow is representative of reality. The process of geological description results in a large number of realizations to be used in the next steps of the study.

Flow scenario design: Herein we define the initial and boundary conditions of the CO₂ injection problem. Also, we specify the injection scenarios. Possible simplifying physical assumptions will be

taken here. Each scenario is implemented in all geological realizations.

Law-based flow modeling: After defining the injection problem, we simulate the flow dynamics in the chosen realizations. We use a two-phase flow model and a standard commercial simulator.

Data-driven flow modeling: Modeling the flow dynamics via formulations of physical laws normally results in complicated equations with large degrees of freedom. The computational cost of solving these equations is high, in particular if these models are used for uncertainty related studies that require a large number of simulations to cover the variation in the uncertain parameters.

The so called data-driven methods, are mathematical functions that are specified by correlating a set of unknown flow attributes to their corresponding uncertain parameter values. These methods need to be tuned by a law-based method before employment. Because these methods are designed to be only dependent on the uncertain parameters, they are normally low in computational costs. However, they may exhibit the pitfall of not following the physical rules and in some cases produce unrealistic results.

Flow responses study: Once the simulation results are obtained from the flow modeling procedure, it is possible to calculate the important flow responses from simulation results. The fate of carbon storage and assessment of the operations can be inferred from these responses. Storage volume capacity and rate, and leakage risk are evaluated from flow responses. Responses include pressure distribution over time, CO₂ plume development, and other quantities describing the dynamics of flow in aquifer.

Sensitivity and risk analysis: The sensitivity analysis is performed in two ways: firstly by using three dimensional two-phase flow simulations on all realizations available for demonstrating the geological variability and via a linear gradient method. In the second method, we employ an approximating polynomial to perform global sensitivity analysis and stochastic uncertainty studies. Using the relatively fast data-driven method, we perform a Monte-Carlo process on 10000 simulation cases.

1.4 Geological description

The central part of a successful CO₂ storage fate modeling is to provide plenary aquifer models that depict the geological heterogeneity in a realistic manner. This requires having an inclusive understanding about model sensitivity with respect to different geological parameters and quantifications of geological uncertainty and its impacts on the process.

The conventional practice of geological modeling includes using geostatistical models. It is possible that two different heterogeneity patterns produce the same geostatistical model, as discussed by Caers [14]. Therefore, a geostatistical model does not represent a unique reservoir image and if we do not include additive information in the process, we might end-up with an unrealistic heterogeneity texture[14, 21]. The primary attention in our work has been on this issue and to provide a more realistic way of geological uncertainty analysis for CO₂ sequestration by including information of geological features and textures in the process.

1.4.1 Uncertainty

Sources of uncertainty can exist in every part of CO₂ storage modeling process. Herein, we briefly describe each of the possible contributions to the uncertainty in modeling within various parts.

Uncertainty in physical modeling: We might ignore some phenomena during the physical modeling of CO₂ storage that can be influential in the flow behavior. This might happen due to lack of awareness of the phenomena or by underestimating the significance of it. For example, we might ignore the heat exchange within the system, assuming that heat transfer does not play an important role in the flow performance. If some parameters in the modeling are sensitive to the heat and change by temperature variations, the assumption to ignore heat transfer effect will introduce considerable uncertainty in the outcome of the modeling.

Mathematical formulation and numerical approximation: A specified physical problem can be formulated mathematically in more than one way. The choice of primary unknowns to be found

can change the mathematical form and nature of the equations. Degrees of non-linearity and coupling between unknowns in the equations can vary in different formulations.

Modeling CO₂ injection and migration in a realistic geological formation results in a complicated mathematical system that in most of the cases can not be solved analytically. The numerical approach to approximate the original mathematical system, normally introduces errors in approximation. Mathematical analysis can help in estimating the error or its order, but it might not be doable for complicated models.

Geological uncertainty: The high costs of data acquisition and technical limitations introduce a huge amount of geological uncertainties in CO₂ storage modeling. The injected CO₂ may travel in a large spatial scale and providing enough geological information and the medium attributes is a big challenge.

User introduced uncertainty: These type of uncertainties are caused by the errors introduced by a user for her/his biased choice of modeling tools and interpretations of modeling results.

1.4.2 Geological parameters

From the flow modeling perspective, sources of geological uncertainty can manifest themselves in the rock parameters that go in the flow equation such as permeability and porosity. To represent the geological uncertainty, it is not enough to randomize these parameters. This approach might work in simple geological models, but it can fail to give plausible results in the realistic heterogeneous problems with uncertain structural and depositional descriptions.

In response to the EU priorities of reducing time to first oil and of improving overall hydrocarbon recovery efficiency, the interdisciplinary SAIGUP study was initiated to increase the understanding of the influence of geological uncertainties in oil field recoveries. SAIGUP stands for 'sensitivity analysis of the impact of geological uncertainties on production forecasting in clastic hydrocarbon reservoirs'. The context in SAIGUP is defined for shallow-marine depositional systems. The main objective of the SAIGUP project has been to perform a quantitative sensitivity analysis to measure the impact of sedimentological and structural variations within geological descriptions on oilfield recovery estimates [38, 46, 48].

Sedimentological variability was modeled in small and large scales and combined to provide realistic variations of reservoir heterogeneities. Structural aspects are modeled via fault modeling within geological description. Faults are considered in different levels of intensity, orientation, and transmissibility. Five waterflood scenarios were designed in various injection-production well patterns, resulting in simulated production behavior for over 35000 full-field reservoir models. All models have the same total pore volume and vary in few number of grid geometries.

Although these models were designed to study the impact of geological heterogeneity on oil recovery, they may also be used to model a scenario in which CO₂ is injected into an abandoned reservoir. Therefore, we have selected five parameters from the setup and varied these parameters by combining different levels for our CO₂ storage study. These features are lobosity, barriers, aggradation angle, progradation, and fault. In the following, we describe each feature briefly.

Lobosity: Lobosity is a metric for describing the interplay between fluvial and wave processes in a shallow-marine depositional system. As the river enters the mouth of the sea, the shore-line shapes where the river flux crash with the waves from sea. The balance between the sediment supply from rivers and the available accommodation space in the shallow sea defines the shore-line shape. Sea waves smear out the shore-line, while fluvial flux from river makes branches into the sea. Less wave effect produces more pronounced lobe shapes around the river entrance into the sea.

The channels made into the sea mouth by fluvial supplies contain good quality rocks with relatively higher porosity and permeability and poor quality rock types are located between the conductive branches. Reservoir quality decreases with distance from the shore-face. Lobosity variation can influence the CO₂ injection operation and plume distribution in the aquifer. In this study, models of three levels of lobosity are used: flat shoreline, one lobe and two lobes, see Fig. 1.4.

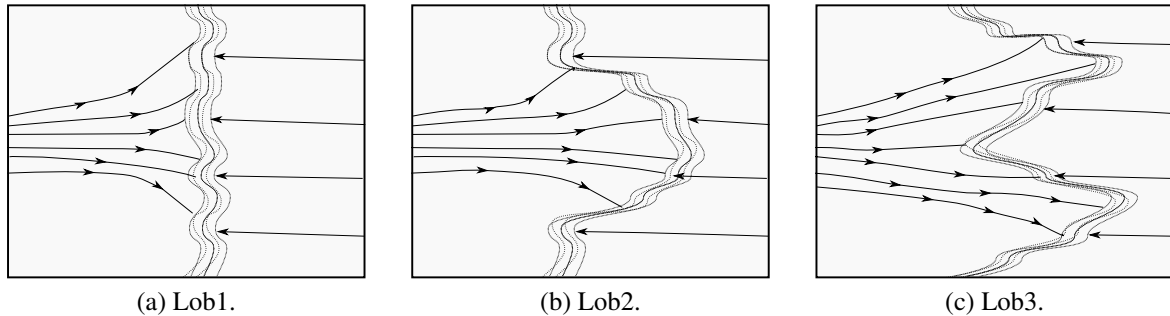


Figure 1.4: Lobosity levels are defined based on the shoreline shape, which is caused by the interplay between fluvial and wave forces.

Barriers: Barriers are mud-draped surfaces sitting between reservoir sections that are caused by periodic floods in a shallow-marine depositional system. Barriers extend in both vertical and lateral directions and are potential significant barriers to flow. In the SAIGUP domain used here, these barriers were modeled by defining areas between layers with zero transmissibility multipliers. The areal coverage designed in three levels: low (10%), medium (50%), and high (90%). We use the same variations in this study, see Fig. 1.5.

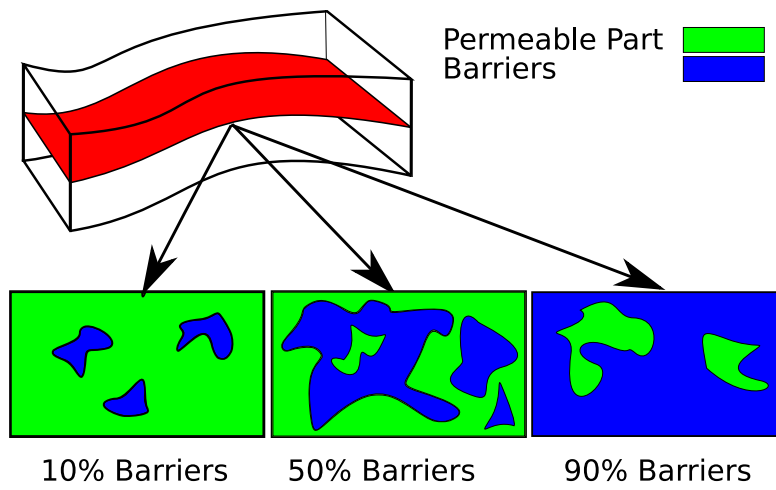


Figure 1.5: Barrier levels caused by periodic floods.

Aggradation angle: In shallow-marine systems, the sediment supply from rivers deposits in a spectrum of large size grains in the land side toward fine grains deep in the basin. Amount of deposition supplied by the river compared to the accommodation space that the sea provides defines the transition of different rock-types between the river and the sea. If the river flux or sea level fluctuates, the equilibrium changes into a new bedding shape based on the balance of these factors.

When the river flux increases, it shifts the whole depositional system into the sea causing an angle between transitional deposits that are stacked on each other because of this shifting. This angle is called aggradation angle. Three levels of aggradation are modeled here: low, medium and high (Fig. 1.6). As we will see later, aggradation can have a major role in influencing the CO₂ flow direction in the medium.

Progradation: Progradation is the depositional-dip direction between the sea and the river. Two types are considered here: up and down the dominant structural dip. Progradation combined with lobosity can influence the plume development in the medium, as the injected CO₂ plume migrates upward to the crest goes through heterogeneities(Fig. 1.7).

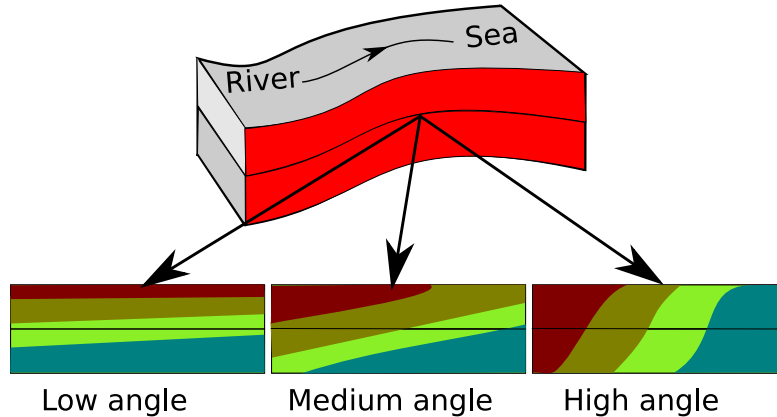


Figure 1.6: Aggradation angle levels.

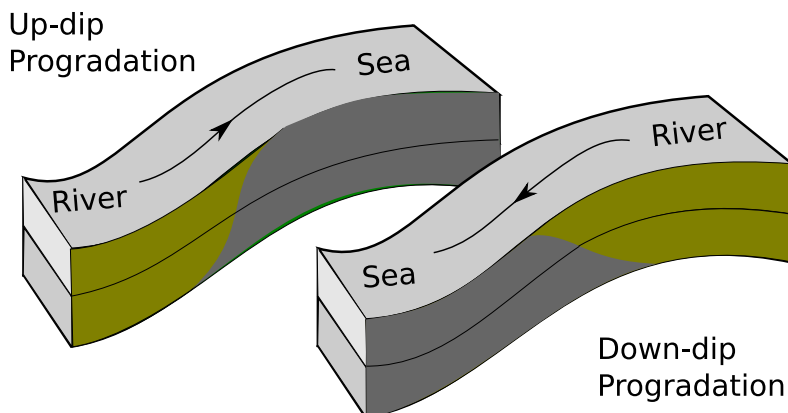


Figure 1.7: Progradation levels.

1.5 Flow equations

After introducing the parameters that make our geological model, we need to define the flow problem. In this section we discuss various formulations of the governing equations describing single and two phase flow in porous medium. We introduce the functionalities and axillary equations required to close the flow equation system. This section also includes a brief mathematical discussion on the flow equations. We discuss various flow regimes in the medium in the next section.

1.5.1 Single phase flow

Assume a porous domain Ω with boundary Γ as shown in Figure 1.8. We write the continuity equation in general form for a single phase flowing in the domain [1, 2, 15]:

$$\text{Accumulation} + \text{In-Out Flux} = \text{Source/Sink} \quad (1.1)$$

$$\int_{\Omega} \frac{\partial}{\partial t} (\phi \rho) d\tau + \int_{\Gamma} (\rho v \cdot n) d\sigma = \int_{\Omega} q d\tau \quad (1.2)$$

In Equation 1.4, ϕ is the rock porosity, ρ is the fluid density, v is the flow velocity, and n is the normal vector to the boundary. The term q denotes the mass source or sink in the system. Integrations are taken over arbitrary domain Ω with boundary Γ (Figure 1.8). Flow velocity is considered at the representative elementary volume (REV) scale for porous media [9].

The resistance of porous medium against flow results in a velocity which can be calculated from pressure and gravity gradient and fluid properties in the medium. This is governed by Darcy equation for single phase flow:

$$\mathbf{v} = -\frac{K}{\mu} \cdot (\nabla P + \nabla D). \quad (1.3)$$

In Equation 1.3, K is the permeability of the medium. Permeability is a function of pore size distribution and connectivity and in the macro scale, it is a measure of medium conductivity when a fluid is flowing through the medium (Figure 1.9). D is the gravity term that is a function of fluid specific gravity and elevation in vertical direction.

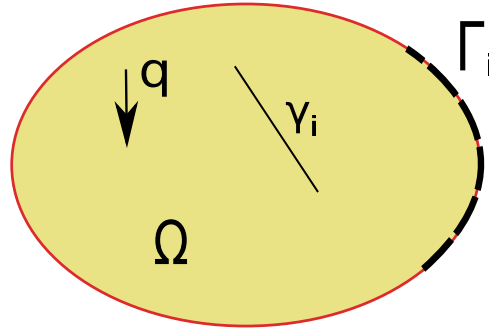


Figure 1.8: Flow domain and boundaries.

Substituting velocity term from Equation 1.3 into Equation 1.4 gives:

$$\int_{\Omega} \frac{\partial}{\partial t}(\phi\rho)d\tau - \int_{\Gamma} (\rho(\frac{K}{\mu} \cdot (\nabla P + \nabla D)) \cdot n)d\sigma = \int_{\Omega} qd\tau. \quad (1.4)$$

As a primary unknown in Equation 1.4, pressure depends upon boundary conditions as it is clear from the second term left hand side of Equation 1.4. Also, any geological discontinuities in the medium (γ in Figure 1.8) appear in Equation 1.4 through K tensor and can influence pressure behavior in the domain.

The second term in Equation 1.4 can be converted into an integration over domain Ω , using divergence theorem resulting in the following:

$$\int_{\Omega} [\frac{\partial}{\partial t}(\phi\rho) + \nabla \cdot (\rho v)]d\tau = \int_{\Omega} qd\tau. \quad (1.5)$$

Equation 1.5 is valid for arbitrary domain Ω , hence the equality is valid for the integrands *almost everywhere* in domain Ω in the *general* situation:

$$\frac{\partial}{\partial t}(\phi\rho) + \nabla \cdot (\rho v) = q. \quad (1.6)$$

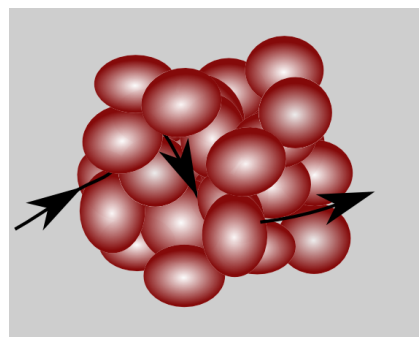


Figure 1.9: Permeability is an indication of how easy it is for the fluids to flow through the medium.

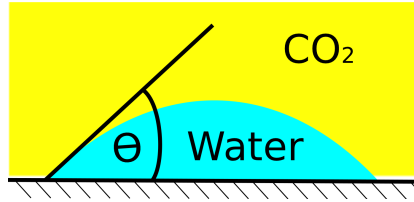


Figure 1.10: Wettability and interfacial tension in water-CO₂ system.

Fluid and rock change in volume with pressure variations. These dependencies are defined by a parameter called total compressibility, which is approximated by a combination of rock and fluid compressibilities:

$$C_T \approx C_{rock} + C_{fluid}, \quad (1.7)$$

where

$$C_{rock} = \frac{\partial \phi}{\partial P}, \quad (1.8)$$

and

$$C_{fluid} = \frac{1}{\rho} \frac{\partial \rho}{\partial P}. \quad (1.9)$$

In Equation 1.8, C_{rock} can be assumed constant in moderate pressure changes depicting a linear relation between pressure and porosity. Also, Equation 1.9 can be expanded resulting in the following [54]:

$$\rho = \rho_0 \left(\frac{P}{P_0} \right)^m \exp[C_{fluid}(P - P_0)]. \quad (1.10)$$

Assuming slight compression gives [63]:

$$\rho \simeq \rho_0 + C_{fluid} \rho_0 (P - P_0) \quad (1.11)$$

By substituting from Equations 1.7, 1.9, 1.8, and Equation 1.3 into Equation 1.6, density vanishes and by defining volumetric source/sink η , we have the single-phase diffusivity equation:

$$C_T \frac{\partial P}{\partial t} - \nabla \cdot \left[\frac{K}{\mu} (\nabla P - \nabla D) \right] = \eta. \quad (1.12)$$

1.5.2 Two-phase flow

In a two-phase flow of CO₂ and water within porous media, interactions between phases lead to loss of energy. This introduces specific phenomena occurring in the pore scale that have impact on the macro scale flow performance. More complicated equations appear in modeling the two-phase flow compared to the single-phase problem. First we describe some of the conceptual two-phase phenomena in the pore scale and then we will continue by deriving the flow equations for two phases in the system, i.e. CO₂ and water.

When CO₂ and water get in contact in the pore scale, an interface forms between them such that the energy in the system is minimized. Water and CO₂ are also in contact with the porous medium and the interface between them forms an angle from the solid phase in the water phase (shown by θ in Figure 1.10) that depends on their competence for wetting the rock. This is called wettability and the phase with the preference of wetting the solid phase is called the wetting phase. The other phase is called the non-wetting phase. Conventionally, θ is measured inside the denser fluid. If $\theta < \frac{\pi}{2}$ then the denser phase is the wetting phase. Wettability in a porous medium depends on the fluids and the rock. It can have a significant influence in the phase displacement within the medium. For water-CO₂ system, normally water is the wetting phase.

At very low water saturations, water covers the rock grains surface in layers that can go to the thickness size order of molecular films. In this situation the water phase is immobile and can not make

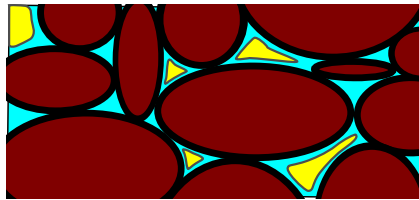


Figure 1.11: Multi-phase flow in the pore scale.

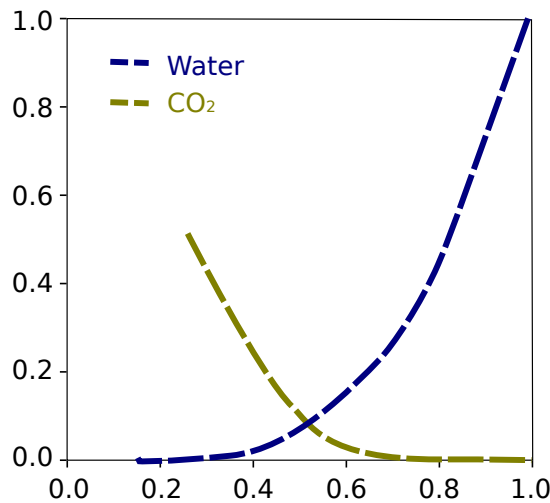


Figure 1.12: Two-phase flow and relative permeability.

a continuous phase moving through the porous medium. As water saturation in the medium increases, the layers covering the rock grains grow in size until the saturation exceeds a critical level, above which the water phase is able to flow in the medium. This saturation is called the critical or connate water saturation. In a water wet rock, once the critical water saturation is reached (for example, during the first deposition of sediments), it can not go below that level by being displaced via a non-wetting phase. Therefore, when we inject CO₂ into an aquifer, there will always be some residuals water saturation in the regions invaded by CO₂.

As a non-wetting phase, CO₂ flows in the middle part of the pore space as shown in Figure 1.11. If CO₂ saturation decreases in the medium, it reaches a critical level under which it can not make a continuous phase flowing through the pore-network. Tiny drops of CO₂ are trapped in the middle of the pore space and only very large pressure difference across the pore can move it out of the pore. This level of CO₂ saturation is called the residual saturation. Higher residual saturation is more interesting for the purpose of immobilizing more volumes of injected CO₂ in the aquifer, which reduces the risk of CO₂ leaking through any breakings in the geological formation and channeling toward surface.

Relative ease for the phase to flow within the medium is described by the relative permeability parameter. Relative permeability is a function of wettability and phase saturation. High phase saturation indicates a higher space available for the phase to flow through that space. A sample of CO₂-water relative permeability functions are shown in Figure 1.12. A library of relative permeability curves for CO₂-water system for various rock-types is available at [10].

The difference in surface tension between water and CO₂ causes a pressure acting on the interface of the two fluids. This pressure is called capillary pressure. In addition, capillary pressure depends on the geometry of pores. Since the pore geometry is very irregular, it is more convenient to use simpler geometry to drive the concept of capillary pressure. Therefore, experimental work in the laboratory is required to specify the capillary pressure functionality in a special case.

Assuming a geometry of pipe to represent a pore structure, after balancing the forces in the pore-system capillary pressure can be written in the following form:

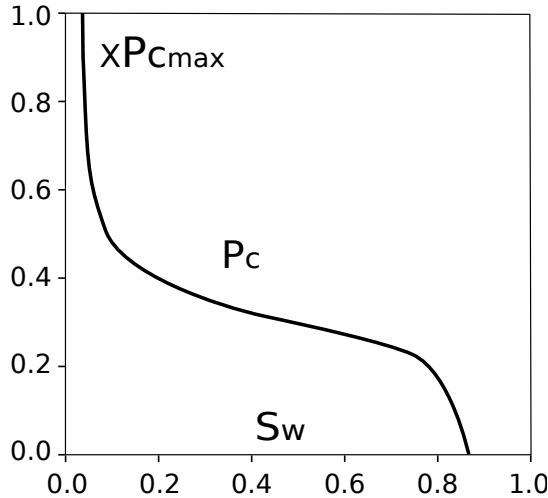


Figure 1.13: Capillary pressure can be expressed as a function of wetting saturation. The plot is a typical curve of capillary pressure function with a maximum of $P_{c\max}$

$$P_c = \frac{2\sigma}{r} \cos\theta, \quad (1.13)$$

where σ is the interfacial tension, θ is the angle between the interface and the solid phase, and r is the radius of the pore.

Capillary pressure is a jump in phase pressure across the interface of the two phases. Therefore, we can relate it to the phase pressures:

$$P_c = P_{nw} - P_w. \quad (1.14)$$

Here, P_{nw} is the non-wetting phase pressure and P_w is the wetting phase pressure.

Capillary pressure can be expressed in an empirical relation as a function of wetting phase saturation. Lower capillary pressure is expected for higher wetting saturations, and capillary pressure values go up for lower wetting saturations (Figure 1.13).

Assume hydrostatic equilibrium for a porous domain in which water and CO₂ are segregated due to buoyancy effect. If capillary forces are considerable in the domain, the sharp interface between water and CO₂ in the macro scale will be replaced by a transition zone with a spectrum of saturations between phases (Figure 1.15). Due to the hydrostatic equilibrium, phase pressure at each depth can be related to the hydrostatic pressure of that phase:

$$P_w = \rho_w g z, \quad (1.15)$$

$$P_{CO_2} = \rho_{CO_2} g z. \quad (1.16)$$

Having the phase pressure, capillary pressure can be calculated by Equation 1.14. As capillary pressure is a function of wetting saturation, the phase saturations can be back-calculated from this functionality and the phase saturation distribution over the medium can be found (Figure 1.14):

$$S_w = P_c^{-1}(P_w). \quad (1.17)$$

We can derive mass and momentum balance for two-phase flow, similar to what we have seen for single-phase flow. The equations must be written for each phase. In Equation 1.4, the accumulation term must be considered only for one phase mass calculated by multiplying the total accumulation mass by phase saturation (S_α). Also the velocity is the phase velocity v_α , and the source/sink term must be written for the phase mass rate q_α .

For phase $\alpha = \{\text{water}, \text{CO}_2\}$, we have:

$$\int_{\Omega} \frac{\partial}{\partial t} (\phi \rho_\alpha S_\alpha) d\tau + \int_{\Gamma} (\rho_\alpha v_\alpha \cdot n) d\sigma = \int_{\Omega} q d\tau. \quad (1.18)$$

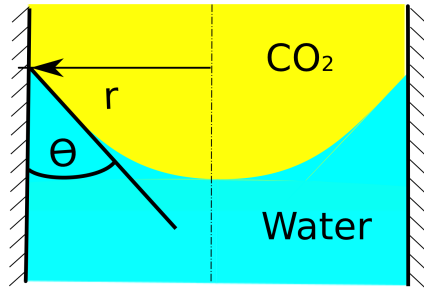


Figure 1.14: Capillary pressure distribution in the transition zone.

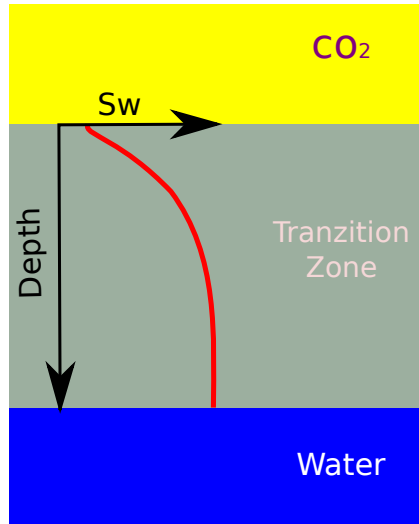


Figure 1.15: Saturation distribution in the capillary transition zone.

Darcy equation for two phases $\alpha = \{\text{water}, \text{CO}_2\}$ can be written in the following form:

$$v_\alpha = -\frac{K_{e\alpha}}{\mu_\alpha} \cdot (\nabla P_\alpha + \nabla D_\alpha). \quad (1.19)$$

Here, $K_{e\alpha}$ is the effective permeability for phase α and can be calculated from:

$$K_{e\alpha} = K_{abs} K_{r\alpha}, \quad (1.20)$$

where K_{abs} is the absolute rock permeability and $K_{r\alpha}$ is the relative permeability of phase α . P_α is the phase pressure and D_α is the gravity term for the phase specific gravity.

Similar to Equation 1.6, differential form of mass balance equation for each of phases $\alpha = \{\text{water}, \text{CO}_2\}$ is as follows:

$$\frac{\partial}{\partial t}(\phi \rho_\alpha S_\alpha) + \nabla \cdot (\rho_\alpha v_\alpha) = q_\alpha. \quad (1.21)$$

In this equation, q_α is the source/sink mass rate for phase α .

The phase saturations are related by the following equation:

$$S_{\text{water}} + S_{\text{co}_2} = 1. \quad (1.22)$$

Fluid properties change by pressure and temperature. Density is mainly a function of pressure and viscosity depends upon temperature. These functionalities, called by convention equation of state (EOS), must be coupled to the system to honor fluid attribute variability [20, 32].

Mass exchange between phases may happen leading to change in composition. That also influences the fluid properties. In the immiscible fluids, the mass exchange can be in small order leading to slight

changes in fluid properties. That can be modeled in a linear functionalities with respect to pressure and temperature.

Extensive mass exchange between phases results in more nonlinear fluid property variations that require a detailed equation of state. Also for highly miscible fluids and high mass transfer between phases, it might be better to write mass and momentum balance equations for components within phases in addition to phase equations.

There are number of approaches to formulate the primary unknowns in the system of flow equations. The direct way is to replace phase velocities from Equation 1.19 into Equation 1.21, leaving the phase pressures and water saturation as the primary unknowns. This ends in a set of strongly coupled equations.

A popular approach for formulating the set of flow equations is the fractional flow method [12]. In this method the total multiphase flow problem is treated as a single-phase flux of multi-phase mixture. Therefore, individual phases are described as a function of total flow. This leads to separate equations for pressure and saturation.

Pressure and saturation are defined for the total flow either global or pseudo globally and relate to the phase pressure and saturation with auxiliary equations. The fractional flow approach keeps the governing equations in the form of single flow equations, and numerical schemes for single-phase flow can be revised into efficient schemes for multi-phase problems.

Pressure and saturation equations have different mathematical nature: pressure has a diffusive character of an elliptical nature, which is numerically more stable than the saturation equation. Saturation equation is of convection-diffusion form with hyperbolic character in the convection part. The convection operator in saturation equation can be highly non-linear due to strong coupling of saturation and phase velocity. This nonlinearity can lead to shocks and discontinuities in the saturation solution.

As an example of fractional flow formulation, global pressure P_t is defined based on phase pressures:

$$P_t = \frac{1}{2}(P_w + P_{CO_2}) - \int_{S_w|P_c=0}^{S_w} (f_w - \frac{1}{2}) P'_c(S_w) dS_w, \quad (1.23)$$

where water fractional flow f_w is defined as:

$$f_w(S_w) = \frac{\frac{K_{rw}}{\mu_w}}{\frac{K_{rw}}{\mu_{co_2}} + \frac{K_{rco_2}}{\mu_{co_2}}}. \quad (1.24)$$

The total velocity is defined as:

$$v_t = v_w + v_{co_2}. \quad (1.25)$$

If capillary and gravity effects are negligible, saturation equation can be solved analytically, e.g. via Buckley-Leverett technique, or method of characteristics.

1.6 Flow regimes

A major part of our studies includes modeling physical phenomena occurring within flow through porous media. Various phenomena occurs during a complete sequence of CO₂ sequestration. During injection the forces imposed by injector dominate the flow behavior in a region around the injector. When CO₂ plumes develop in a thin layer moving along the stratigraphical structure, a large interface between water and CO₂ enhances the diffusion phenomena and lets more CO₂ to be dissolved into water. Convection of water with dissolved CO₂ into the initial water in place leads to complicated flow regimes.

The injected CO₂ undergoes various stages until it is stored underground. We consider two stages in our studies: injection (and early migration), and long term migration. Many forces act on flow within medium, each of which requires a set of modeling parameters. Simplifying assumptions for flow modeling can be justified at each stage with relevance to dominating forces in the medium.

The following can be recognized as forces acting on the medium in the scale at which Darcy velocity is defined:

- Forces due to pressure gradient, mostly imposed by injectors (and/or producing wells)
- Gravity, due to buoyancy with density contrast between flowing phases. Gravity acts in the vertical direction.
- Capillary forces, due to interfacial tensions.
- Hysteresis, due to sequencing of imbibition and drainage during flow in the porous medium.
- Convection forces, due to gradient of density in one phase.
- Diffusion, due to concentration gradient of one component.
- Reaction, due to chemical reaction between phases and rock.

Modeling all forces acting on porous media is not practical, and we need to look at each flow regime separately by neglecting some forces that have a minor role. Herein, we discuss main forces during injection and within long term migration.

1.6.1 Injection and early migration

Injection of CO₂ in the underground happens by forcing CO₂ mass through injector into the medium. This pose a pressure gradient around the injector causing flow within the near bore region. Some authors call the force due to pressure difference ‘viscous force’, since viscosity has an important role in transferring the stress due to pressure difference in the porous medium resulting in fluid mobility. We use the same term throughout this thesis.

Viscous and gravity forces are the two major forces acting on the region around injector during injection. Depending on medium-fluid properties and distance from injection point, force balance changes. Gravity causes rapid phase separation resulting in upward movement of CO₂. Gravity forces dominate two-phase regions far from injector with lower viscous flow velocity compared to near well locations, where the flow velocity is high. At each place in the medium, a force balance results in a total force vector that may cause flow in a particular direction (Figure 1.16a).

Attempts in the literature on evaluating force interplay during a multiphase flow regime incorporating injection in the porous medium, employ sensitivity analysis on flow attribute such as flow velocity and pressure. Many authors try devising an analytical solution to the fairly simplified flow equations that are reduced by justified assumptions and are applicable to the problem [11, 16, 19, 26, 27, 56, 60, 69, 70]. Utilizing analytical solutions gives the flexibility of examining a wide range of parameter variations within the model, enjoying a fast evaluation of the corresponding flow behavior. Semi-analytical and numerical sensitivity analysis are also vastly performed in the literature to involve more physical modeling features in the flow performance evaluations[4, 5, 62].

The flow equations can be normalized to a dimensionless version that is used in many studies discussing the capillary and gravity influence on the flow. Herein, we give the method reported in [27]. If we assume an incompressible flow in one dimensional space for a location in domain Ω without any source/sink, Equation 1.21 reduces to the following for the wetting phase:

$$\phi \frac{\partial s_w}{\partial t} + \frac{\partial v_w}{\partial x} = 0, \quad (1.26)$$

in the x spatial dimension and Darcy equation for one dimension flow becomes:

$$v_w = -K \frac{k_{rw}}{\mu_w} \left(\frac{\partial P_w}{\partial t} + \rho_w g z \right). \quad (1.27)$$

Here, z is the elevation of flow and g is the gravitational acceleration. The system is closed by Equations 1.22 and 1.14. We can define the dimensionless variables as follows:

$$X^* = \frac{x}{L}; T^* = \frac{tv_t}{L\phi}; \text{ and } P_c^* = \frac{P_c}{\pi_c}, \quad (1.28)$$

where L is a length constant in the problem, and π_c is a capillary pressure normalizing constant. After reformulating Equation 1.26, fractional flow can be written in the following form:

$$f_w = G(S_w) + C(S_w) \frac{S_w}{X^*}, \quad (1.29)$$

where S_w is the normalized wetting phase saturation, G is the gravity contribution, and C is the capillary contribution to the flow. The gravity and capillary contributions, G and C , are expressed by quantities relative to the viscous force [34] and we have:

$$G(S_w) = F_w(1 - N_G k_{rnw}), \quad (1.30)$$

$$C(S_w) = N_{nw} F_w k_{rnw} \frac{dP_c}{dS_w}, \quad (1.31)$$

wherein:

$$F_w = \left(1 + \frac{k_{rnw}}{\mu_{nw}} \frac{\mu_w}{k_{rw}}\right)^{-1}, \quad (1.32)$$

$$N_c = \frac{k\pi_c}{\mu_{nw} L v_t}, \quad (1.33)$$

$$N_G = \left(k \frac{(\rho_w - \rho_{nw}) g z}{\mu_{nw} v_t}\right). \quad (1.34)$$

Having these definitions, Equation 1.26 reshapes into:

$$\frac{\partial S_w}{\partial T^*} + \frac{dG(S_w)}{dS_w} \frac{\partial S_w}{\partial X^*} + \frac{\partial}{\partial X^*} \left(C(S_w) \frac{\partial S_w}{\partial X^*} \right) = 0. \quad (1.35)$$

Applying specific type of capillary pressure and relative permeability function may lead to simplified forms of Equation 1.35 with the possibility of having an analytical solution[70].

Some important conclusions in the literature from sensitivity studies on capillary, gravity and viscous forces are summarized here and inferred for CO₂ injection application:

- The gravity and capillary pressure will only influence the flow speed significantly for slow displacement rates. Therefor, around the injection point where normally fluids are flowing relatively with a high speed, the viscous forces are dominant.
- If capillary is of any significance, ignoring capillary forces in modeling the injection of CO₂ results in a pessimistic CO₂ sweep efficiency. Capillary helps in the spreading of CO₂ in the frontal CO₂-water interface.
- Less capillary forces in the porous medium, allows more space for CO₂. This in the macro scale enhances the density segregation due to gravity forces.

The main focus in the series of work in this thesis has been to assess the flow influence by heterogeneity during injection time and early CO₂ migration. For CO₂ injection problems, one objective is to maximize the rate of injection and aligned with that we use relatively high injection rates in our studies. Therefore, we did not include capillarity forces for modeling the high displacement rates within heterogeneities which can be justified by the results in the literature.

Table 1.1: Spatial scales for CO₂ storage. Ranges are extracted from [15].

Feature	Spatial scale
Capillary fringe	10cm->10m
Plume radius	10km->100km
Pressure perturbation	50km->500km
Migration distance	50km->500+km

Table 1.2: Temporal scales for CO₂ storage. Ranges are extracted from [15, 33].

Feature	Temporal scale
Density segregation	1 month->5+ years
Capillary segregation	1 year->50 years
Injection period	5 years->50 years
Convective mixing	20 years->1000 years
Plume migration	few hundred years->1000 years
Mineral reaction	500 years->100000 years

1.6.2 Long term migration

The injected CO₂ volume in the geological formation will travel below the sealing cap by buoyancy forces due to the density difference between water and CO₂. One concern is to have it stored safely, and the mobile CO₂ is at risk of leaking through any imperfections in the sealing layers and abandoned wells. Molecular diffusion occurs in the interface of water and CO₂ and this mass transfer from CO₂ plume into water increases the water density. Transition form of CO₂ from mobile phase into water with dissolved CO₂ is helping the safe storage of CO₂: the heavier water with dissolved CO₂ has the tendency of moving downward. Time scale for the convective mixing is of the order of several hundreds years (Table 1.2). Yet, this is not the end and the dissolved CO₂ can react with the porous medium ending up in a solid phase and it can be stored permanently in a process called mineral trapping. This is an extremely slow process and it can long to even hundreds of thousands of years [33].

Mixing of CO₂ and water in the long term happens through phases in different time scales and with various physical phenomena. Diffusion of CO₂ in water continues and the layer of water with dissolved CO₂ builds up below the CO₂ plume until it forms heavy parts convecting in the form of unstable fingers, as shown in Figure 1.16b.

The onset time for the convective mixing is important in terms of storage safety. This time depends on the Rayleigh number in the medium:

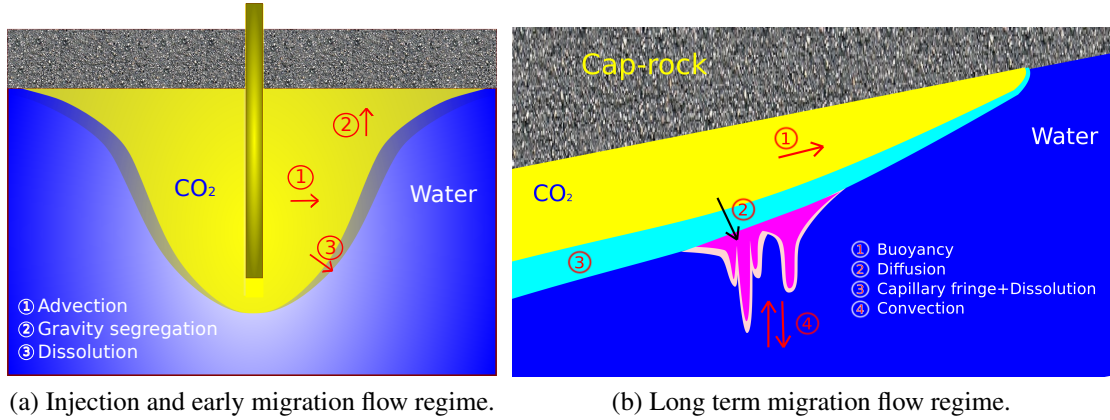
$$Ra = \frac{Kg\Delta\rho H}{D_c\phi\mu}. \quad (1.36)$$

Here, $\Delta\rho$ is the density difference between water and CO₂ phases and D_c is the diffusion coefficient of CO₂ into water phase. The higher density sitting on top of lower density makes an unstable system and the medium must have a minimum Rayleigh number in order to have a growing instability for a small perturbation in the medium. Heterogeneities in the medium can initiate perturbations, reducing the instability onset time [22, 35]. Therefore, heterogeneity is an important factor that must be considered when we are choosing an aquifer for CO₂ storage.

Capillary fringe in the plume can enhance the convective mixing onset. It can speed up the process up to five times [23].

The flow equations for convective mixing are a set of mass and momentum balance for component $c = \{\text{Water}, \text{CO}_2\}$ within phase $\alpha = \{\text{Wetting}, \text{Non-Wetting}\}$:

$$\frac{\partial}{\partial t} \sum_{\alpha} \phi S_{\alpha} \rho_{\alpha} X_{\alpha}^c + \nabla \cdot \sum_{\alpha} \rho_{\alpha} X_{\alpha}^c v_{\alpha} = 0, \quad (1.37)$$

Figure 1.16: Flow regimes in geological CO₂ storage.

and

$$v_\alpha = -\frac{k_{r\alpha} K}{\mu_\alpha} [\nabla P_\alpha - \rho_\alpha g z]. \quad (1.38)$$

where X_α^c is the mole fraction of component c in phase α [24].

1.7 Vertical averaging

In this section we discuss the common approach used in modeling the migration of CO₂ in large scale aquifers. This is a specific type of multi-scale modeling, at which we work with two models with two and three dimensions. A 2D model is extracted from the corresponding 3D model to reduce the computation costs and in some cases the accuracy can be enhanced by reducing the numerical diffusion as we will discuss here.

Spatial gradients of flux and pressure appear in the the flow equations can be decomposed into lateral and vertical components. For a three dimensional problem with the set of unit vectors $\{\vec{i}, \vec{j}, \vec{k}\}$, the gradient operator can be written as the following:

$$\nabla = \nabla_\ell + \nabla_v, \quad (1.39)$$

where:

$$\nabla = \frac{\partial}{\partial x} \vec{i} + \frac{\partial}{\partial y} \vec{j} + \frac{\partial}{\partial z} \vec{k}, \quad (1.40)$$

$$\nabla_\ell = \frac{\partial}{\partial x} \vec{i} + \frac{\partial}{\partial y} \vec{j}, \quad (1.41)$$

$$\nabla_v = \frac{\partial}{\partial z} \vec{k}. \quad (1.42)$$

x , y , and z are the location space components in the three directions.

The geological formation tops are not necessarily oriented horizontally, but they are normally close to horizontal. In CO₂ storage problems the lateral scale is orders of magnitude larger than the vertical direction. Therefore, the variations in the vertical direction are relatively negligible and for a quantity of interest Ψ we have:

$$\int_A \nabla \Psi d\tau \gg \int_\zeta \nabla \Psi dz, \quad (1.43)$$

where A is an arbitrary horizontal surface in the model and ζ is the vertical interval of the domain. Hence, with large lateral scales we can consider average values across the vertical direction for parameters and variables in the flow equations. This reduces the problem from 3D to 2D. In this case we

need to relate the parameters in the two dimensional and three dimensional problems. If this relation is not extremely non-linear the flow solutions can be obtained considerably faster on a two dimensional problem.

In a distance from the injection point, vertical equilibrium assumption is applicable. The density difference between water and CO₂ results in a rapid segregation of the two phases. A layer of CO₂ sits on top of water table and in the presence of considerable capillary forces a capillary transition zone forms between water and CO₂ zones (Figure 1.17).

The vertical equilibrium assumption facilitates the flow equation averaging across the vertical direction ζ . The phase distribution can be calculated from the volume calculations and capillary inverse function for the transition zone as mentioned in 1.5. Phase pressure variation versus depth follows the hydrostatic gravitational gradient for each phase.

The two dimensional version of flow equation can be written in the following form, assuming incompressible fluids [15, 52]:

$$\tilde{\phi} \frac{\partial \tilde{S}_\alpha}{\partial t} - \nabla_\ell \cdot \tilde{v}_\alpha = \tilde{\eta}_\alpha, \quad (1.44)$$

which follows by two dimensional Darcy equation:

$$\tilde{v}_\alpha = -\tilde{K} \tilde{\lambda}_\alpha (\nabla_\ell \tilde{P}_\alpha - \tilde{\rho}_\alpha \tilde{g}). \quad (1.45)$$

Herein, tilde sign denotes the two dimensional parameter or variable that is the vertically averaged of corresponding parameters and variables in the three dimensional problem. The averaging over vertical direction care defined in the following:

$$\tilde{\phi} = \frac{1}{H} \int_0^H \phi dz, \quad (1.46)$$

$$\tilde{K} = \frac{1}{H} \int_0^H K dz, \quad (1.47)$$

$$\tilde{\lambda}_\alpha = \frac{1}{H} K^{-1} \int_0^H K \lambda_\alpha dz. \quad (1.48)$$

Note that $\tilde{\lambda}_\alpha$ is a tensor, because it is defined such that the 2D Darcy equation is consistent with the 3D Darcy equation. The variables in the 2D equations are defined in the following:

$$\tilde{v}_\alpha = \frac{1}{H} \int_0^H v_\alpha dz, \quad (1.49)$$

$$\tilde{s}_\alpha = \frac{1}{\tilde{\phi} H} \int_0^H \phi s_\alpha dz, \quad (1.50)$$

$$\tilde{P}_\alpha = p_\alpha(z_D), \quad (1.51)$$

$$\tilde{\eta}_\alpha = \frac{1}{H} \int_0^H \eta_\alpha dz. \quad (1.52)$$

The hydrostatic equilibrium results in a constant phase pressure gradient over the vertical direction. Therefor, the phase pressure at any datum depth z_D in the medium can be used into the 2D flow equations.

Accuracy of vertical averaging approach within CO₂ storage context has been examined in many works in the literature [17, 31, 44, 52]. It has been shown that vertical averaging is applicable to large scale CO₂ studies. The numerical aspects and speed up of the method compared to three dimensional problem are studied in [31, 45], where a second order speedup is reported. Lie et al. [44] have shown the influence of vertical discretization in the three dimensional models which can fail in low resolutions to capture the thin layer of CO₂ plume migrating beneath the top sealing surface in the formation. The vertical averaging approach can handle this issue by considering the water and CO₂ interface in

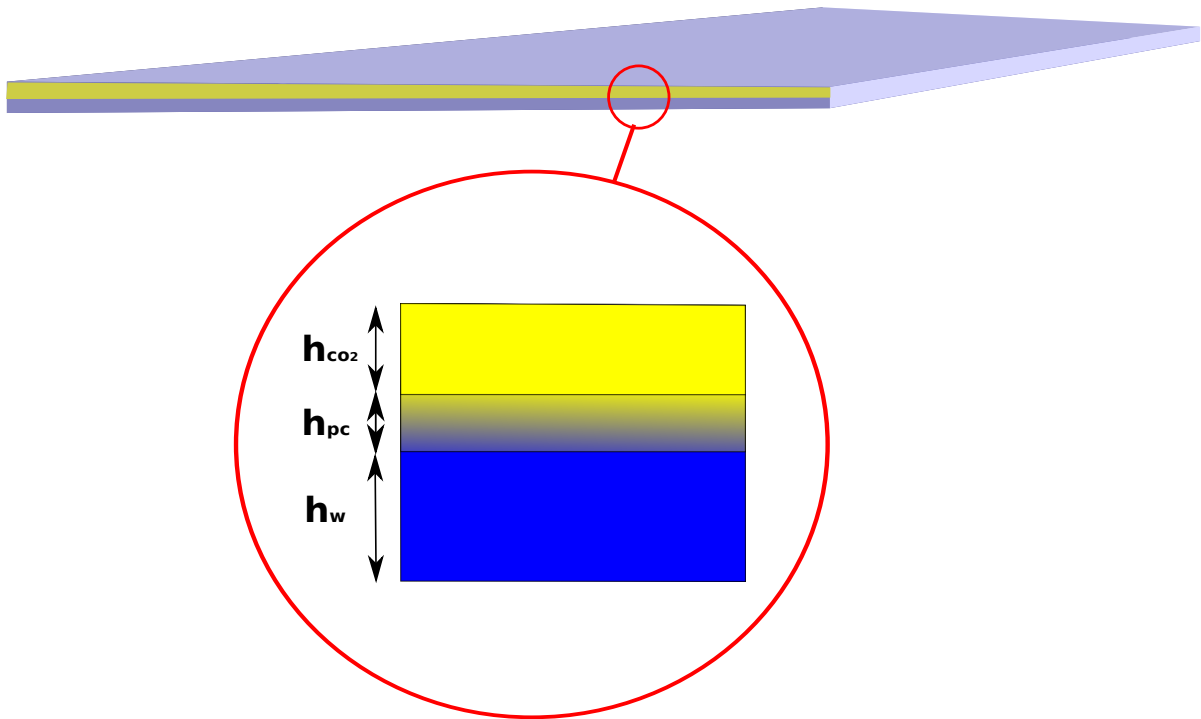


Figure 1.17: Hydrostatic equilibrium condition results in three zones: the CO_2 zone with thickness h_{CO_2} , the water table with thickness h_w , and the capillary transition zone h_{pc} .

calculating the vertically averaged parameters in the model. A comparison between three and two dimensional models has been done on various aspects in [52].

The influence of topography in modeling the CO_2 migration and estimating the storage fate has been shown in [31, 66] by examining different geometries and heterogeneities in the domain. These conclusions suggest that the significance of the model top surface is more than the small order flow in the model vertical thickness.

The studies reported in this thesis concern the flow near injector and early times of plume development. Therefore vertical equilibrium would benefit larger scales with big portion of model in vertical equilibrium. We do our flow modeling by including the three dimensions and for the quantitative uncertainty analysis we employ a polynomial approximation (Section 1.9).

1.8 Flow modeling

We use a standard porous media simulator to solve the flow equations in the medium. The solution is based on finite difference method and the following assumptions are taken:

- Two compressible phases are considered in the medium: water and super critical CO_2 .
- No mass exchange occurs between the two considered phases.
- No heat exchange is considered.

1.8.1 Numerical scheme

The employed simulator uses two-point finite difference scheme to solve Equation 1.21 on a Cartesian grid. The Darcy equation for two-phases can be written in a difference. This makes the flow equation into cell a from the neighboring cell b:

$$F_{ab\alpha} = T_{ab} M_{a\alpha} \Delta \psi_\alpha. \quad (1.53)$$

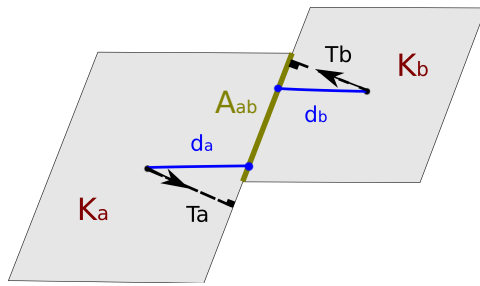


Figure 1.18: Transmissibility calculation for two cells a and b.

Here, T_{ab} is the transmissibility of medium between the two cells. $M_{a\alpha}$ is the mobility of phase α that is taken upstream of the flow from cell a, and $\Delta\psi_\alpha$ is the pressure and gravity term difference between two cell centers.

Transmissibility for two neighboring cells (i.e., sharing a face area, see Figure 1.18) is calculated by harmonic average of transmissibilities from the center of each cell to the center of the cells mutual face within that cell:

$$T_{ab} = \frac{1}{\frac{1}{T_a} + \frac{1}{T_b}}. \quad (1.54)$$

Each half transmissibility is calculated by an inner product between the permeability of the cell K_a , the mutual area between cells A_{ab} , and the distance from cell center to the mutual face center d_a :

$$T_a = K_a \cdot d_a \cdot A_{ab}. \quad (1.55)$$

Mobility term in Equation 1.53 is defined as follows:

$$M_{a\alpha} = \frac{k_{r\alpha}}{B_\alpha \mu_\alpha}, \quad (1.56)$$

where $k_{r\alpha}$ is the relative permeability of phase α , μ_α is the viscosity of phase α , and B_α is the formation volume factor of phase α which is defined as :

$$B_\alpha = \frac{\text{Volume at surface condition}}{\text{Volume at formation condition}} = \frac{V_{s\alpha}}{V_{r\alpha}}. \quad (1.57)$$

Formation volume factor definition is connected to compressibility of the fluid to change volume at surface and in the geological formation condition, but it is defined in this way in the simulator to honor cases where a fluid like oil loses its dissolved gas while being produced at surface pressure. Since we assume no mass exchange between phases in our study, here the formation volume factor works like compressibility of the fluid. Formation volume factor is a function of pressure.

Slight compressibility is considered for phases in our study, and phase density is defined as a function of pressure:

$$\rho_\alpha(P) = \frac{\rho_{0\alpha}}{B_\alpha(P)}. \quad (1.58)$$

Here, $\rho_{0\alpha}$ is the density of phase α at surface condition.

Wells are defined as source or sink in Equation 1.21. In reality wells are a void space drilled in the porous medium and the flow into the well-bore and up to surface for production wells (and vice-versa for injectors) goes through a pressure change that must be modeled separately from the porous medium.

Figure 1.19 shows a schematic pressure distribution around the injector. The well radius is much smaller than the simulation cell containing the well and the pressure in the bottom-hole is different than the cell pressure. The well bottom-hole pressure can be related to the cell pressure containing the well by a separate approximation that can be coupled with the flow equations in the grid model. Flow equation for phase α between the cell center and the well for an injector is written as follows:

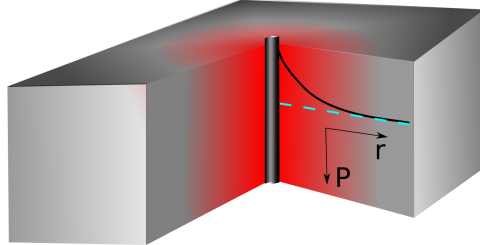


Figure 1.19: Well modeling inside a simulation cell.

$$\eta_\alpha = T_w \cdot M_\alpha \cdot [P_w - P_1]. \quad (1.59)$$

η_α is the volumetric injection rate of phase α , P_w is the injector bottom-hole pressure, P_1 is the cell pressure, T_w is the transmissibility between the cell and the injection well-bore, and M_α is the mobility of injection flow into the cell.

A region can be assumed by a radius r_e at which the pressure is equal to the cell pressure. Approximating the flow near the well-bore by Equation 1.12, the transmissibility for this region can be found from the analytical solution to Equation 1.12:

$$T_w = \frac{cK \cdot h}{\ln(\frac{r_e}{r_w})}, \quad (1.60)$$

where c is a unit conversion constant, h is the medium thickness, K is the medium rock permeability, and r_w is the well radius. Here, we assume that the well is completed and connected in the entire thickness of the cell h and there is no skin effect in the well. The Equation 1.60 can be extended to model wells with partial completions and skins. r_e in Equation 1.60 is estimated from Peaceman formula and can be related to the cell geometry:

$$r_e = 0.28 \frac{\left[\delta_x^2 \left(\frac{K_y}{K_x} \right)^{\frac{1}{2}} + \delta_y^2 \left(\frac{K_x}{K_y} \right)^{\frac{1}{2}} \right]^{\frac{1}{2}}}{\left(\frac{K_y}{K_x} \right)^{\frac{1}{4}} + \left(\frac{K_x}{K_y} \right)^{\frac{1}{4}}}. \quad (1.61)$$

Here, K_x and K_y are the permeabilities in X and Y directions and δ_x and δ_y are the cell sizes in these directions. This equation assumes a vertical well and a diagonal permeability tensor. It can be modified for more general cases.

1.8.2 Flow scenarios

All of the realizations have dimensions of $3 \text{ km} \times 9 \text{ km} \times 80 \text{ m}$, which is enough to capture variations in the designed geological features. While the volume of the realizations is large enough to capture major parts of the injected volume, the pressure disturbance imposed by the injector can go beyond this scale. To compensate for the size, we choose hydrostatics boundary conditions for the models. The open boundaries are modeled by considering a huge pore volume for the outer cells in the model that represent the boundary. Figure 1.20 shows the boundary condition defined in the model.

We consider the injection of 20% of the total model pore volume, which amounts to 40 MM m^3 . This volume is injected into realizations in three different scenarios. In the first scenario, the injection is forced to finish in 30 years and the pressure in the system is allowed to rise unlimitedly. Linear relative permeability functions are considered in this scenario. The purpose of the first scenario is to examine the flow distribution in the medium influenced by geological heterogeneity. Linear assumption for relative permeabilities is taken to speed up the flow within the medium. The relative permeability curvature has shown a significant influence on the pressure behavior in the aquifer.

In the second scenario, the injector operates with the same fixed rate as in the first scenario and the relative permeability curves are chosen to be quadratic functions. Quadratic relative permeability curves

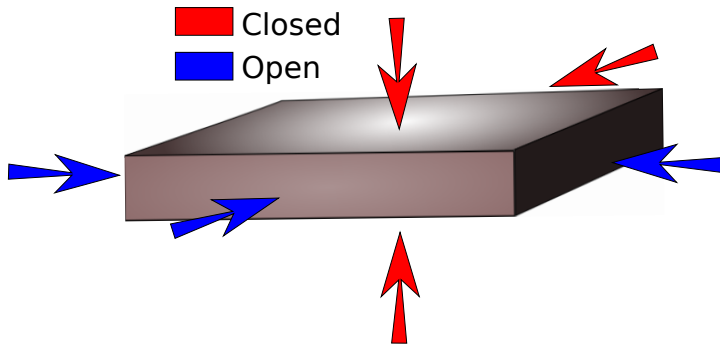


Figure 1.20: Top, bottom, and upper side boundaries are closed and the rest are open to the flow.

cause lower flow mobility in the medium compared to the linear function, and by forcing the injector with a fixed volumetric rate of injection, the pressure rises significantly in the aquifer. This leads us to the third injection scenario, where the injector is controlled by pressure rather than volumetric rate. Thus, injection time is variable depending on the injectivity of the medium.

Only one injector is considered in the study. With one injector, it is easier to study the flow behavior and the plume development within the medium. The injector is located in the flank and to increase the sweep efficiency for the up-moving CO₂ plume, the injector is completed only in the lower part of the aquifer. The injector location and the completed layers are fixed for all of the realizations. The studies here aim to identify the influence of uncertainty on injectivity and fixing a place for injection helps in achieving this goal. In a deterministic case, we can complete the well in the best quality layers.

There are few locations of distorted geometries in the faulted realizations that may be considered as structural traps for the injected CO₂. The topography in the SAIGUP realizations is simple and does not cover the variational space to be used in a sensitivity analysis. The slight inclination in the structural geometry of the medium, from the flank up to the crest, leads the injected CO₂ to accumulate in the crest and below the faulted side of the aquifer. The structural trapping due to variational morphology is studied in IGEMS, which is a sister project to MatMora (for example, see [66]).

In a homogeneous medium, we expect the CO₂ to accumulate under the cap-rock. A small fraction of the injected CO₂ will escape through the open boundary near the injection well and the rest of it will stay within the medium in two forms that we refer to as mobile and residual volumes. As the CO₂ moves through the rock, part of it stays in the smaller pores by capillary trapping process and can not be discharged by brine. The other parts move through the larger pores and can be displaced by water in an imbibition process. This volume is called mobile. As we are interested in storing the CO₂ permanently and safely, increasing the trapped volume is in line with the objective of minimizing the leakage risk and maximizing the storage capacity. Likewise, the more mobile volume of CO₂ exists in the medium, the more will be the risk of leakage.

Defining the boundary condition of the aquifer of interest can influence the flow behavior in the system. One advantage of aquifers for carbon storage is the availability of large aquifers to provide the required accommodation space. Computational costs make that more feasible to model the flow locally and in the part of the aquifer that is going through more pronounced changes in flow behavior. Therefor, we can choose the boundaries of the model inside the aquifer in a volume that is containing the injection wells and the areas effected by them. Hydrostatic open boundary condition is a choice for the system boundaries to include the aquifer parts that fall outside the boundaries (Fig. 1.21).

The underground network of aquifer systems can be connected via geological channeling and conductive features. Some aquifers might be active and connected to the surface and expand in volume by variations in water influx due to seasonal rains. This can impose an external force on the system boundaries considered in a storage problem. Fig. 1.21 shows the water influx through the boundaries of the system due to external aquifer activities. We consider the external support by imposing a higher pressure than the hydrostatic pressure on the boundary of the model.

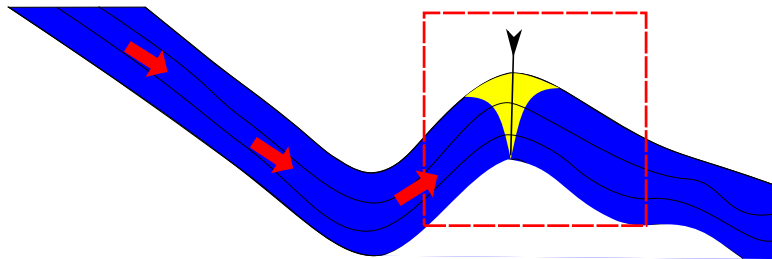


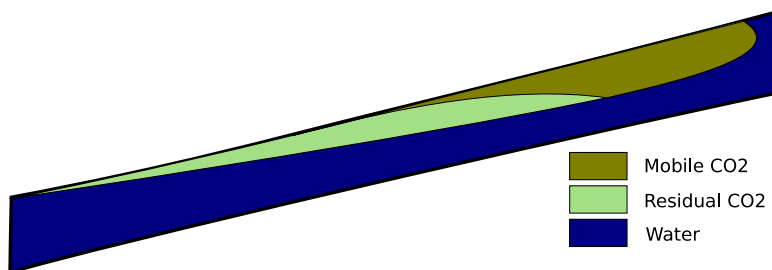
Figure 1.21: External pressure drive.

1.8.3 Flow responses

The primary unknowns in the flow model are the CO₂ pressure and the saturation distribution at different times. From the simulation output, we can derive quantities that address the feasibility of CO₂ injection, these quantities include a number of flow responses related to the CO₂ injection and migration problems. Each of these responses are directly or indirectly a measure of success for the operation within a specific realization. In the following, we give a brief description of each of them:

Boundary fluxes: The flux out of open boundaries is a measure of sweep efficiency for the CO₂ plume. Channeling can lead to early CO₂ breakthrough at boundaries and we prefer cases with less out-fluxes through open boundaries. The out-flux through the down open boundary, which is closer to the injector, is a potential loss for the injected volume. After the injection stops, some of the CO₂ that has left the domain comes in again due to gravity segregation effect.

Total mobile and residual CO₂ volume: If the CO₂ saturation is below the critical value, it will be immobile in the bulk flow, although not in the molecular sense. Less mobile CO₂ means less risk of leakage and more residual volumes (with saturations less than the critical) resulting from a more efficient volume sweep as preferable. We use critical saturation of 0.2 for both water and CO₂. During injection time the flow process is mainly drainage but after injection imbibition also happens and increases the residual trapped CO₂.

Figure 1.22: Mobile and residual CO₂ volume.

Total number of CO₂ plumes and largest plume: To estimate the risk of leakage from the cap-rock, we assume that all mobile CO₂ connected to a leakage point will escape out of the reservoir. Hence, it is preferable if the total mobile CO₂ volume is split into smaller plumes rather than forming a big mobile plume. Though the area exposed to potential leakage points will increase by splitting the plume, yet the volume reduction is overtaking the area effect. We looked at the largest plume size, the number of plumes, and other statistical parameters.

Average aquifer pressure: Average aquifer pressure is one of the most important responses to be considered. The pressure response in general shows a sharp jump at the start of injection and a declining trend during the injection and plume migration.

As soon as the injection starts, a pulse of pressure goes through the medium, introducing a pressure buildup in the aquifer. When the pressure wave reaches the open boundary, the aquifer pressure starts declining to a level maintained by the injector. When the injector stops operation, the pressure support will be removed and the pressure drops and declines until it reaches equilibrium.

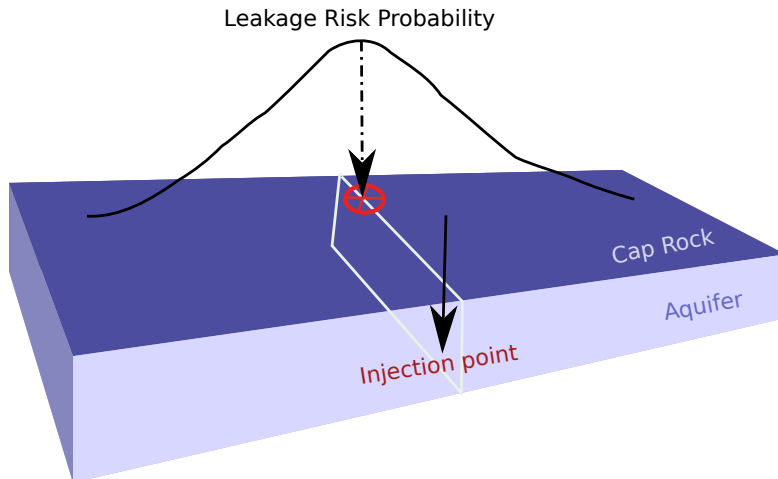


Figure 1.23: We use a 2D Gaussian distribution for leakage probability on the cap-rock.

Leakage risk: During injection operation the foremost important issue is the aquifer pressure which as discussed earlier may lead to fractures in the cap-rock. On the other hand, the cap-rock break depends on lithology and sealing thickness and differs from point to point. Some weaker locations can be the most probable to break and start leaking if any mobile CO₂ exists there.

Geo-mechanical modeling of aquifer combined with flow modeling in the medium are very costly to be used in uncertainty assessment processes. To avoid expensive computations, the idea in this thesis is to model the possible breakings on the cap-rock (considering the stress stream in the medium) by introducing a probability measure on the cap-rock. This measure can be used to evaluate different cases for their risk of leakage, considering the CO₂ distribution under the cap-rock.

Here, we define the probability of leakage as a measure on the cap-rock that assigns a value to each point of the cap-rock, modeling the relative weakness of the cap-rock and the medium at that point. If for example both the cap-rock and the aquifer are continuous homogeneous layers with constant thickness, then the point of cap-rock that sits on the highest point of the injection slice can be the most probable place for leakage in case of dramatic pressure increase in the well: the stress stream is more in the injection slice and the CO₂ accumulation occurs on the topmost part of the mentioned slice. Then one may consider a 2D-Gaussian probability distribution on the cap-rock, centered above the injection slice.

If the medium is heterogeneous or tilted, the injected CO₂ may be distributed in different number and sizes of plumes below the cap-rock. Therefore, in addition to the probability of breaking for each point of cap-rock, one must consider the CO₂ connected volume that is attached to that point.

Since we have neither the cap-rock model nor the geo-mechanical properties of the SAIGUP models, we use a simple 2D-Gaussian leakage probability distribution centered at a point on the crest which is in the same slice as the injection point (Fig. 1.23). We calculate the probability of each cell in the top layer and using the simulation results for the case, we weight it by the CO₂ saturation of that cell and the plume size that the cell is attached to. Summing up the values of the topmost cells, we assign a single number to the case which we call leakage risk of the case. One may weight the case risk value with the average pressure in the system, such that higher pressure gives a bigger weight.

One way to report the described responses and their relations to the uncertain parameters in one graph is to use scatter plots. Each case will then be represented by a marker sign with attributes dedicated to the set of geological parameter levels used in that case. Figure 1.24 shows some of the codes used in the study. That will be used later in the thesis in the papers reporting from our study.

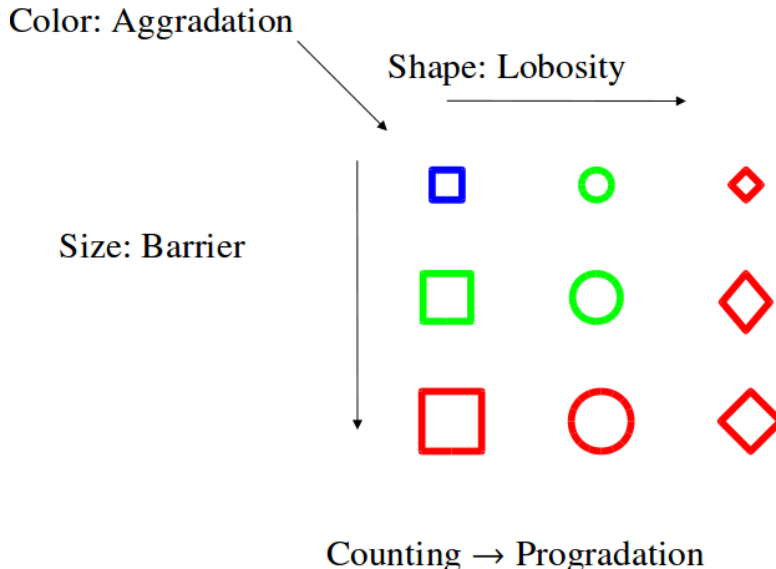


Figure 1.24: Marker codes used to plot the simulation results of all cases together.

1.9 Sensitivity and risk analysis

Mathematical models developed to approximate the injected CO₂ in the storage sites consist of several steps, including the determination of parameters which are the most influential on the model outputs. Sensitivity analysis can serve as a guide to any further use of the model.

In the initial sensitivity analysis performed on geological uncertain parameters of our studies, we use the large number of detailed flow simulations and measure the variability of model responses with respect to each level of the uncertain parameters.

We can obtain histograms of response Γ for three different levels of parameter α (i.e., low, medium, and high) by performing simulations over all geological realizations. Measuring the mean response value on each histogram results in an average for all cases with a fixed level for parameter α . Having three average points for low, medium, and high levels of parameter α , a line can be fitted to those points that approximates the trend of variations of response Γ versus the increase in levels of para α .

Assuming an equal probability for each level, the model output variations are examined by looking at each response at two important simulation times, i.e., end of injection and end of simulation. In order to study the input variations over a higher resolution, demands for a fast flow modeler. We use a response surface method that is explained in the next section in details.

1.9.1 Stochastic analysis

Complicated physical phenomenon must be modeled as a stochastic process. Uncertainty reduction in different part of modeling requires a better understanding and description of input parameters and dependency rules within the system. Parameters can be ranked in the order of their influence on the model output. Knowing the most influential parameters helps in treating the stochastic nature of the process.

Sensitivity analysis serves in identification and evaluation of important model parameters. The European commissions and the United States environment protection agency recommend using sensitivity analysis in the context of extended compact assessment for uncertainty reduction strategies and policy making [64].

As discussed in the earlier sections, various sources of uncertainties are embedded within CO₂ storage modeling and operations. The devotion of our research has been on geological uncertainty and its consequences. The procedure used here to identify the relative importance of uncertain geological

parameters via sensitivity analysis and the corresponding risk assessment is a general work-flow that can be applied to any type of uncertainties in the model inputs.

Our research continues by employing a stochastic response surface method that approximates the flow responses by projecting them on high-dimensional polynomials. In particular, we use arbitrary polynomial chaos (aPC) expansions, which consists of orthogonal polynomial bases that are constructed according to the uncertainties in the input parameters. The approach is flexible with respect to the quantification of probabilities for uncertain parameters and can be applied in studies with limited knowledge of probabilities.

The reduced model approximated by aPC is considerably faster than the original detailed one, and thus it provides a promising start point for global sensitivity analysis and probabilistic risk assessment. Variance based global sensitivity analysis methods have shown success in non-linear and complex problems[61].

The system can be decomposed into approximating functions of input parameters, and this makes it easy to implement methods based on variance. The bottle-neck of variance-based approaches can be their computational costs. In our case, the variance in output responses can be set equal to the variance of polynomial components calculated for each input parameters. Polynomials are relatively very fast and this makes it efficient to implement a variance based sensitivity analysis. Furthermore, the fact that the response surface has known polynomial properties simplifies the approach significantly. Finally, the speed of polynomial approximation makes it feasible to perform an intensive probabilistic risk assessment via Monte-Carlo process over high resolution input variation.

1.9.2 Arbitrary polynomial chaos expansion

Statistical accuracy of a Monte-Carlo process is highly sensitive to the resolution of variational inputs. A response surface method assisting a Monte-Carlo procedure must be constructed on a dense Cartesian grid, which will be computationally demanding. We explore an alternative method which only requires a minimum number of model evaluations to construct the approximating response surface. The approach we use is based on the aPC as described in [57]. The main idea is to construct the approximating response surface by projecting the response on orthogonal polynomial bases within uncertain parameter space. Therefore, uncertainty of input parameters is involved in the process from the initial steps of the work-flow. This approach is an advanced statistical regressor method that offers an efficient and accurate way of including non-local effects in stochastic analysis, see e.g., [25, 28, 71]. The method is examined for accuracy and one attractive feature of PCE is the high-order approximation of error propagation as well as its computational speed [58] when compared to Monte-Carlo processes.

Earlier PCE techniques put the restriction of specified types of uncertainty distribution functions to be used in the work-flow. In contrast, the arbitrary polynomial chaos (aPC) is flexible to accommodate for a wide range of data distribution [57]. The aPC can work even in cases with limited uncertainty information reduced in a few statistical moments of samples. They can be specified either analytically (as probability density, cumulative distribution functions), numerically as histograms, or as raw data sets. In terms of performance, the aPC approach shows an improved convergence applied to input distribution that fall outside the range of classical PCE.

In general, an approximation of system response Γ , can be written as a functionality of uncertain input parameters Θ :

$$\Gamma \approx \Upsilon(\Theta). \quad (1.62)$$

Uncertainty of input parameters Θ can be represented by mapping h from random variable space xi to random input space Θ

$$\Theta = h(\xi). \quad (1.63)$$

As discussed earlier, h can be an analytical or numerical representation. Approximation 1.62 can be expressed in the parametric mathematical form. We use a polynomial expression to approximate the

flow responses. This polynomial consists of coefficients that do not necessarily have a direct physical interpretation. Instead, we must define these coefficient such that the prediction by our polynomial functional matches some available realistic responses. These responses must be obtained either from real data measurements or via detailed flow modeling tools. This type of approximation is data-driven and we can rewrite approximation in 1.62 as follows:

$$\Gamma \approx \Upsilon(\Theta) = v(\Theta, \alpha). \quad (1.64)$$

In this relation, Θ is the input parameters and α is in the data driven parameter space, which represents the dependency between input and output of the system. First, we specify α . Then given Θ , the responses Γ can be estimated. In many practical problems, input parameters are expressed in terms of random variables and a functional form is defined to quantify the system responses. This functional expression can be in different forms, from simple linear mapping to very complicated non-linear forms.

The aPC approach involves the uncertainty of input parameters in constructing the polynomial bases. The responses of the system can be expanded into the space of these bases. This expression is specified by constant coefficient c_i :

$$\Gamma \approx \sum_{i=1}^{n_c} c_i \Pi_i(\Theta). \quad (1.65)$$

Here, n_c is the number of expansion terms, c_i are the expansion coefficients, and Π_i are the multi-dimensional polynomials for the variables Θ , $\Theta = [\theta_1, \dots, \theta_n]$. The number n_c of unknown coefficients c_i depends on the degree d of the approximating polynomial, and the number of considered parameters n :

$$n_c = \frac{(d+n)!}{d! \times n!}. \quad (1.66)$$

Polynomials Π_i in the Expansion 1.65 consist of polynomial bases P_l , with l ranging from zero up to the approximation degree d . These bases are orthogonal, i.e., every pair of non-identical bases fulfill the following condition:

$$\int_{I \in \Omega} \omega P_l P_m d\tau(\Theta) = \delta_{lm}, \quad (1.67)$$

where ω is a weight function, δ is the Kronecker delta function, and τ is the measure for input variable space. We choose the weight to be one, i.e., $\omega := 1$.

According to [57], the orthogonal polynomial basis satisfying Equation (1.67) can be obtained from the solution of the following linear system of equations:

$$\begin{bmatrix} \mu_0 & \mu_1 & \dots & \mu_k \\ \mu_1 & \mu_2 & \dots & \mu_{k+1} \\ \dots & \dots & \dots & \dots \\ \mu_{k-1} & \mu_k & \dots & \mu_{2k-1} \\ 0 & 0 & \dots & 1 \end{bmatrix} \begin{bmatrix} P_0^{(k)} \\ P_1^{(k)} \\ \dots \\ P_{k-1}^{(k)} \\ P_k^{(k)} \end{bmatrix} = \begin{bmatrix} 0 \\ 0 \\ \dots \\ 0 \\ 1 \end{bmatrix}, \quad (1.68)$$

Here, μ_k is the k^{th} non-central (raw) statistical moment of random input variable, which is defined as:

$$\mu_k = \int_{\Theta \in \Omega} \Theta^k d\tau(\Theta). \quad (1.69)$$

Thus, arbitrary polynomial chaos expansion base on Equation 1.68 only demands the existence of a finite number of moments, and does not require the exact knowledge or even existence of probability density functions. An interesting aspect is that only moments up to twice the order of expansion matter. This means, that there is no need for any kind of assumptions for data probability distribution leading to subjectivity artifacts as discussed earlier.

The PCE techniques are divided into intrusive [30, 49, 68] and non-intrusive [39, 41, 42, 58] approaches. Intrusive techniques require modifications in the system of governing equations. In some

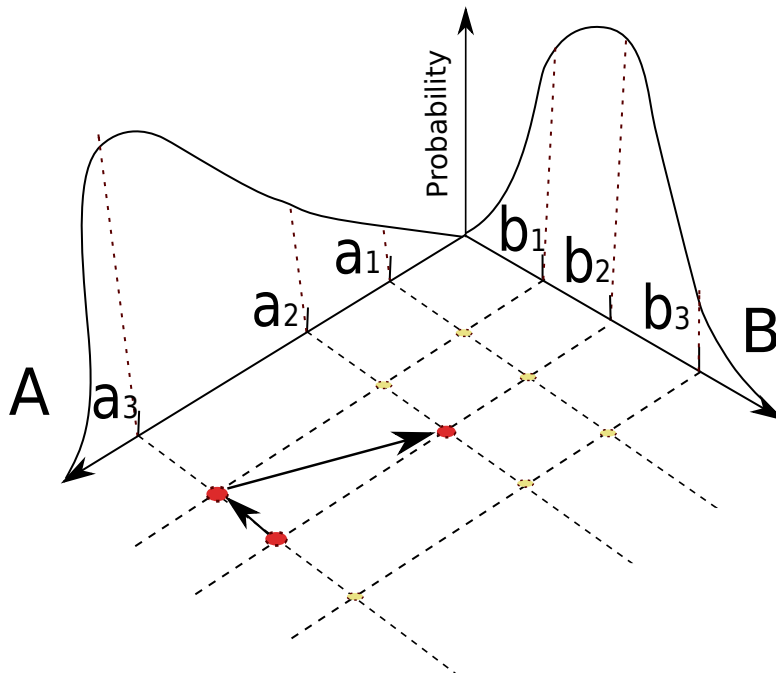


Figure 1.25: Collocation points are combined in different uncertainty directions such that the total probability in all directions is maximized.

cases, this can end up in semi-analytical methods that are used for simpler stochastic analysis studies (e.g., stochastic Galerkin method). However, the intrusive approaches can be very complex and analytically cumbersome and can not be implemented for industrial applications. In contrast to intrusive techniques, the non-intrusive methods are vastly used in practical studies. These methods do not require any symbolic manipulations of the governing equations. The sparse quadrature and the probabilistic collocation method (PCM, [42, 58]) are among the non-intrusive technique. In a simple sense, PCM can be considered as a mathematically optimized interpolation of model output for various parameter sets. The polynomial interpolation is based on minimal model evaluations in optimally chosen set of parameters that are called collocation points. Hence, the challenge in these techniques is to find a balance between accuracy and speed to evaluate the uncertainty in the physical processes.

The collocation formulation has the advantage of treating the model as a black-box. This formulation requires the corresponding output to be known in the collocation set of input parameters obtained from any acceptable mapping between input and output in the system.

According to [67], the optimal choice of collocation points corresponds to the roots of the polynomial of one degree higher ($d + 1$) than the order used in the chaos expansion (d). This strategy is based on the theory of Gaussian integration (e.g., [3]).

For multi-parameter analysis, the full tensor grid of available points from the original integration rule is $(d + 1)^n$, which is larger than the necessary number M of collocation points. This might be used for low-order (1st, 2nd) analysis of limited number of parameters. However, for large number of parameters and high order of polynomial approximations, the full grid becomes computationally cumbersome. In the collocation approach, minimal tensor of grid point set is chosen that is a scarce set of collocation points that are chosen from the most probable regions based on the parameter probability distributions (See [42, 57, 58]). This way the modeler can extract a lot of information in the main range of the parameter distribution (Figure 1.25).

We implement the probabilistic collocation method for computing the coefficients c_i in Equation 1.65. The weighted-residual method in the random space is defined as [42]:

$$\int \left[\Gamma - \sum_{i=1}^{n_c} c_i \Pi_i(\Theta) \right] w(\Theta) p(\Theta) d\tau = 0, \quad (1.70)$$

where $w(\Theta)$ is the weighting function and $p(\Theta)$ is the joint probability density function of Θ . By substituting the weight function in Equation 1.70 with Delta function, the equation reduces to

$$\Gamma_c - \sum_{i=1}^{n_c} c_i \Pi_i(\Theta_c) = 0. \quad (1.71)$$

In this equation, Γ_c and Θ_c are the responses and input parameters in the collocation points. Having the Θ_c chosen based on the probability distributions of input parameters, and Γ_c from the minimal model evaluations on Θ_c , we can solve Equation 1.71 and find the coefficients c_i .

1.9.3 Sensitivity analysis

Sensitivity analysis helps in understanding the degree of dependency of system responses to the input parameters. When the input parameters are uncertain in value, the model predictions will consist of uncertainties that must be eliminated for a robust and precise prediction. Therefore, sensitivity analysis can be useful both in optimizing the system performance and in studying the variation in performance coming from the stochastic nature of the system.

Global sensitivity analysis covers the entire variational space for uncertain parameters, while other methods, like the gradient-based methods, are limited in the scope influence of the parameters.

Variance-based methods are very popular among different types of sensitivity analysis methods. Variance-based methods provide global sensitivity and work for general non-linear problems. When the response is decomposed into simpler components (for instance, polynomial bases), it is easier to decompose the unconditional variance in the output into terms due to individual parameters and the interaction between them. It is possible then to rank the input parameters based on their contribution to the output variance [61, 65].

Following the linear sensitivity analysis performed initially in the study on the extensive detailed simulations, we tackle the global sensitivity analysis based on the aPC technique. This approach is well described in [57, 59]. Morris method [53] considers a uniform importance of input parameters within predefined intervals. We use a weighted global sensitivity in a more flexible approach accounting for arbitrary bounds and parameters with different importance defined by weighting functions. The big advantage of aPC-based sensitivity methods is their low computational costs for obtaining global sensitivity analysis. The aPC based-method places the parameter sets for model evaluation at an optimized spacing in parameter space. This can be interpreted as fitting polynomials to the model response. These polynomials approximate the model over the entire parameter space in a weighted least-square sense. This is more beneficial to computing a tangent or local second derivatives (compare FORM, SORM methods, e.g., [40]) that approximate the model well just around one point in the parameter space.

As an advantage, in variance based methods one can work with arbitrary system as a black-box and calculations are based on inputs and outputs only. More recent works are concerned about expediting calculation pace [18, 57, 59]. The idea is to replace the system with an approximating function which gives benefits in sensitivity calculations, because it is easy to relate the output variances to the input variables.

We expand the variance of output solution into components. Assume that we break the system output into components:

$$\Gamma = \Gamma_0 + \sum_i \Gamma_i + \sum_{i < j} \Gamma_{ij} + \dots \quad (1.72)$$

A single index shows dependency to a specific input variable, whereas more than one index shows interaction of input variables. If we consider input vector Θ to be of n components θ_i for $i = 1, \dots, n$, then

$\Gamma_i = f_i(\theta_i)$ and $\Gamma_{ij} = f_{ij}(\theta_i, \theta_j)$. In practice, we consider a finite number of terms in Equation (1.72). The first order sensitivity index, so called Sobol index, is defined as follows [65]:

$$S_i = \frac{V[E(\Gamma | \theta_i)]}{V(\Gamma)}, \quad (1.73)$$

where $E(\Gamma | \theta_i)$ is the conditional expectation of output Γ given θ_i and V is the variance operator. Since θ_i can be fixed at any value in its uncertainty interval, each of those values produce a distinct expectation $E(\Gamma | \theta_i)$. Equation 1.73 is a measure for variations of these expectations, which indicates the direct contribution of parameter θ_i in the output variance. For more than one index, a higher-order Sobol index can be defined as:

$$S_{ij} = \frac{V[E(\Gamma | \theta_i, \theta_j)] - V[E(\Gamma | \theta_i)] - V[E(\Gamma | \theta_j)]}{V(\Gamma)}. \quad (1.74)$$

Here, $V[E(\Gamma | \theta_i, \theta_j)]$ is the variance of output expectations after fixing θ_i and θ_j . This index represents significance of variation in output generated from uncertainty in input variables together, i.e., the interaction of uncertain parameters. If we add all indices that contain variable θ_i , the sum is called the total Sobol index:

$$S_{Ti} = S_i + \sum_{j \neq i} S_{ij} + \sum_{j \neq i} \sum_{k \neq i} S_{ijk} + \dots \quad (1.75)$$

To clarify the subject, we go through a simple analytical example given in [6]. Suppose that the exact expression for response Γ to be known and can be written as a polynomial with parameters θ_1 , θ_2 , and θ_3 :

$$\Gamma(\theta_1, \theta_2, \theta_3) = \theta_1^2 + \theta_2^4 + \theta_1\theta_2 + \theta_2\theta_3. \quad (1.76)$$

The Sobol indices can be calculated from functions F that are defined based on orthogonality condition used to decompose the solution and for input with Gaussian distribution Φ_n in uncertainty domain R^n they are as follows:

$$F_0 = \int_{R^n} \Gamma(\Theta) \Phi_n(\Theta) d\Theta, \quad (1.77)$$

$$F_i = \frac{\int_{R^{n-1}} \Gamma|_{\theta_i} \Phi_{n-1}(\theta_{\sim i}) d\theta_{\sim i}}{\Phi_1(\theta_i)} - F_0, \quad (1.78)$$

$$F_{i,j} = \frac{\int_{R^{n-2}} \Gamma|_{\theta_i, \theta_j} \Phi_{n-2}(\theta_{\sim i}, \theta_{\sim j}) d\theta_{\sim i} d\theta_{\sim j}}{\Phi_2(\theta_i, \theta_j)} - F_0 - F_i(\theta_i) - F_j(\theta_j). \quad (1.79)$$

$\Gamma|_{\theta_i}$ and $\Gamma|_{\theta_i, \theta_j}$ are the Γ values at fixed θ_i and $\{\theta_i, \theta_j\}$ respectively. $\theta_{\sim i}$ is the vector of dummy variables corresponding to all but the component θ_i of uncertain parameters Θ .

Let us denote the variances by D :

$$D = V[F(\Theta)] = \int F^2(\Theta) d\Theta - F_0, \quad (1.80)$$

that can be decomposed into

$$D_i = \int F_i^2(\theta_i) d\theta_i, \quad (1.81)$$

and

$$D_{i,j} = \int F_{i,j}^2(\theta_i, \theta_j) d\theta_i d\theta_j. \quad (1.82)$$

Then the Sobol indices can be found from:

$$S_i = \frac{D_i}{D}, \quad (1.83)$$

$$S_{i,j} = \frac{D_{i,j}}{D}. \quad (1.84)$$

Finally, the total Sobol index can be found from Equation 1.75. Applying the calculations of Equations 1.77 to 1.82 for our example (i.e., the expression in Equation 1.76) we can obtain the following Sobol indices, assuming Gaussian distributions for the parameters over the interval $[0, 1]$:

$$\begin{aligned} S_1 &= 0.0005 & S_2 &= 0.4281 & S_3 &= 0.0000 \\ S_{12} &= 0.0007 & S_{13} &= 0.0000 & S_{23} &= 0.5708 \\ S_{123} &= 0.0000 \end{aligned}$$

and the total sobol indices are:

$$S_{T1} = 0.0012 \quad S_{T2} = 0.9996 \quad S_{T3} = 0.5708 .$$

The total Sobol index can be used as a sensitivity measure to rank parameters for their influence in the results variation. In this example, we can see that the ranking that the total Sobol indices suggests is consistent with what can be inferred directly from the simple expression in Equation 1.76: θ_2 is the most influential parameters, because it appears in two terms, and in one of them with a forth degree. Interactions are represented by two indices, and S_{13} is zero, because there exist no term in Equation 1.76 that contains both θ_1 and θ_3 .

With known polynomial coefficients, Sobol indices are easy to calculate. When the number of parameters is large, it is possible to do initial sensitivity analysis with lower degree polynomials to filter out pertinent parameters. Then the analysis continues on the filtered parameters with a higher degree polynomial approximation.

1.9.4 Risk analysis

The risk is the impact of uncertainty on objectives. Quantifying the risk requires calculating this impact, which consist of two parts: quantification of the uncertainty and evaluation of the system consequences. Risk R of a process is quantitatively defined as the consequence C caused by the process multiplied by the probability P of that consequence to happen:

$$R = P \times C. \quad (1.85)$$

In the case of CO₂ injection into deep aquifers, the amount of CO₂ which stays mobile and undissolved in the medium for a time after injection can be considered as a consequence, bearing the potential of leakage up to the surface if exposed to a geological leakage point. The risk could be the expected amount of CO₂ that will leak through ill-plugged abandoned wells or cracks in the sealing rocks.

We consider looking at responses and the probability of them to happen. We initially examine this probability by drawing the histogram of response values obtained from detailed simulations on large number of realizations and corresponding to important time, like end of injection and end of simulation. Yet larger number of points in the uncertain parameter space are studied employing the data-driven aPC method, which requires a considerably short time for evaluating the responses. This way it is possible to perform an intensive Monte-Carlo process in a full tensor grid of input parameter variational space, resulting in a high resolution output probability distribution.

1.10 Implementation of work-flow

This thesis incorporated working with large number of realizations, various flow scenarios, and different procedures and softwares. While the study progresses, new ideas and challenges rises that require manipulation of parts of the work-flow. In order to achieve the defined goals of the research, an automated work-flow is required that connects different parts of the study and converts data type in-between them. This makes the study feasible in terms of saving time for any necessary modifications.

Matlab programming language is used for implementing the work-flow in this research. The main reason for this choice, apart from the rich facilities available within Matlab toolboxes, is to use many

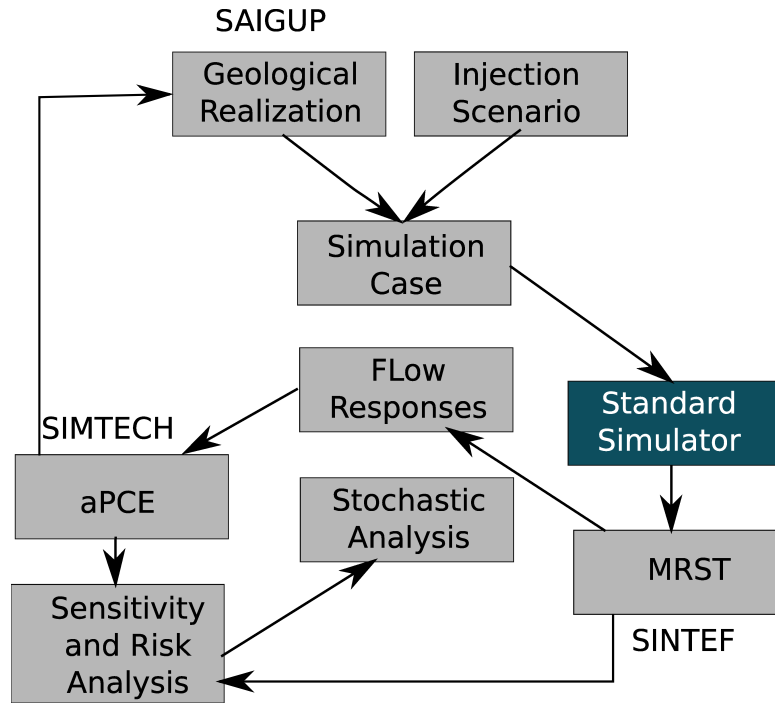


Figure 1.26: Flow-chart of work process implemented in an automated procedure.

functions within the Matlab Reservoir Simulation Toolbox (MRST) [43, 47] available as free and open-source software in Matlab language. For flow simulation a commercial software is used, which is a standard simulator for oil and gas industry and research. The simulator is using finite difference for flow modeling.

Figure 1.26 shows the elements of the work-flow implemented by a large number of Matlab functions. Functions from MRST at SINTEF and the stochastic tools of SIMTECH group in Stuttgart university are utilized and merged into the work-flow. The design is made such that the work-flow is flexible and general. Some research has been done by replacing the commercial simulator with in-house simulators at SINTEF, but the main study was performed using the black-box commercial simulator.

One thing to notice in Figure 1.26 is the link between designing geological realizations and implementation of aPCE method. A normal procedure must start by finding the collocation points from the given geological uncertainty, and then based on those collocation points we design the geological realizations.

Chapter 2

Introduction to the papers

2.1 Introduction

The main scientific part of this thesis consist of five papers. They come in a sequence to show the research progress withing this PhD program. Paper I is presented in the proceedings of the Computational Methods in Water Resources (CMWR) conference in Barcelona, 2010. Utilizing the feed back from that conference and including more uncertain parameters in the study ended up in paper II presented in the proceedings of the ECMOR XII in Oxford, 2010. Paper III includes a detailed study on the flow responses and effect of relative permeability on the flow and it is submitted to the International Journal of Greenhouse Gas Control (IJGGC). Pressure is an important model response during injection operations. Therefore, a special study is dedicated to pressure analysis in the system. This is reported in paper IV, which is submitted to the IJGGC. Finally, paper V reports modern stochastic techniques used to perform detailed quantitative sensitivity analysis and probabilistic risk assessments. This paper is submitted to special issue of the IJGGC.

2.2 Summary of papers

Paper I: Impact of geological heterogeneity on early-stage CO₂ plume migration

Summary:

It is a conventional practice in the context of CO₂ storage study to simplify the geological modeling in order to achieve an easier force balance study in the medium. Assuming a homogeneous medium is the first step to quantify the time and space scales in CO₂ storage problems by a dimensionless analysis on the analytical solution of flow equation. However, in practice the real flow performance is very much influenced by geological heterogeneity.

We use a set of SAIGUP realizations selected to cover the variability of four sedimentological and structural parameters. The selected parameters are lobosity, barriers, aggradation angle, progradation direction. Each of these parameters varies over three levels, except the progradation direction, which includes up-dip and down-dip directions. Combining the available parameters makes 54 realizations.

30 years of injection and 70 years of early migration of CO₂ are simulated and flow responses related to the storage capacity and leakage risk objectives are defined and calculated from the simulation results. The responses are reported in scatter plots at end of injection and end of early migration time.

This work is specific in examining how heterogeneity influences flow behavior by using a number of geological realizations. Flow responses defined in this work are specific to CO₂ studies and differ from the responses used in the original SAIGUP project to study oil recovery. We simulate the aquifer average pressure, model boundary fluxes, residual and mobile CO₂ saturation, and spatial distribution of connected CO₂ volumes. These responses can be considered to discuss the site storage capacity and risk of CO₂ leakage to surface.

Comments:

This work initially is presented in Edinburgh 2010 ACM conference, in a brief proceedings presentation, and more details of the work are reported in a proceedings for CMWR 2010 conference in Barcelona. The aim of this paper is to investigate the impact of geological heterogeneity on a typical CO₂ injection problem.

The main concern here is to include realistic geological heterogeneity knowledge into flow simulation work-flow, which is specific to the CO₂ storage problem. Results of this work conclude that the range of variability in flow responses indicate the significance of geological heterogeneity in modeling the CO₂ flow. Geological features are ranked by for their impact on each of the defined flow responses and in particular, aggradation angle has shown a big impact in most of the responses.

This paper received a comment on lacking the quantitative sensitivity analysis. This was added in the later works.

Paper II: *Impact of geological heterogeneity on early-stage CO₂ plume migration: sensitivity study*

Summary:

In this paper, we consider faults in addition to the four geological parameters used in Paper I. In the SAIGUP study, fault modeling is performed in an intensive variability over structural parameters and transmissibility across the fault. In order to keep the work less succinct and conclusive in studying the dynamics of flow, we fix the structural variability in its medium level and vary the transmissibility over three main levels: unfaulted, open faults and closed faults.

The flow responses analyzed are the same as defined in Paper I. In addition, we perform a linear sensitivity analysis for the flow responses with respect to the geological variations. The outcome of sensitivity analysis shows that the flow behavior is highly sensitive to aggradation angle. Barriers and faulting will also influence the flow responses significantly. In this work, similar to the previous report, we clearly see the range variation in flow responses that indicates how significant is to model the geological features accurately.

Comments:

The following issues have been addressed for the works reported in this paper:

- *The SAIGUP realizations*

This paper is presented in ECMOR conference in Oxford, 2010. This is a complementary to proceedings works presented in ACM Edinburgh, 2009 and CMWR in Barcelona, 2010.

Topography is a major player in the gravity dominated flow behavior. The SAIGUP realizations include variability in topography of the geological layering via structural changes due to faults and also barriers in the model. These are good enough for early migration when the CO₂ and water segregate and plumes accumulate below cap-rock and start the longer migration. In the long-term migration, top surface geometry is an important geological parameter and larger models than the SAIGUP models with a better resolution of the top surface are needed to get good predictions of the long-term migration phase. This was considered in the next generation of geological studies performed following this study [55, 66] under the IGEMS research project.

- *Physical assumptions*

The work concentrates on how geological heterogeneity impacts the flow performance. We need to measure the volumetric sweep efficiency of CO₂ plumes to evaluate the residual trapping. The most important parameter is the rock transmissibility, rather than fluid properties. Including more physics in the modeling will add the computational costs specially when the flow modeling is used in a sensitivity analysis or risk assessment process. Therefore, we used simple fluid models for PVT.

To accelerate the flow, we used linear relative permeability curves. This increases the flow mobility in the low saturation values. Hysteresis effects are modeled by changing the endpoints in the relative permeability curves and no scanning-curves is considered here. During injection, the main process is drainage. After injection, the imbibition process starts and mostly is a replacement of CO₂ by water due to gravity segregation. This justifies the usage of simple hysteresis model, and more detailed study can be done to investigate this influence in a quantitative manner.

- *Uncertainty considerations*

The geological parameters are changed in value between low and high levels. These values are assumed with the same probability, which is a reasonable start point for sensitivity analysis. In general, this probability might not be uniform, depending to the regional geology of the storage site.

Paper III: Impact of geological heterogeneity on early-stage CO₂ plume migration: sensitivity study

Summary:

In this paper, we use the same setup that is used in the previous paper. Five geological features are examined, which are lobosity, barriers, aggradational angle, progradational direction, and faults. Also, the same injection scenario is used: 30 years of CO₂ injection and 70 years of early migration. The injector is controlled by a constant rate and no pressure constraint is set to allow for all ranges of pressure, including those that are unrealistic. Moreover, we define an additional model output that is related to the risk of CO₂ leakage through any breakings in the cap-rock.

We examine the influence of simplifying assumptions considered in our works regarding linearity of relative permeability function. We perform a detailed flow analysis on various geological realizations using two different relative permeability relations: linear and quadratic functions. The non-linearity in relative permeability hinders the flow in the lower saturation values of the displaced phase, i.e., water phase. We discuss the influence of curvature on CO₂ flow dynamics within the aquifer.

Comments:

Results show that using linear relative permeability function ends up in conservative conclusions with respect to CO₂ distributions in the domain in terms of storage safety. Since computational costs are much lower for linear relative permeability scenario than quadratic relative permeability, it sounds a good strategy to perform sensitivity analysis by using linear relative permeability function on flow responses that are based on CO₂ distribution in the domain.

However, dramatic pressure build-up can happen in the medium during injection in the quadratic relative permeability scenario. This suggests that for pressure studies we must use more realistic relative permeability functions.

Following this work, a detailed pressure study with more realistic relative permeability curves is performed, which is reported in the next paper.

Paper IV: Geological storage of CO₂: heterogeneity impact on pressure behavior

Summary:

After observing the influence of relative permeability curvature on pressure response for CO₂ injection studies, in this paper we perform a detailed pressure study on the chosen geological realizations.

Pressure is an important criteria that can determine the success and failure of CO₂ storage operations. Over-pressurized injections can induce new fractures and open the existing faults and fractures that increases the risk of leakage for the mobile CO₂ in the domain. On the other hand, the pressure disturbance imposed on the system travels within the domain beyond the scales of CO₂ distribution. If the CO₂ is injected into a saline aquifer connected to fresh water aquifers, the pressure pulse may result in fresh water contaminations by the brine far from the injection point. We define specific pressure responses to examine the pressure disturbance in the system during injection.

Two injection scenarios are examined for the same 160 geological realizations setup. In the first scenario, the injector is set to a fixed volumetric rate to inject the CO₂ volume in 30 years into the domain, allowing for an unlimited pressure build-up. In the second scenario, a pressure constraint is set on the injector that results in various rates of injection in different geological realizations to inject the same amount of CO₂ volume considered in the first injection scenario.

Comments:

Pressure response sensitivity study with respect to different geological features indicates the significance of aggradational angle, progradational direction, and faults during injection. A probabilistic pressure analysis is also performed based on the 160 simulations on the available realizations.

Paper V: Geological storage of CO₂: global sensitivity analysis and risk assessment using the arbitrary polynomial chaos expansion**Summary:**

In this paper, we perform a stochastic sensitivity and risk analysis. We obtain a high resolution global sensitivity and probabilistic study on the flow responses that are defined and discussed in the previous papers. We choose barriers, aggradation angle, and faults from the SAIGUP geological parameters. Faults are considered by changing the transmissibility value across them, which is a continuous parameter. One more parameter is added to the study which is common in the literature and models the external pressure support from other aquifers attached to the model (regional groundwater effect).

Flow simulation on high resolution variational geology demands a huge computational costs. To enhance the calculation speed, we use a data-driven method that does not need to solve the full physical flow equations. We approximate the flow solver by a response surface method that is a polynomial and relates the system output to the input with a minimal computational cost. We use the arbitrary polynomial chaos expansion (aPC) to approximate the flow responses. The aPC method considers the uncertainty in the input variables.

A global sensitivity analysis is performed by employing Sobol indices that are based on variances of responses. The method is shown to be robust in problems of high levels of complexity and non-linearity.

And finally, we perform a Monte-Carlo process using the approximating polynomial on a high resolution input variations. This makes it possible to perform a high resolution probabilistic study on the flow responses. This way, extreme cases can be identified by probability of occurrence.

Comments:

In order to implement our stochastic technique, we choose geological parameters in this study that can be interpolated between two levels of their values. For example, it makes sense to use barriers coverage level of 25% between the low (10%) and medium (50%) levels used in the previous studies. Some of the geological parameters are discrete and can not be interpolated between two values. For instance, lobosity can only be varied over three points and we can not define a 1.5-lobe.

Having a large number of points in the input values interval requires intensive geological modelings to be used in the flow simulations. Using the data-driven polynomial, the approach only needs evaluating the polynomial in the defined values, and there is no need for full geological modeling except in the collocation points, i.e., point values that the polynomial coefficients must be calculated.

The work reported here is to demonstrate the work-flow of using the aPC for global sensitivity analysis and probabilistic risk assessment. A normal work-flow starts by defining the uncertainties in the input parameters and follows by building the geological models that are based on those uncertainties. To perform this study on the SAIGUP models that are consistent with a uniform uncertainty in the geological parameters, with no loss of generality, we used uniform uncertainty distributions for our study. However, the aPC method is not limited to uniform uncertainty descriptions.

Geological features are ranked based on the sensitivity analysis results. The results are in agreement with dynamics of the flow in the aquifer. Aggradation angle is the most influential parameter, while the regional groundwater has the least influence in the model responses. The study is not limited to the assumed uncertainty of input parameters and the conclusion may change for a very different uncertainty description.

Chapter 3

Scientific results

Paper I

3.1 Impact of geological heterogeneity on early-stage CO₂ plume migration

M. Ashraf, K.A. Lie, H.M. Nilsen, J.M. Nordbotten & A. Skorstad

Proceedings of *International Conference on Water Resources (CMWR)*, Barcelona, Spain (2010)

IMPACT OF GEOLOGICAL HETEROGENEITY ON EARLY-STAGE CO₂ PLUME MIGRATION

**Meisam Ashraf^{*,§,1}, Knut-Andreas Lie^{*,§,2}, Halvor M. Nilsen^{§,3}, Jan M.
 Nordbotten^{*,4}, Arne Skorstad^{†,5}**

*Department of Mathematics, University of Bergen, NO-5008 Bergen, Norway

§SINTEF ICT, Department of Applied Mathematics, NO-0314 Oslo, Norway

†Norwegian Computing Center, NO-0314 Oslo, Norway

¹Meisam.Ashraf@uni.no, ²Knut-Andreas.Lie@sintef.no, ³HalvorMoll.Nilsen@sintef.no
⁴Jan.Nordbotten@math.uib.no, ⁵Arne.Skorstad@nr.no

Key words: CO₂ storage, heterogeneity, sensitivity, shallow marine

Summary. In an effort to determine the influence of geological heterogeneity on CO₂ storage efficiency, we study injection and early-stage migration of CO₂ in 54 different realizations of a shallow-marine reservoir.

1 INTRODUCTION

Academic studies of CO₂ injection frequently employ simplified or conceptualized reservoir descriptions in which the medium is considered nearly homogeneous. However, geological knowledge and experience from petroleum production show that the petrophysical characteristics of potential CO₂ sequestration sites can be expected to be heterogeneous on the relevant physical scales, regardless of whether the target formation is an abandoned petroleum reservoir or a pristine aquifer. Geological uncertainty introduces tortuous subsurface flow paths, which in turn influence reservoir behavior during injection. It is paramount that the effect of the geological heterogeneity is quantified by the research community. This will facilitate both improved understanding of subsurface flow at operational CO₂ injection sites, and allow comparison with simulated flow in ideal homogeneous models and upscaled versions of these.

Within oil recovery, the impact of geological uncertainty on production forecast has been thoroughly investigated in the SAIGUP project [2, 3, 4] focusing on shallow-marine reservoirs. To study different factors, synthetic realistic models were made and several thousand cases were run for different production scenarios. The results showed that realistic heterogeneity in the structural and sedimentological description had a strong influence on the production responses.

Meisam Ashraf, Knut-Andreas Lie, Halvor M. Nilsen, Jan M. Nordbotten and Arne Skorstad

The main objectives of CO₂ storage studies are to maximize the injection volume/rate and to minimize the risk of leakage [1]. The problem of CO₂ storage differs from oil recovery prediction not only in the objectives of study, but also in the time scales considered for the process (thousands of years compared to tens of years for CO₂ migration). In addition, the characteristic length scale of the flow is much larger. Working with long temporal and spatial scales and huge amounts of uncertainties poses the question of how detailed the geological description should be. The motivation of this work is mainly to answer two questions related to CO₂ storage:

- How sensitive is the injection and early-stage migration to uncertainty and variability in the geological description?
- What simplifying assumptions are allowed in averaging the geological attributes over scales?

To this end, we use a subset of the synthetic models from the SAIGUP study to perform a preliminary sensitivity analysis for CO₂ sequestration in aquifers. Heterogeneity classes are defined based on different sequence-stratigraphy parameters and levels of shale barriers. We assume two-phase flow with slight compressibility for supercritical CO₂. The injection scenarios are defined based on the objectives outlined above, and important responses are discussed to evaluate the efficiency and risk of the process.

2 Geological descriptions

In this work we question the widespread use of simplified geological descriptions that ignore the detailed heterogeneity in modeling. Our hypothesis is that heterogeneity features like channels, barriers, sequence stratigraphy of facies, and fault intensity/geometry all have a particular effect on flow behavior, both locally and globally, and may significantly alter the injection and migration of CO₂ plumes.

Sound geological classifications and descriptions of key geological features are important to give a realistic description of the sensitivity of CO₂ storage performance. To this end, we have selected four parameter spaces of geological variations from the SAIGUP study [2, 3, 4]. The parameters span realistic intervals for progradational shallow-marine depositional systems with limited tidal influence. In the following, we give a brief description of each.

Lobosity: Lobosity is defined by the plan-view shape of the shore-line. As a varying parameter, lobosity indicates the level at which the shallow-marine system is dominated by each of the main depositional processes. Two depositional processes are considered in the SAIGUP study: fluvial and wave processes. The higher amount of sediment supply from rivers relative to the available accommodation space in the shallow sea, the more fluvial dominant the process will be. As the river enters the mouth of the sea, it can divide into different lobes and branches. Wave processes from the sea-side smear this effect and flatten the shoreline shape. Less wave effect produces more pronounced lobe shapes around the river mouths. Very high permeability and porosity can be found in

Meisam Ashraf, Knut-Andreas Lie, Halvor M. Nilsen, Jan M. Nordbotten and Arne Skorstad

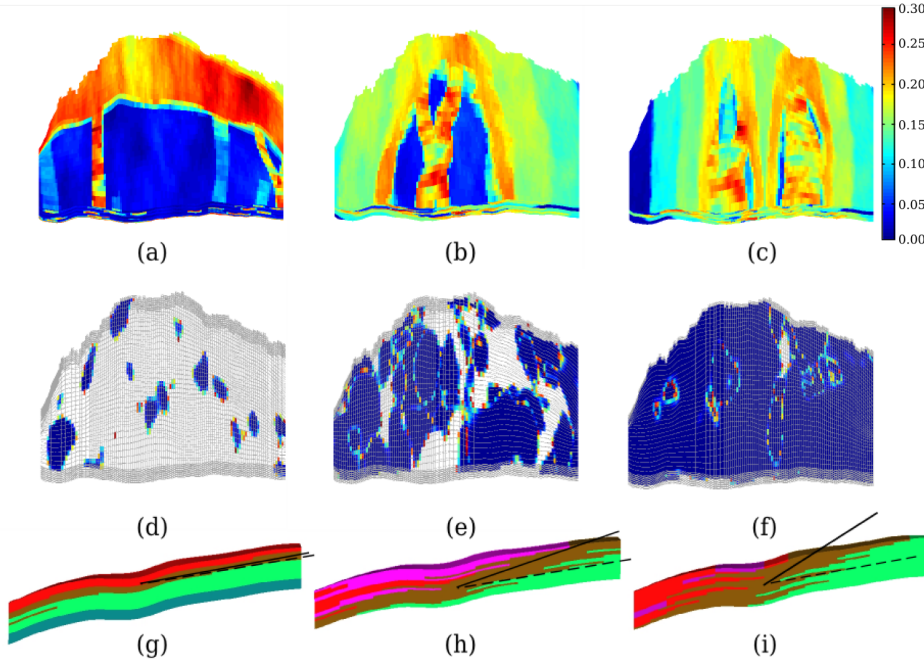


Figure 1: Different geological features considered in this study. Top row shows 'lobosity' in porosity distribution: (a) flat shore-line, (b) one lobe, (c) two lobes. The middle row shows 'barrier' by the distribution of zero transmissibility multipliers: (d) low, (e) medium, (f) high. The lower row shows 'aggradation' in rock-type distribution: (g) low angle of interface between the transitional rock-types leads to parallel layers; this angle is increasing in cases (h) and (i), which correspond to higher levels of aggradation. An up-dip progradation direction is shown in (b), and if the lobe flips over the long axis, we will have down-dip progradation.

the channeling branches, while dense rock with low permeability fills the space between them. Reservoir quality decreases with distance from the shoreface. We expect that the level of lobosity can have a considerable effect on the CO₂ injection and plume size in the aquifer. In this study, models of three levels of lobosity are used: flat shoreline, one lobe and two lobes, see Fig. 1.

Barriers: Periodic floods result in a sheet of sandstone that dips, thins, and fines in a seaward direction. In the lower front, thin sheets of sandstone are interbedded with the mudstones deposited from suspension. These mud-draped surfaces are potential significant barriers to both horizontal and vertical flow. In the SAIGUP domain used here, these barriers were modeled by transmissibility multipliers in three levels of zero value percentage: low (10%), medium (50%), and high (90%). We use the same variations in this study, see Fig. 1.

Aggradation: In shallow-marine systems, two main factors control the shape of the transition zone between the river and the basin: amount of deposition supplied by the river and the accommodation space that the sea provides for these depositional masses. One can imagine a constant situation in which the river is entering the sea and the flow

Meisam Ashraf, Knut-Andreas Lie, Halvor M. Nilsen, Jan M. Nordbotten and Arne Skorstad

slows down until stagnation. The deposition happens in a spectrum from larger grains depositing earlier in the land side to fine deposits in the deep basin. If the river flux or sea level fluctuates, the equilibrium changes into a new bedding shape based on the balance of these factors.

In the SAIGUP study, the progradational cases are considered in which, for example, the river flux increases and shifts the whole depositional system into the sea. The angle at which the transitional deposits are stacked on each-other because of this shifting, is called aggradation angle. Three levels of aggradation are modeled here: low, medium and high (Fig. 1). As we will observe later, aggradation can have a dramatic influence on the injection and migration process.

Progradation: The final factor varied is the progradation or the depositional-dip direction. Two types are considered here: up and down the dominant structural dip. Since the model is tilted a little, this corresponds to the lobe direction from flank to the crest or vice-versa (Fig. 1). This has a potential influence on the CO₂ flow from the injection point up to the crest.

3 Simulation workflow

A fully automated workflow was designed for this study, starting from variational parameters in the SAIGUP models and ending into comprehensive result outputs based on the objective of the work. As a first step, 54 representative cases are studied using a commercial simulator (Eclipse). However, the parallel aim of future work is to develop fast simulation methods that are suitable for performing thousands of runs, using e.g., a vertically-averaged formulation [5].

4 Scenario design

After studying several scenarios for a typical CO₂ injection, we ended up using an injector down in the flank and hydrostatic boundary conditions on the sides, except the faulted side on the crest (Fig. 2). No-flow boundary conditions are imposed on the top and bottom surfaces of the model. The well is completed only in the last three layers.

Simple linear saturation functions with zero capillarity are used. This can be justified because the permeability contrast in channels has the dominating effect on the flow. Also, simple PVT data for a slightly compressible supercritical CO₂ is used. To model the hydrostatic boundaries in Eclipse, high multipliers are used to magnify the pore volume of the outer cells in the model. About 40MM m³ of supercritical CO₂ is injected for thirty years, which amounts to 20% of the models' pore volumes. After the injection period, seventy years of early plume migration is simulated.

5 Results

As our objective function, we seek to maximize the CO₂ storage volume and minimize the risk of leakage. These quantities are measured indirectly by various simulation outputs

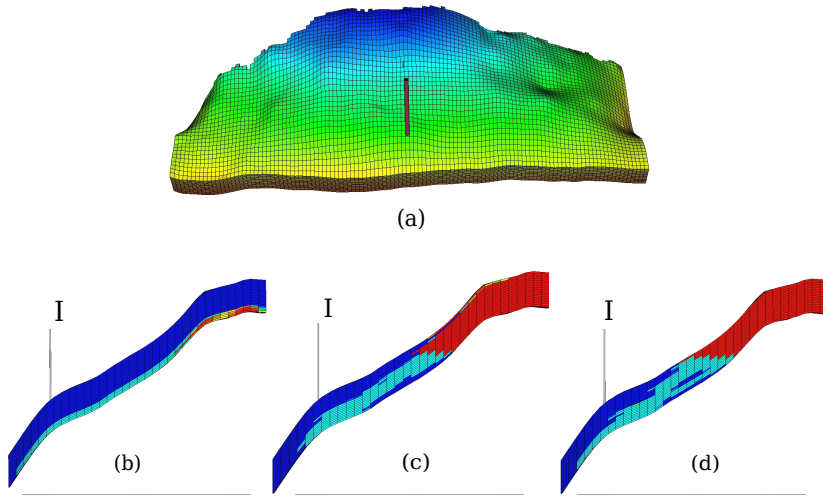


Figure 2: (a) Model geometry and well position. Model dimensions are 3km×9km×80m with 20 layers. The bottom row shows the side view of CO₂ distribution (in red) at the end of simulation in different aggradation cases, from low (b) to high (d). The vertical direction is exaggerated.

that are discussed below.

In all outputs, we recognize the effect of aggradation. Cases with low aggradation have continuous facies layering parallel to the horizontal direction of the grid. Because the three lowest layers, in which the well is completed, are sealing in the cross-layering direction, the flow is forced to stay in the same layers rather than accumulating in the crest (Fig. 2).

Reservoir pressure: The pressure response in general shows a sharp jump at the start of injection and a declining trend during the injection and plume migration. Pressure behavior of different cases at the end of the injection period is shown in Fig. 3. Low aggradation cases show higher pressure.

Boundary fluxes: The flux out of the open boundaries is a measure of the sweep efficiency of the CO₂ plume. As channeling can lead to early CO₂ breakthrough at boundaries, we prefer cases with less fluxes out of the boundaries. The down boundary that is closer to the injector is a potential loss for the injected volume (Fig. 4). Again, the flow is led readily to the boundaries in cases with low aggradations .

Total mobile/residual CO₂: If the CO₂ saturation is below the critical value, it will be immobile in the bulk flow, although not in the molecular sense. Less mobile CO₂ means less risk of leakage and more residual volumes (with saturations less than the critical) resulting from a more efficient volume sweep as preferable (Fig. 4). We use critical saturation of 0.2 for both water and CO₂.

Connected CO₂ volumes: To estimate the risk of leakage from the caprock, we

Meisam Ashraf, Knut-Andreas Lie, Halvor M. Nilsen, Jan M. Nordbotten and Arne Skorstad

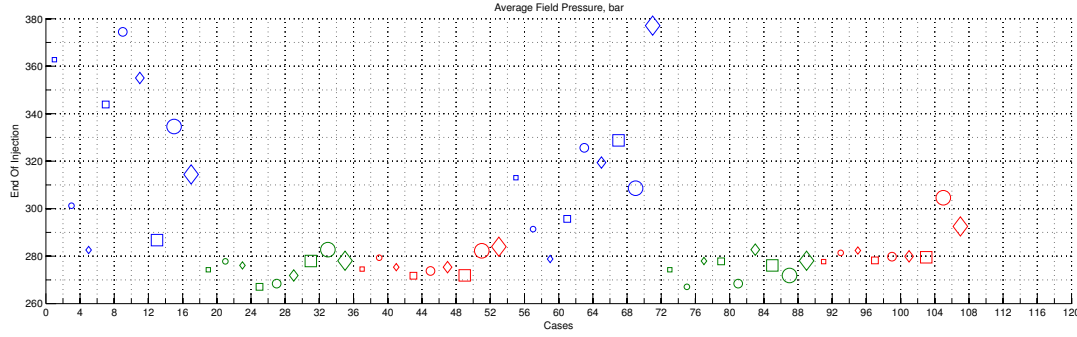


Figure 3: Average reservoir pressure plot for all cases. Colors represent 'aggradation' level: blue for low, green for medium, and red for high levels. Size represents 'barrier': small for low, medium for medium, and large for high level of barrier. Marker shape represents 'lobosity': square for flat shore-line, circle for one lobe, and diamond for two lobes. The first half of the case numbers refer to 'progradation' up-dip towards the crest, and the second half represent 'progradation' down-dip.

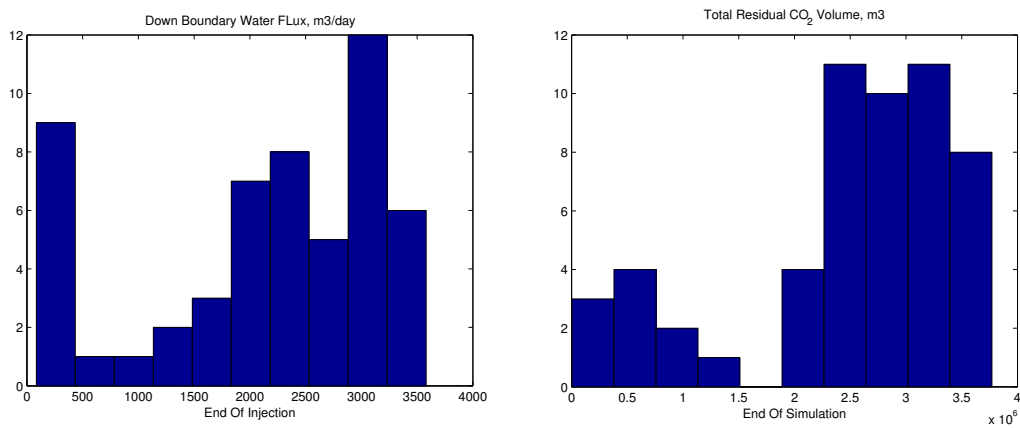


Figure 4: (a) Flux histogram for down boundary: cases with low aggradation show high values. (b) Total residual CO₂ volume; cases with low aggradation show less values in a separate family.

Meisam Ashraf, Knut-Andreas Lie, Halvor M. Nilsen, Jan M. Nordbotten and Arne Skorstad

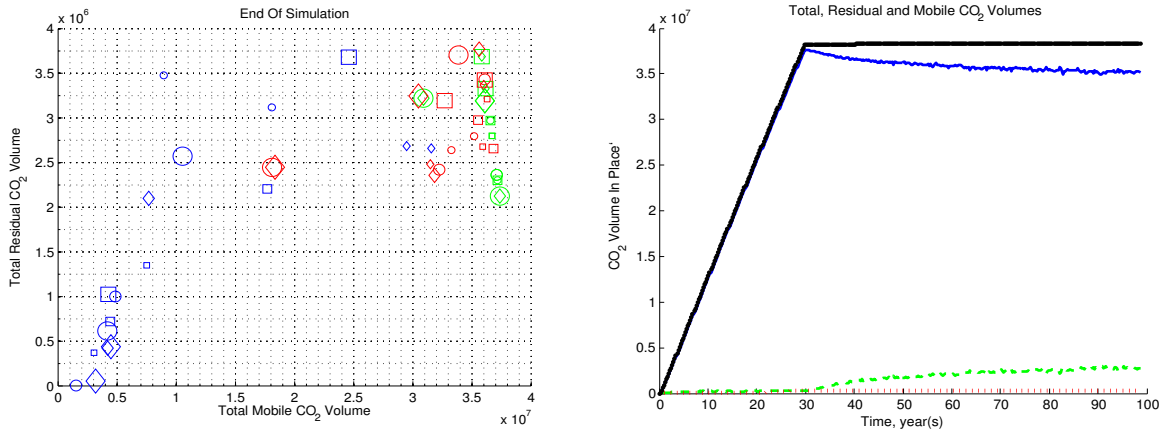


Figure 5: CO₂ volumes. Left: residual versus mobile volume at the end of simulation. Most of the green colored cases follow a linear trend, which is expected because the injected CO₂ must be conserved if no CO₂ leaves the system. For the rest of the cases, some CO₂ goes out of boundaries. Right: Total CO₂ volumes with time plotted for one case. Green curve is the residual volumes, dotted red denotes volumes that have left the domain, solid blue is mobile volumes, and the solid black shows the summation, which is the total volume and stays constant after injection because no more CO₂ is added to the system.

assume that all mobile CO₂ connected to a leakage point will escape out of the reservoir. Hence, it is preferable if the total mobile CO₂ volume is split into smaller plumes rather than forming a big mobile plume. Though the area exposed to potential leakage points will increase by splitting the plume, yet the volume reduction is overtaking the area effect.

On the other hand, the split CO₂ plumes can sweep more cross-areas than a big single plume. The no-flow faulted side can be considered to be connected to an imaginary large volume available for long-term plume migration. Thus, it makes sense to talk about plume sweeping cross area. Larger areas leave more residual CO₂ in the tail of the plume. Hence, we looked at the largest plume size, the number of plumes, and other statistical parameters. The number of plumes at the end of simulation for all cases are given in Fig. 6. Two-lobed cases include more branching channels which result in more plume numbers. Also barrier effect increases the lateral distribution of the plume.

6 Conclusions

Herein, we have reported on a preliminary study of the influence of various geological parameters on the injection and early-stage migration of CO₂ in progradational shallow-marine systems. Large variations in the flow responses show the importance of considering uncertainty in the geological parameters. In particular, our results highlight how variation in aggradation and barriers significantly change the flow direction within the medium. Therefor we believe that effort should be put into detailed geological modeling of potential injection sites. This way, one can better balance the influence of simplifications made in the models of geology and flow physics.

Meisam Ashraf, Knut-Andreas Lie, Halvor M. Nilsen, Jan M. Nordbotten and Arne Skorstad

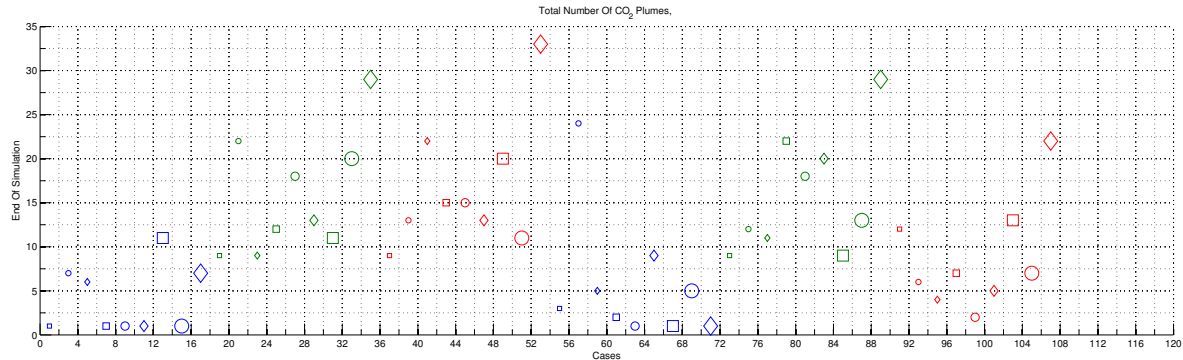


Figure 6: CO₂ plume number at end of simulation, see explanation in Fig. 3.

Finally, we stress that these are very preliminary conclusions drawn from a limited number of simulations performed on a suite of synthetic models that were made to study petroleum production. A more thorough investigation should generate new synthetic geological realizations that are more representative of typical injection sites.

REFERENCES

- [1] J. M. Nordbotten: *Sequestration of Carbon in Saline Aquifers: Mathematical and Numerical Analysis*, Doctor Scientiarum Thesis, Department of Mathematics, University of Bergen,(2004).
- [2] J. A. Howel, A. Skorstad, A. MacDonald, A. Fordham, S. Flint, B. Fjellvoll, and T. Manzocchi: *Sedimentological parameterization of shallow-marine reservoirs*, Petroleum Geoscience, Vol. 14, No. 1, pp. 17-34, (2008).
- [3] T. Manzocchi, J. N. Carter, A. Skorstad, B. Fjellvoll, K. D. Stephen, J. A. Howell, J. D. Matthews, J. J. Walsh, M. Nepveu, C. Bos, J. Cole, P. Egberts, S. Flint, C. Hern, L. Holden, H. Hovland, H. Jackson, O. Kolbjørnsen, A. MacDonald, P. A. R. Nell, K. Onyeagoro, J. Strand, A. R. Syversveen, A. Tchistiakov, C. Yang, G. Yielding, and R. W. Zimmerman: *Sensitivity of the impact of geological uncertainty on production from faulted and unfaulted shallow-marine oil reservoirs: objectives and methods*, Petroleum Geoscience, Vol. 14, No. 1, pp. 3-15, (2008).
- [4] J. D. Matthews, J. N. Carter, K. D. Stephen, R. W. Zimmerman, A. Skorstad, T. Manzocchi, and J. A. Howell: *Assessing the effect of geological uncertainty on recovery estimates in shallow-marine reservoirs: the application of reservoir engineering to the SAIGUP project*, Petroleum Geoscience, Vol. 14, No. 1, pp. 33-44, (2008).
- [5] S. E. Gasda, J. M. Nordbotten, and M. A. Celia: *Vertical equilibrium with sub-scale analytical methods for geological CO₂ sequestration*, Computational Geosciences, Volume 13, Number 4, pp. 469-481, (2009).

Paper II

3.2 Impact of geological heterogeneity on early-stage CO₂ plume migration: sensitivity study

M. Ashraf, K.A. Lie, H.M. Nilsen & A. Skorstad

Proceedings of *ECMOR XII*, Oxford, UK(2010)

**IMPACT OF GEOLOGICAL HETEROGENEITY ON
EARLY-STAGE CO₂ PLUME MIGRATION: SENSITIVITY
STUDY**

M. Ashraf^a, K.A. Lie^a, H.M. Nilsen^a & A. Skorstad^{bc}

^a SINTEF ICT, Department of Applied Mathematics, NO-0314 Oslo, Norway

^b Norwegian Computing Center, NO-0314 Oslo, Norway.

^c Present address Roxar Software Solutions, Lysaker Torg 45, NO-1366 Lysaker, Norway

July 30, 2010

Introduction

Academic studies of CO₂ injection frequently employ simplified or conceptualized reservoir descriptions in which the medium is considered nearly homogeneous. However, geological knowledge and experience from petroleum production show that the petrophysical characteristics of potential CO₂ sequestration sites can be expected to be heterogeneous on the relevant physical scales, regardless of whether the target formation is an abandoned petroleum reservoir or a pristine aquifer. Geological uncertainty introduces tortuous subsurface flow paths, which in turn influence reservoir behaviour during injection. It is paramount that the effect of the geological heterogeneity is quantified by the research community. This will facilitate both improved understanding of subsurface flow at operational CO₂ injection sites, and allow comparison with simulated flow in ideal homogeneous models and upscaled versions of these.

Within oil recovery, the impact of geological uncertainty on production forecast has been thoroughly investigated in the SAIGUP project [3, 4, 5] focusing on shallow-marine reservoirs. To study different factors, synthetic realistic models were made and several thousand cases were run for different production scenarios. The results showed that realistic heterogeneity in the structural and sedimentological description had a strong influence on the production responses.

The main objectives of CO₂ storage studies are to maximize the injection volume/rate and to minimize the risk of leakage [1, 2]. The problem of CO₂ storage differs from oil recovery prediction not only in the objectives of study, but also in the time scales considered for the process (thousands of years compared to tens of years for CO₂ migration). In addition, the characteristic length scale of the flow is much larger. Working with long temporal and spatial scales and huge amounts of uncertainties poses the question of how detailed the geological description should be. The motivation of this work is mainly to address two questions related to CO₂ storage:

- How sensitive is the injection and early-stage migration to uncertainty and variability in the geological description?
- What simplifying assumptions are allowed in averaging the geological attributes over scales?

To this end, we use a subset of the synthetic models from the SAIGUP study to perform a preliminary sensitivity analysis for CO₂ sequestration in aquifers. Heterogeneity classes are defined based on different sequence-stratigraphy parameters and levels of shale barriers. We assume two-phase flow with slight compressibility for supercritical CO₂. The injection scenarios are defined based on the objectives outlined above, and important responses are discussed to evaluate the efficiency and risk of the process.

Geological descriptions

In this work we question the widespread use of simplified geological descriptions that ignore the detailed heterogeneity in modelling. Our hypothesis is that heterogeneity features like channels, barriers, sequence stratigraphy of facies, and fault intensity/geometry all have a particular effect on flow behaviour, both locally and globally, and may significantly alter the injection and migration of CO₂ plumes.

Sound geological classifications and descriptions of key geological features are important to give a realistic description of the sensitivity of CO₂ storage performance. To this end, we have selected four parameter spaces of geological variations from the SAIGUP study [3, 4, 5]. The parameters span realistic intervals for progradational shallow-marine depositional systems with limited tidal influence. In the following, we give a brief description of each.

Lobosity: Lobosity is defined by the plan-view shape of the shore-line. As a varying parameter, lobosity indicates the level at which the shallow-marine system is dominated by each of the main depositional

processes. Two depositional processes are considered in the SAIGUP study: fluvial and wave processes. The higher amount of sediment supply from rivers relative to the available accommodation space in the shallow sea, the more fluvial dominant the process will be. As the river enters the mouth of the sea, it can divide into different lobes and branches. Wave processes from the sea-side smear this effect and flatten the shoreline shape. Less wave effect produces more pronounced lobe shapes around the river mouths. Very high permeability and porosity can be found in the channelling branches, while dense rock with low permeability fills the space between them. Reservoir quality decreases with distance from the shore-face. We expect that the level of lobosity can have a considerable effect on the CO₂ injection and plume size in the aquifer. In this study, models of three levels of lobosity are used: flat shoreline, one lobe and two lobes, see Fig. 1.

Barriers: Periodic floods result in a sheet of sandstone that dips, thins, and fines in a seaward direction. In the lower front, thin sheets of sandstone are interbedded with the mudstones deposited from suspension. These mud-draped surfaces are potential significant barriers to both horizontal and vertical flow. In the SAIGUP domain used here, these barriers were modelled by transmissibility multipliers in three levels of coverage of barrier sheet: low (10%), medium (50%), and high (90%). We use the same variations in this study, see Fig. 1.

Aggradation: In shallow-marine systems, two main factors control the shape of the transition zone between the river and the basin: amount of deposition supplied by the river and the accommodation space that the sea provides for these depositional masses. One can imagine a constant situation in which the river is entering the sea and the flow slows down until stagnation. The deposition happens in a spectrum from larger grains depositing earlier in the land side to fine deposits in the deep basin. If the river flux or sea level fluctuates, the equilibrium changes into a new bedding shape based on the balance of these factors.

In the SAIGUP study those cases are considered in which, for example, the river flux increases and shifts the whole depositional system into the sea. The angle at which the transitional deposits are stacked on each-other because of this shifting, is called aggradation angle. Three levels of aggradation are modelled here: low, medium and high (Fig. 1). As we will observe later, aggradation can have a dramatic influence on the injection and migration process.

Progradation: The next factor varied is the progradation or the depositional-dip direction. Two types are considered here: up and down the dominant structural dip. Since the model is tilted a little, this corresponds to the lobe direction from flank to the crest or vice-versa (Fig. 1). This has a potential influence on the CO₂ flow from the injection point up to the crest.

Fault: There are three variational dimensions considered for faults in the SAIGUP study: fault type, intensity and transmissibility. However we did not include all of these variations in our work and confined this step to two transmissibilities of almost open and closed faults. Fig. 2 shows the effect of fault transmissibility on the flow pattern. Here we took the compartment type of faults of medium intensity ([3, 5]).

Simulation workflow

A fully automated workflow was designed for this study, starting from variational parameters in the SAIGUP models and ending into comprehensive result outputs based on the objective of the work. As a first step, 54 representative cases are studied using a commercial simulator. However, the parallel aim of future work is to develop fast simulation methods that are suitable for performing thousands of runs, using e.g., a vertically-averaged formulation [6].

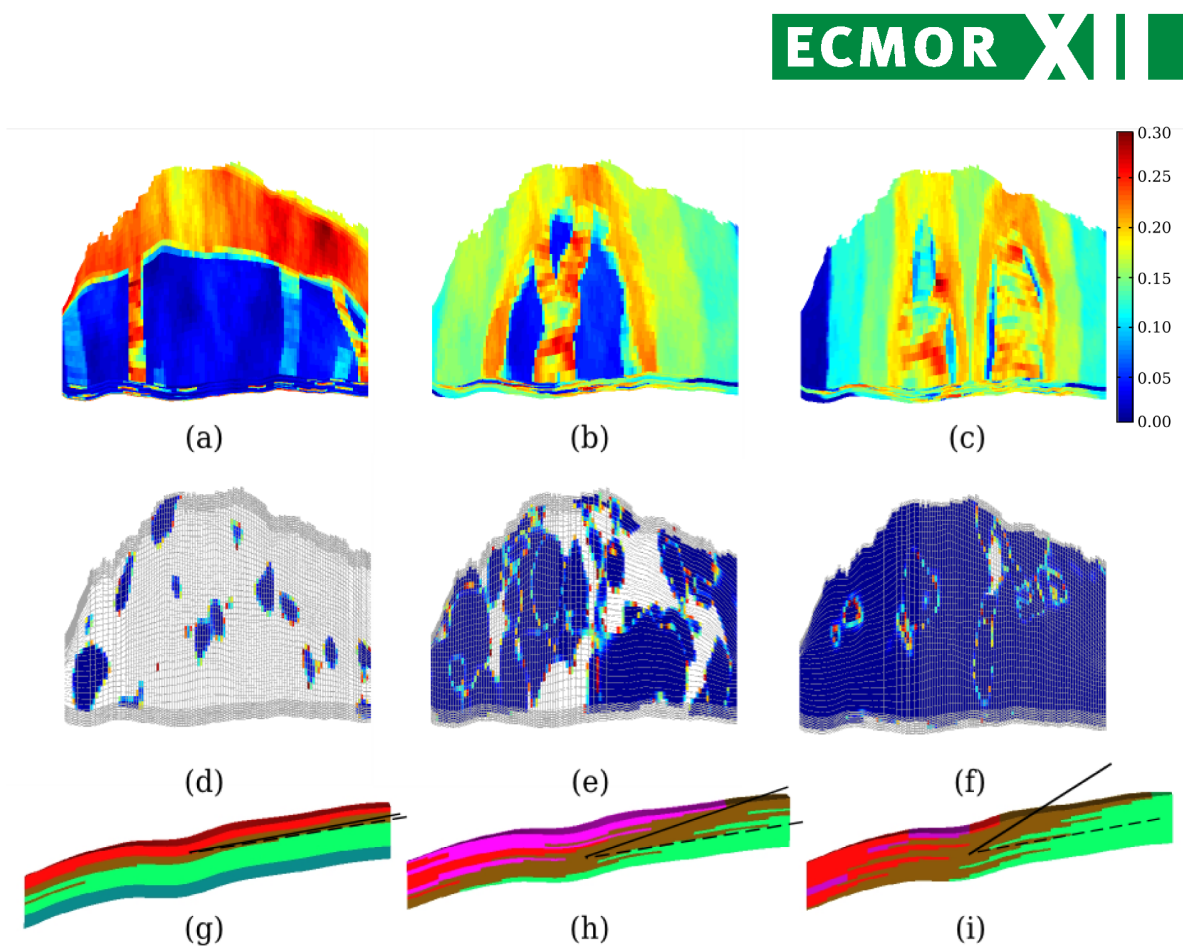


Figure 1 Different geological features considered in this study. Top row shows 'lobosity' in porosity distribution: (a) flat shore-line, (b) one lobe, (c) two lobes. The middle row shows 'barrier' by the distribution of zero transmissibility multipliers: (d) low, (e) medium, (f) high. The lower row shows 'aggradation' in rock-type distribution: (g) low angle of interface between the transitional rock-types leads to parallel layers; this angle is increasing in cases (h) and (i), which correspond to higher levels of aggradation. An up-dip progradation direction is shown in (b), and if the lobe flips over the long axis, we will have down-dip progradation.

Scenario design

We are using an injector down in the flank and hydrostatic boundary conditions on the sides, except the faulted side on the crest (Fig. 3). No-flow boundary conditions are imposed on the top and bottom surfaces of the model. The well is completed only in the last three layers.

Simple linear saturation functions with zero capillarity are used. This can be justified because the permeability contrast in channels has the dominating effect on the flow. Also, simple PVT data for a slightly compressible supercritical CO₂ is used. To model the hydrostatic boundaries in used simulator, high multipliers are used to magnify the pore volume of the outer cells in the model. About 40MM m³ of supercritical CO₂ is injected for thirty years, which amounts to 20% of the models' pore volumes. After the injection period, seventy years of early plume migration is simulated.

Results

As our objective function, we seek to maximize the CO₂ storage volume and minimize the risk of leakage. The results are discussed in three parts: first we look at model responses, then correlation between these responses. Afterwards we consider the sensitivity of each response to the studied geological feature.

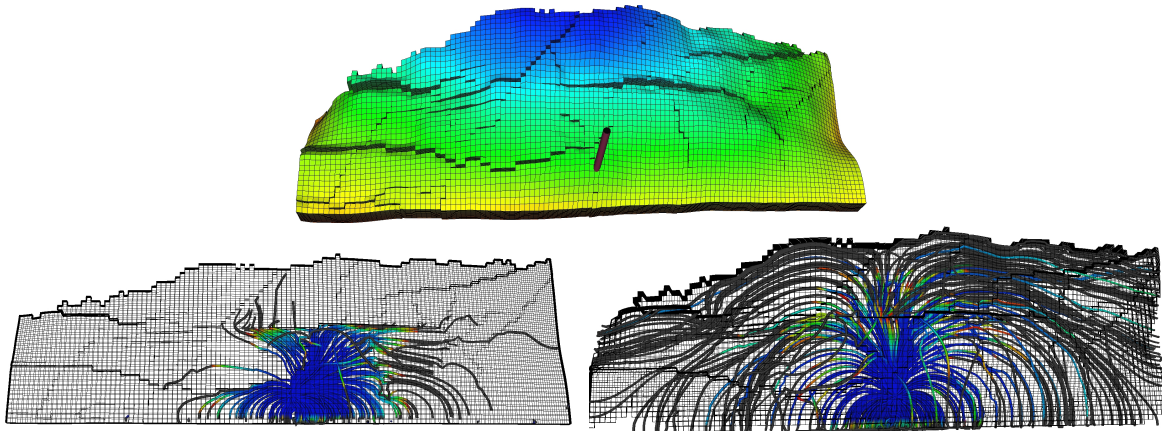


Figure 2 The studied fault features: the picture on the top shows the orientations and intensity of the faults, down left picture shows the flow path in almost closed faults case and the one on the right is showing the flow in the almost open faulted medium. The streamlines are shown for the same time step in both pictures. Notice that the flow is confined in the closed faults model.

In all outputs, we recognize the effect of aggradation. Cases with low aggradation have continuous facies layering parallel to the horizontal direction of the grid. Because the three lowest layers, in which the well is completed, are sealing in the cross-layering direction, the flow is forced to stay in the same layers rather than accumulating in the crest (Fig. 3).

Important responses

Reservoir pressure: The pressure response in general shows a sharp jump at the start of injection and a declining trend during the injection and plume migration. Pressure behaviour of different cases at the end of the injection period is shown in Fig. 4. Low aggradation cases show higher pressure.

Boundary fluxes: The flux out of the open boundaries is a measure of the sweep efficiency of the CO₂ plume. As channelling can lead to early CO₂ breakthrough at boundaries, we prefer cases with less fluxes out of the boundaries. The down boundary that is closer to the injector is a potential loss for the injected volume (Fig. 5(a)). Again, the flow is led to the boundaries in cases with low aggradations.

Total mobile/residual CO₂: If the CO₂ saturation is below the critical value, it will be immobile in the bulk flow, although not in the molecular sense. Less mobile CO₂ means less risk of leakage and more residual volumes (with saturations less than the critical) resulting from a more efficient volume sweep as preferable (Fig. 5(b)). We use critical saturation of 0.2 for both water and CO₂.

Connected CO₂ volumes: To estimate the risk of leakage from the cap-rock, we assume that all mobile CO₂ connected to a leakage point will escape out of the reservoir. Hence, it is preferable if the total mobile CO₂ volume is split into smaller plumes rather than forming a big mobile plume. Though the area exposed to potential leakage points will increase by splitting the plume, yet the volume reduction is overtaking the area effect.

On the other hand, the split CO₂ plumes can sweep more cross-areas than a big single plume. The no-flow faulted side can be considered to be connected to an imaginary large volume available for long-term plume migration. Thus, it makes sense to talk about plume sweeping cross area. Larger areas leave more residual CO₂ in the tail of the plume. Hence, we looked at the largest plume size, the number of plumes, and other statistical parameters. The number of plumes at the end of simulation for all cases are given

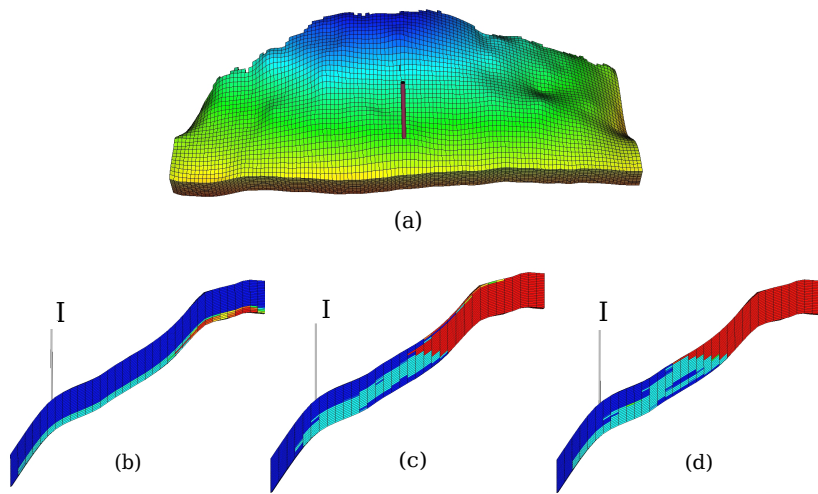


Figure 3 (a) Model geometry and well position. Model dimensions are 3km×9km×80m with 20 layers. The bottom row shows the side view of CO₂ distribution (in red) at the end of simulation in different aggradational cases, from low (b) to high (d). The vertical direction is exaggerated.

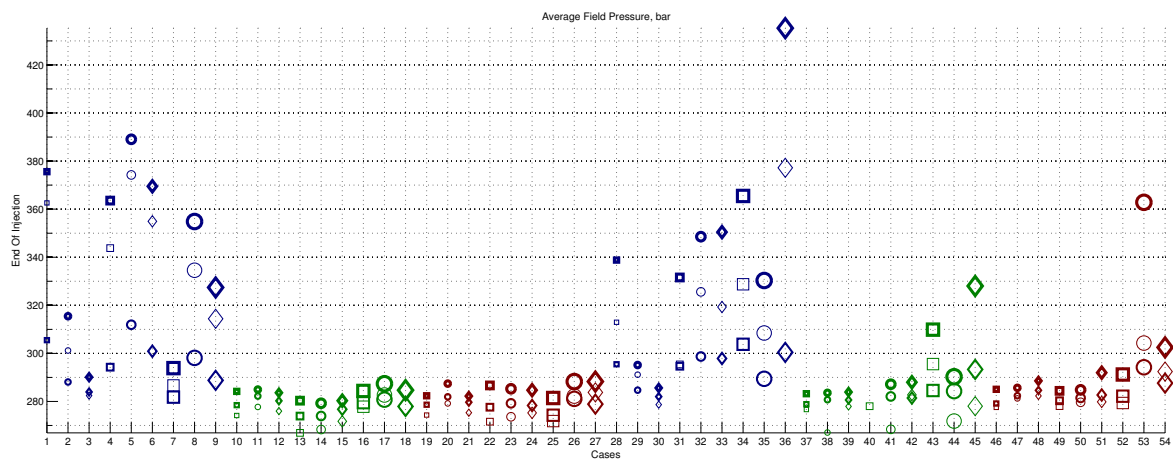


Figure 4 Average reservoir pressure plot for all cases. Colours represent 'aggradational' level: blue for low, green for medium, and red for high levels. Size represents 'barrier': small for low, medium for medium, and large for high level of barrier. Marker shape represents 'lobosity': square for flat shore-line, circle for one lobe, and diamond for two lobes. The first half of the case numbers refer to 'progradation' up-dip towards the crest, and the second half represent 'progradation' down-dip. Thickness shows the fault criteria: thin for unfaulted, medium for open faulted and thick for closed faulted cases.

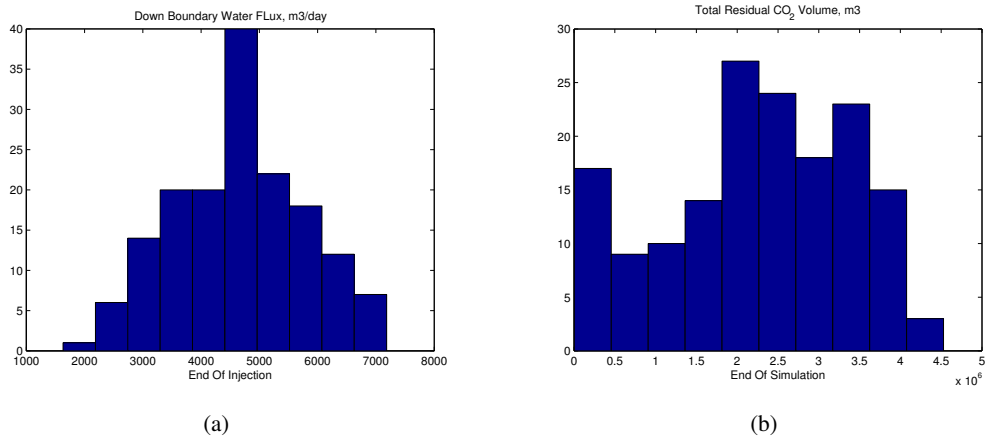


Figure 5 (a) Flux histogram for down boundary (b) Total residual CO₂ volume; cases with low aggradation show less values in a separate family.

in Fig. 7. Two-lobed cases include more branching channels which result in more plume numbers. Also barrier effect increases the lateral distribution of the plume.

Correlation between responses

Here we relate the responses by plotting them against each other. This helps in understanding the degree of correlations between the responses. By looking at these plots we can relate the trends to geological features. This in turn helps in evaluating the effect of uncertainty of each feature on the uncertainty of the simulation outputs.

Fig. 8 shows down boundary CO₂ flux versus average field pressure at the end of injection. Two linear trends can be recognized in the plot: first one starting from 280 bar going until 290 bar in a near vertical slope. The other one starts from 290 bar on the pressure axis and goes about 400 bar in a lower slope. The first trend shows that average pressure is not changing a lot with the increase of CO₂ out-flux. But the second trend shows a dramatic change in pressure corresponding to the change in the down flux rate.

The second trend is made mainly by the cases of blue colour. This is again showing the effect of low aggradation in the flow and pressure behaviour. In low aggradation cases, as the CO₂ flux out of the down boundary increases, the average pressure also increases in the aquifer. Effect of other geological features combined with the low aggradation dictates the amount of CO₂ which goes up to the crest or stays in the bottom-most layers going out from the down boundary. Since the lower layers have poor quality rock, more flow through these layers towards down boundary result in higher pressure in the aquifer.

In Fig. 9, the total number of CO₂ plumes are plotted against total residual CO₂ volumes at end of simulation. The general trend shows positive correlation between these two responses. This is consistent with our discussion in the previous section about the plume size and sweep efficiency. Split plume introduces more residual CO₂. On the other hand, there is a separation in the plotted cases based on the fault criteria. Thin signs are clustered in the lower part of the graph. The medium thickness markers are clustered on the higher part of the graph and the very thick signs are sitting in between. This implies that the unfaulted cases show higher residuals with lower number of plumes, and the open faulted cases introduce more number of plumes. This can be justified by looking at a flow pattern in unfaulted and open faulted case which are shown in Fig. 10. In the open faulted cases, the flow is more laterally distributed. The closed faulted cases restrict the plume migration in the fault compartments and this

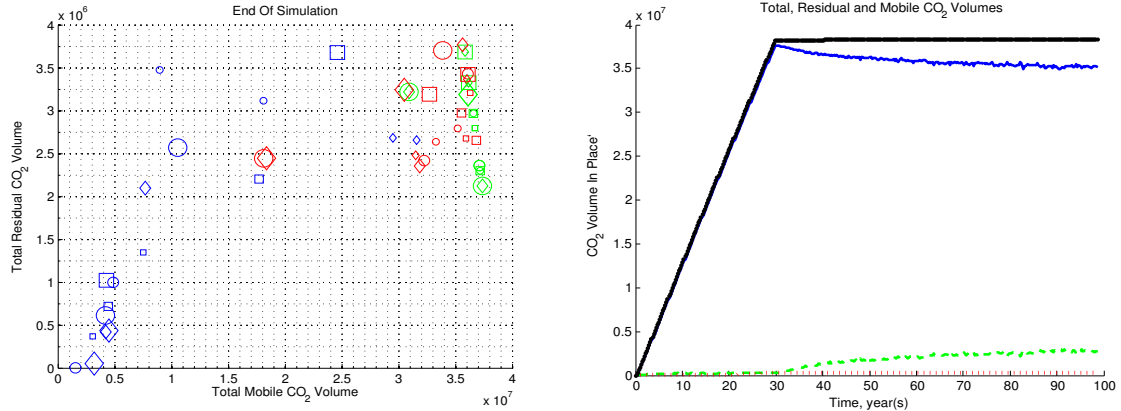


Figure 6 CO₂ volumes. Left: residual versus mobile volume at the end of simulation. Most of the green coloured cases follow a linear trend, which is expected because the injected CO₂ must be conserved if no CO₂ leaves the system. For the rest of the cases, some CO₂ goes out of boundaries. Right: Total CO₂ volumes with time plotted for one case. Green curve is the residual volumes, dotted red denotes volumes that have left the domain, solid blue is mobile volumes, and the solid black shows the summation, which is the total volume and stays constant after injection because no more CO₂ is added to the system. The faulted cases are not included in this figure.

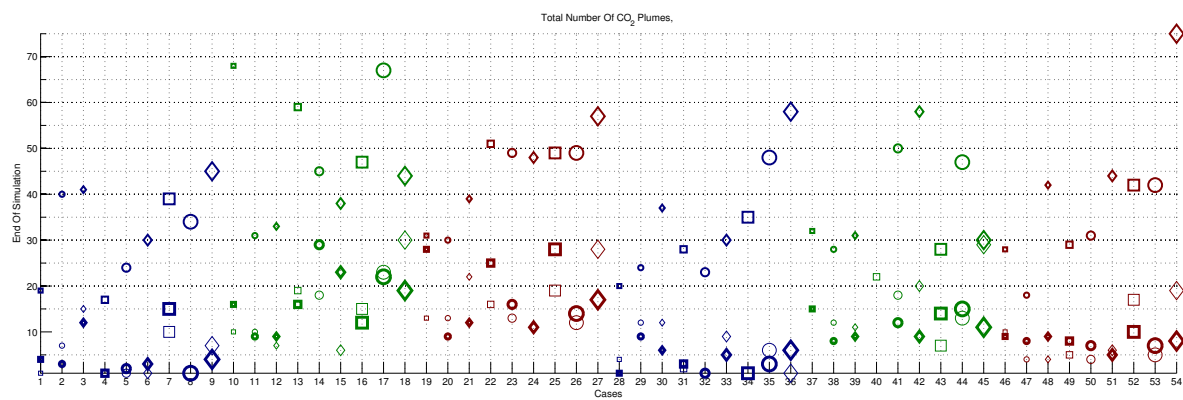


Figure 7 CO₂ plume number at end of simulation, see explanation in Fig. 4.

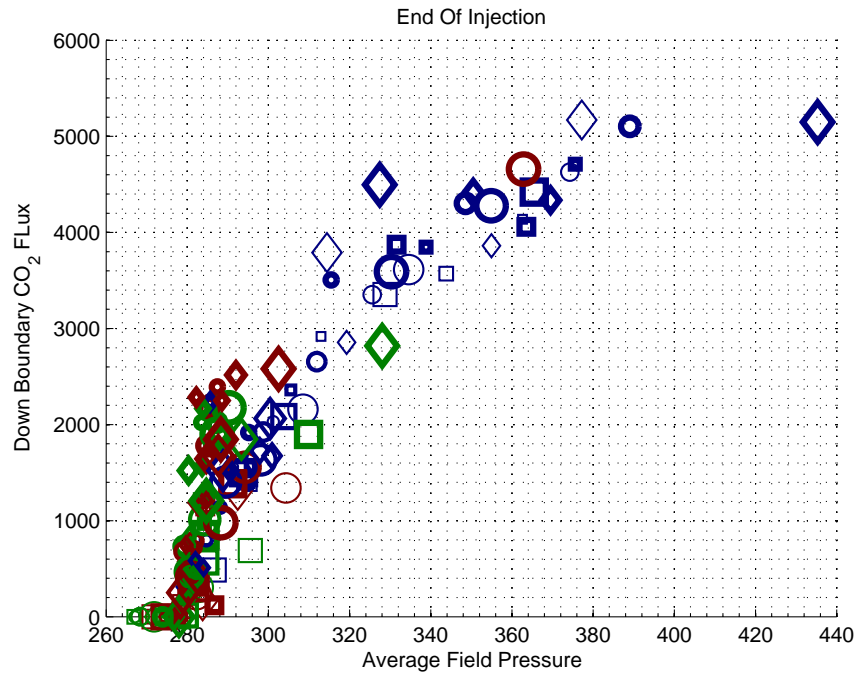


Figure 8 Down boundary CO₂ flux versus average pressure, at end of injection.

introduces lower number of plumes with lower volumes of residuals which make these cases to fall in between (Fig. 2).

Finally we look at total CO₂ residuals versus down boundary CO₂ fluxes at end of injection. We can recognize a negative correlation in an almost linear trend in Fig. 11. Higher out-flux through the down boundary leaves less CO₂ in the domain to migrate and this lowers the residual volumes in the domain.

Sensitivity of responses

In this section, we try to quantify the sensitivity of flow responses to each of the geological features. To achieve this, we define a gradient for each of the features. To make it clear, we use the example of barriers which are easier to explain.

We have three levels of barrier: low, medium and high. Suppose that we are interested in calculating the gradient of average field pressure with respect to barriers. We do this in two steps: first we average the average field pressure for cases of the same level of barriers. This results in three averaged pressure values corresponding to each level of barriers. In the next step, we fit a line through these three points and calculate the tangent of this line. This represents the average pressure increase due to one level increase in barriers.

For other features like fault and lobosity, we follow the same procedure. Though the feature variation is not apparent like barrier, that points to change in the type of the feature. For example, first level of fault criteria relates to unfaulted cases, the second relates to the open faulted and the third one is for the closed faulted cases. Or regarding progradation, we have two levels: up-dip and down-dip direction. The positive and negative gradient is defined based on the way we vary the defined levels.

Fig. 12 shows the average pressure sensitivity to different features at end of injection and end of sim-

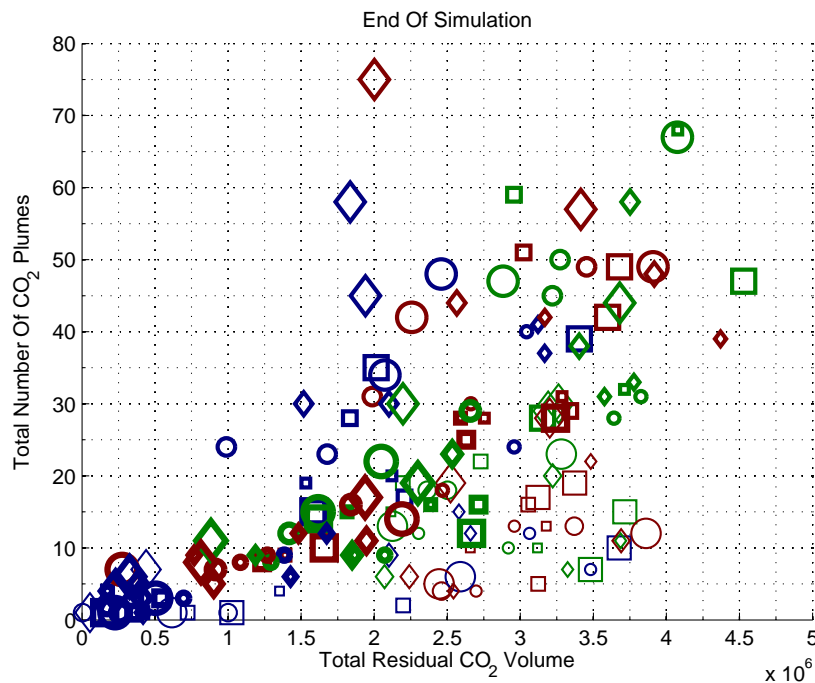


Figure 9 Plume number versus residuals at end of simulation.

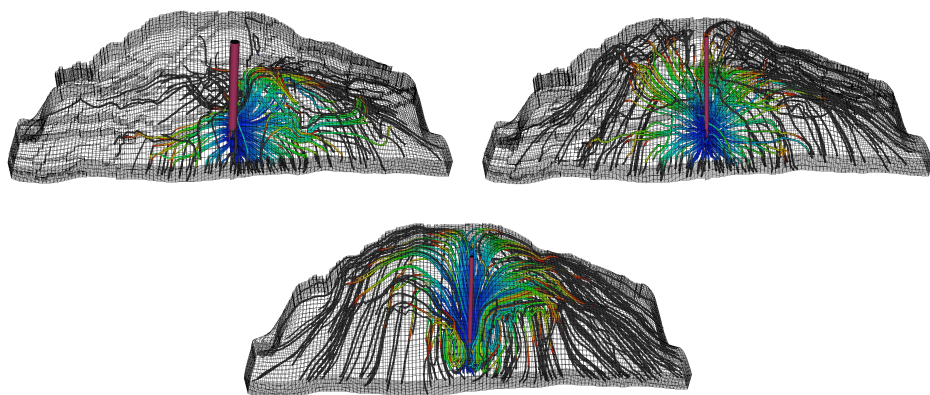


Figure 10 Effect of fault structure on the flow pattern: top left picture shows the closed faulted case, top right picture shows the open faulted case and the bottom picture shows the unfaulted case. Open faults enhance the lateral flow, while the flow in the unfaulted case is mainly upward heading the crest.

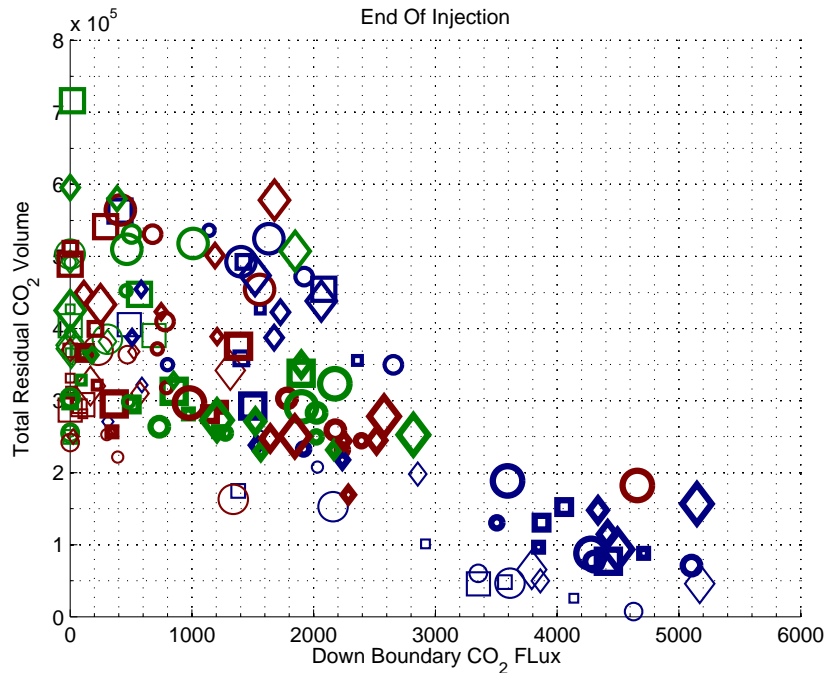


Figure 11 CO₂ residual volume versus down boundary CO₂ flux.

ulation. These results show that in the injection period the dominating effect is related to aggradation, while at end of simulation the most influential feature is the fault criteria. During injection, the flow is dictated by the viscous force imposed by the injector. This force is more sensitive to the feature. In the low aggradation cases, flow is forced to stay in the lower layers with lower permeability values. This increase the pressure in the aquifer. In the higher aggradation level, CO₂ can flow upward through channels with higher permeabilities. This lowers the average pressure in the domain. This is why the gradient is negative for aggradation at end of injection, since lower aggradation level introduces higher pressure.

After stopping the injection, the dominating force is the gravity. The main flow direction is vertical and the pressure is now more sensitive to fault criteria. This is what we see in Fig. 12(b).

The effect of progradation switches from positive to negative after stopping the injection. During injection period, injecting in up-dip direction is easier than injecting in down-dip direction, while for the plume migration after injection the down-dip opens more conductive medium in front of the plumes moving towards the crest.

In Fig. 13 plume number sensitivity is shown. During injection (Fig. 13(a)), barriers are the most influential features. They enhance the lateral flow and the plume splits rather than accumulating in the crest. At end of simulation (Fig. 13(b)), progradation plays an important role relatively. Note that at this time, the open faults are introducing large number of plumes, while the unfaulted and closed faulted cases introduce small number of plumes which in average cancels out to a low gradient.

Finally Fig. 14 shows gradients for total CO₂ residuals. During injection (Fig. 14(a)) aggradation is the most influential feature. Fault criteria is playing the most important role in the plume migration period after injection (Fig. 14(b)).

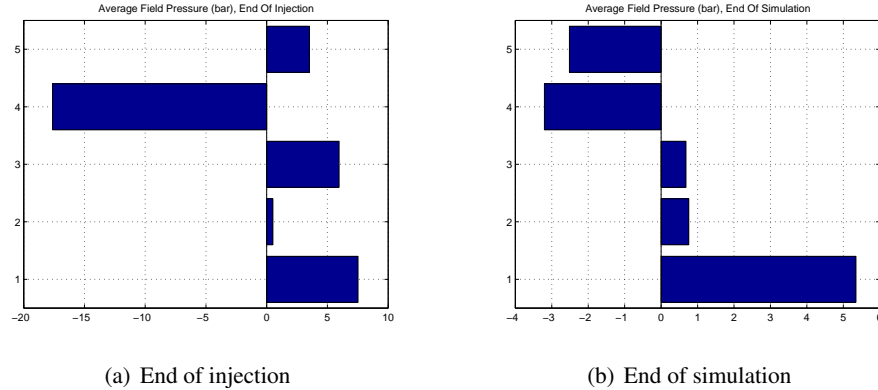


Figure 12 Average pressure sensitivity to different geological features. In these pictures, the vertical axis shows the different geological features from bottom to top: 1-fault, 2-lobosity, 3-barrier, 4-aggradation and 5-progradation. Notice the different range in the horizontal axis at end of injection and end of simulation.

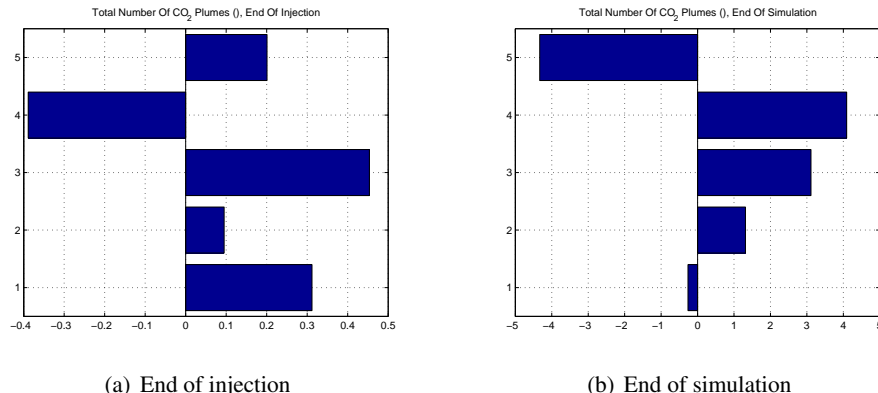


Figure 13 CO₂ plume number sensitivity to different geological features. See Fig. 12 for the vertical axis explanation.

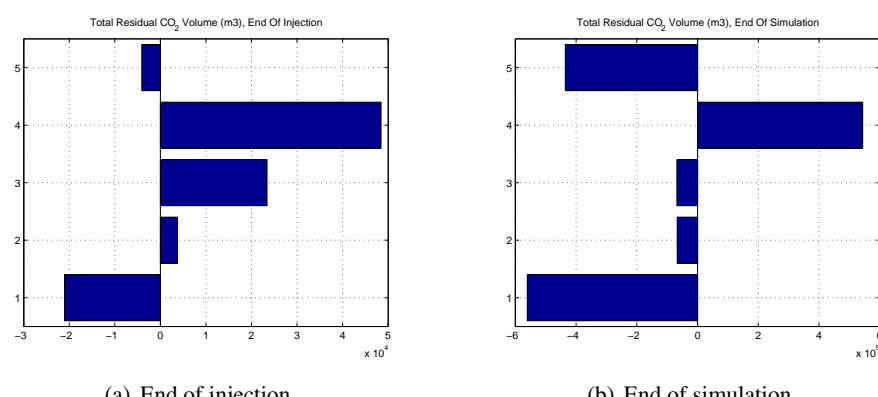


Figure 14 Total residual CO₂ sensitivity to different geological features.

Conclusions

Herein, we have reported on a preliminary study of the influence of various geological parameters on the injection and early-stage migration of CO₂ in progradational shallow-marine systems. The important responses related to storage capacity and risk of leakage are calculated for all the cases and discussed accordingly. The correlations between responses are investigated and a sensitivity measure is introduced and discussed for different responses.

Large variations in the flow responses show the importance of considering uncertainty in the geological parameters. Moreover, we have demonstrated that different geological parameters can have a different impact on the CO₂ migration during injection and during the later migration. In particular, our results highlight how variation in aggradation, fault criteria and barriers significantly change the flow direction within the medium. Therefore we believe that effort should be put into detailed geological modelling of potential injection sites. This way, one can better balance the influence of simplifications made in the models of geology and flow physics.

References

- [1] J. M. Nordbotten: *Sequestration of Carbon in Saline Aquifers: Mathematical and Numerical Analysis*, Doctor Scientiarum Thesis, Department of Mathematics, University of Bergen, (2004).
- [2] S. Bachu: *CO₂ storage in geological media: Role, means, status and barriers to deployment*, Progress in Energy and Combustion Science, ELSEVIER, (2008).
- [3] J. A. Howell, A. Skorstad, A. MacDonald, A. Fordham, S. Flint, B. Fjellvoll, and T. Manzocchi: *Sedimentological parameterization of shallow-marine reservoirs*, Petroleum Geoscience, **14** (1), pp. 17-34, (2008).
- [4] T. Manzocchi, J. N. Carter, A. Skorstad, B. Fjellvoll, K. D. Stephen, J. A. Howell, J. D. Matthews, J. J. Walsh, M. Nepveu, C. Bos, J. Cole, P. Egberts, S. Flint, C. Hern, L. Holden, H. Hovland, H. Jackson, O. Kolbjørnsen, A. MacDonald, P. A. R. Nell, K. Onyeagoro, J. Strand, A. R. Syversveen, A. Tchistiakov, C. Yang, G. Yielding, and R. W. Zimmerman: *Sensitivity of the impact of geological uncertainty on production from faulted and unfaulted shallow-marine oil reservoirs: objectives and methods*, Petroleum Geoscience, **14** (1), pp. 3-15, (2008).
- [5] J. D. Matthews, J. N. Carter, K. D. Stephen, R. W. Zimmerman, A. Skorstad, T. Manzocchi, and J. A. Howell: *Assessing the effect of geological uncertainty on recovery estimates in shallow-marine reservoirs: the application of reservoir engineering to the SAIGUP project*, Petroleum Geoscience, **14** (1), pp. 33-44, (2008).
- [6] S. E. Gasda, J. M. Nordbotten, and M. A. Celia: *Vertical equilibrium with sub-scale analytical methods for geological CO₂ sequestration*, Computational Geosciences, **13** (4), pp. 469-481, (2009).

Paper III

3.3 Impact of geological heterogeneity on early-stage CO₂ plume migration: sensitivity study

M. Ashraf, K.A. Lie, H.M. Nilsen & A. Skorstad

Submitted to *International Journal of Greenhouse Gas Control (IJGGC)*

Impact of Geological Heterogeneity on Early-Stage CO₂-Plume Migration: Sensitivity Study

Meisam Ashraf Knut-Andreas Lie Halvor M. Nilsen Arne Skorstad

November 29, 2011

1 Introduction

Underground sequestration of CO₂ produced from localized sources like power plants and oil and gas recovery sites has been proposed as a possible solution to reduce the rate of anthropogenic CO₂ emission into the atmosphere [5, 2]. Much of the technology required to inject CO₂ into saline aquifers, unminable coal seams, and abandoned reservoirs is already available from the petroleum and mining industry. However, before large-scale storage operations can be initiated, answers to practical questions regarding operational safety and the fate of the injected CO₂ need to be answered. The main concern for policy makers and the general public is the risk of leakage, i.e., how likely it is that the injected CO₂ (or highly saline brine) will migrate into water resources, active petroleum reservoirs, or back to the surface via conductive features like fractures and faults, through ill-plugged wells [10], or through caprocks broken by the high pressure imposed to the system during the injection operation. Likewise, there is a concern about pressure buildup, which may extend much further than the injected CO₂ plume (the effluent of CO₂ into brine). In other words, the operator of a potential injection site needs to maximize storage volumes while minimizing leakage risks and effects on areas surrounding the injection point.

The flow of CO₂ in the subsurface is governed by a very complex interaction between physical forces acting on the reservoir fluids and properties of the reservoir rock itself. To determine the fate of the injected CO₂, it is necessary to develop effective (numerical) models that can be used to accurately describe the pertinent flow dynamics during injection and the subsequent migration period. Moreover, the numerical models must also properly account for geological heterogeneity—i.e., variations in hydraulic conductivity and fluid storage—and how this heterogeneity influences the flow dynamics. Geological heterogeneity is recognized as a major control mechanism within petroleum production [3] and an important constraint on many aspects of quantitative hydrogeology. For this reason, much effort has been devoted to understand and represent geological heterogeneity in flow models, see e.g., [4]. The understanding of the geology of a specific reservoir or aquifer is typically limited and the description of the geological heterogeneity will usually have large uncertainties attached. If flow simulations are to be used to assess risks associated with a storage operation, the numerical flow model must properly account for the impact of uncertainty in the geological description. Yet, academic studies of CO₂ injection commonly employ simplified or conceptualized reservoir descriptions, in which the medium is considered (nearly) homogeneous, and instead focus on developing complex flow models, discretization schemes, and solvers.

Within oil recovery, the impact of geological uncertainty on production forecasts has been thoroughly investigated in the SAIGUP project [8, 6, 9], in which an ensemble of synthetic but realistic models of shallow-marine reservoirs were generated and several thousand cases were run for different production scenarios. The results showed that realistic variations in the structural and sedimentological description has a strong influence on production responses. Simulation of CO₂ storage involves temporal and spatial scales and density ratios that are quite different from those encountered in oil recovery. Potential storage sites may also have geological characteristics that differ from those seen in producible oil reservoirs. For these reasons, one cannot expect that knowledge of how geological heterogeneity impacts flow predictions of oil-water systems can be carried directly over to CO₂-brine systems relevant for CO₂ injection scenarios. Nevertheless, we will herein consider a scenario in which CO₂ is injected into an abandoned shallow-marine reservoir and use geological realizations generated as part of the SAIGUP project to study the impact of geological heterogeneity on the early-stage

migration of the CO₂ plume. How heterogeneity impacts the injection operation will be studied in a separate work, in which we also discuss more realistic pressure constraints on the injection operation.

Our work is a continuation of an early study reported in [1], which focused on a few primary flow responses. Herein, we will also include flow responses that relate more directly to leakage risk. In addition, we evaluate how curvatures in the relative-permeability model influences plume migration; this as a complement to previous studies of endpoint and hysteresis effects, see e.g., [11, 7].

2 Model Setup

In this study, we will consider a storage operation in which supercritical CO₂ is injected into a shallow-marine reservoir underneath a sealing caprock that forms a type of structural trap that is often seen in petroleum reservoirs. To represent the aquifer geology, we use an ensemble of synthetic models developed in the SAIGUP study [8]. In this study, data were collected from many different sources to develop representative, parametrized models that span realistic parameter intervals for progradational shallow-marine depositional systems with limited tidal influence [6]. An ensemble of geostatistical realizations were then made from the parametrized model, each having a heterogeneity and geometrical complexity as seen in real-life models of petroleum reservoirs. In our study, we have selected the following five parameters that altogether give 160 realizations:

Lobosity – is defined by the plan-view shape of the shoreline. As a varying parameter, lobosity indicates the level at which the shallow-marine system is dominated by each of the main depositional processes. Two depositional processes are considered in the SAIGUP study: fluvial and wave processes. The higher the amount of sediment supply provided from rivers is relative to the available accommodation space in the shallow sea, the more fluvial dominant the process will be. As the river enters the mouth of the sea, it can divide into different lobes and branches. Wave processes from the sea-side smear this effect and flatten the shoreline shape. Less wave effect produces more pronounced lobe shapes around the river mouths. Very high permeability and porosity can be found in the channeling branches, while dense rock with low permeability fills the space between them. Reservoir quality decreases with distance from the shore-face. We expect that the level of lobosity can have a considerable effect on the CO₂ injection and plume size in the aquifer. In this study, models of three levels of lobosity are used: flat shoreline, one lobe and two lobes, as illustrated in the upper row of Figure 1.

Barriers – Periodic floods result in a sheet of sandstone that dips, thins, and fines in a seaward direction. In the lower front, thin sheets of sandstone are interbedded with mud-stones deposited from suspension. These mud-draped surfaces will potentially act as significant barriers to both horizontal and vertical flow, and are modeled by transmissibility multipliers corresponding to three levels of coverage for the barrier sheet: low (10%), medium (50%), and high (90%), as illustrated in the middle row of Figure 1.

Aggradation – In shallow-marine systems, two main factors control the shape of the transition zone between river and basin: amount of deposition supplied by the river and the accommodation space that the sea provides for these depositional masses. One can imagine a constant situation in which the river is entering the sea and the flow slows down until stagnation. The deposition happens in a spectrum from larger grains depositing at the river mouth to fine deposits in the deep basin. If the river flux or sea level fluctuates, the equilibrium changes into a new bedding shape based on the balance of these factors. The SAIGUP data models cases in which, for instance, the river flux increases and shifts the whole depositional system into the sea. The angle at which the transitional deposits are stacked on each-other because of this shifting, is called aggradation angle. Three levels of aggradation are modeled here: low, medium, and high angles. The three parameter choices are illustrated in the bottom row of Figure 1, where we in particular notice how a low aggradation angle gives continuous facies layering parallel to the dip direction of the model.

Progradation – denotes the direction of the depositional dip. Two types are considered here: up and down the dominant structural dip. Because the model is tilted a little, this corresponds to the lobe direction from flank to crest or vice versa.

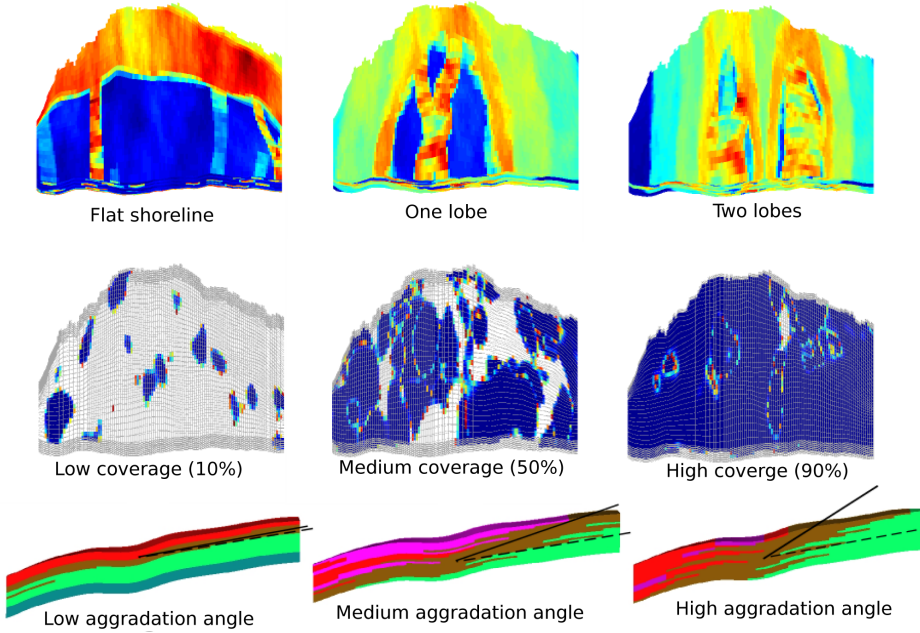


Figure 1: Illustration of geological parameters from the SAIGUP study: the top row shows three different lobosities for up-dip progradation (if the lobes flip over the long axis, we will have down-dip progradation); the middle row shows barriers representing different degrees of mud-draped coverage; and the bottom row shows aggradational angle.

Table 1: Geological features from the SAIGUP project included in this study. The last column reports markers used to distinguish different features in the plots.

Feature	Levels	Marker
Lobosity	flat, one-lobe, two-lobe	square, circle, diamond
Barrier	low(10%), medium(50%), high(90%)	small, medium, large
Aggradational angle	low(parallel layering), medium, high	blue, green, red
Progradation	up-dip, down-dip	first half, second half
Fault	unfaulted, open faults, closed faults	thin, medium, thick

Fault – are represented by three different parameters in the SAIGUP study: fault type, intensity, and transmissibility. Herein, we limit our study to compartment faults of medium intensity and consider three parameter choices: no faults, open faults, and closed faults.

Table 1 lists the markers (shape, size, color, thickness) that will be used to signify different parameters values in plots of simulation results later in the paper.

We will consider storage of forty million cubic meters of supercritical CO₂, which amounts to approximately 20% of the total pore volume in the aquifer and will be injected from a single well over a period of thirty years. After the injection period, seventy years of plume migration is simulated for all cases. If the medium was homogeneous, we would expect that the injection will create one big plume that moves upward because of the gravity force until it accumulates under the structural trap of the caprock, i.e., migrating from the injection point and upward to the crest of the aquifer. The idea is therefore to inject as deep as possible to increase the travel path and the volume swept by the plume before it reaches the crest. To this end, the injector is placed down in the flank and only completed in the three lowest layers of the aquifer. Hydrostatic boundary conditions are imposed on the sides, except at the faulted side on the crest, and no-flow boundary conditions are imposed on the top and bottom surfaces.

The injected CO₂ is assumed to be a supercritical fluid with density 700 kg/m³ and viscosity 0.04 cP. The supercritical fluid is modeled as a dead oil with a formation factor of 1.1 at 0 bar and 0.95 at 400 bar. Brine is assumed to be slightly compressible ($3.03 \cdot 10^{-6}$ psi⁻¹) with density 1033 kg/m³ and

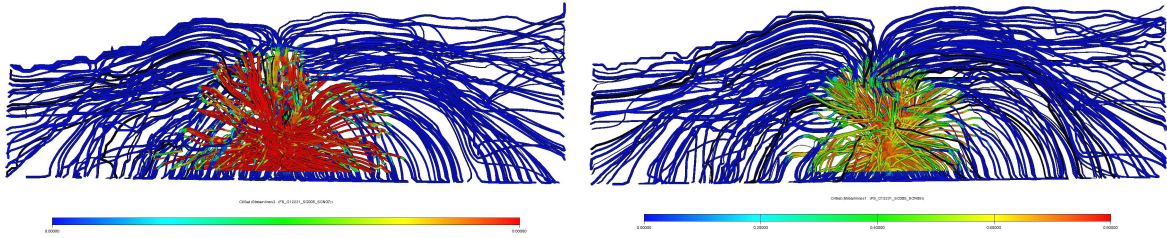


Figure 2: CO₂ saturation plotted on streamlines for linear relative permeabilities (left) and quadratic permeabilities (right).

viscosity 0.4 cP. The rock compressibility is set to $3 \cdot 10^{-7}$. For both fluids, we will use Corey-type relative permeability functions

$$k_{rCO_2} = (1 - S)^\alpha, \quad k_{rw} = S^\alpha, \quad \alpha = 1, 2$$

where S denotes the saturation of brine normalized for end points 0.2 and 0.8.

3 Basic Flow Responses

In this section we will give a qualitative discussion of how some basic flow responses like the wave speeds of the plume migration, average aquifer pressure, mobile and residually trapped volumes, and plume sizes are affected by variations in the geological parameters.

3.1 Effect of relative permeability curvature

How the geological heterogeneity impacts the plume migration will depend upon the fluid model. We therefore start by discussing the choice of relative permeability functions. Previous studies have mainly looked at hysteresis and effects from saturation endpoints, see e.g., [7]. However, the curvature of relative permeability function will also play a significant role and in the following we will therefore consider both linear and quadratic relative permeability curves. In oil recovery processes, the efficiency of flooding increases by the higher viscosity of displacing fluid. For example in water-flooding, increasing the water viscosity using additives is a way to increase the process efficiency. For CO₂ storage, on the other hand, we are interested in mixing brine and CO₂ to increase the rate of dissolution; a lower viscosity of CO₂ compared to brine helps this aim.

With linear relative permeability and a CO₂ viscosity of tenth of the brine viscosity, there will be no sharp displacement front in the system and CO₂ invades the brine zone in a spectrum of rarefaction waves from zero to the maximum possible saturation (0.8 in our case). On the other hand, with quadratic relative permeability functions, there will be a sharp displacement front with a saturation around 0.4 followed by rarefactions.

To illustrate the different behavior of linear and quadratic relative permeabilities, we have picked one of the SAIGUP models which includes one shoreline lobe, medium level of barriers, high aggradation angle, up-dip progradation, and open faults. Figure 2 shows the CO₂ distribution resulting from the two different relative permeability functions. Although the streamline paths appear to be almost identical, there are significant differences in the extent of the plume and the saturation profile inside. With linear relative permeability and a CO₂ viscosity of tenth of the brine viscosity, there will be no sharp displacement front in the system and CO₂ invades the brine zone as a rarefaction fan from zero to the maximum possible saturation. In the left plot of Figure 2, this is observed as a spectrum of saturations ranging from zero to 0.8 and then a bank of constant saturation down to the injector (the red color region around the well). With quadratic relative permeabilities, on the other hand, there will be a sharp displacement front followed by a rarefaction fan. The front (with a saturation around 0.4) is recognizable followed by rarefactions down to the injector in the right plot of Figure 2.

In the simulation we observe that a significantly larger volume of injected CO₂ escapes through the down boundary in the quadratic case. The reason is that the mobility will be higher in the linear case and the wave speed at the tip of the rarefaction fan is significantly faster than the wave speed of the

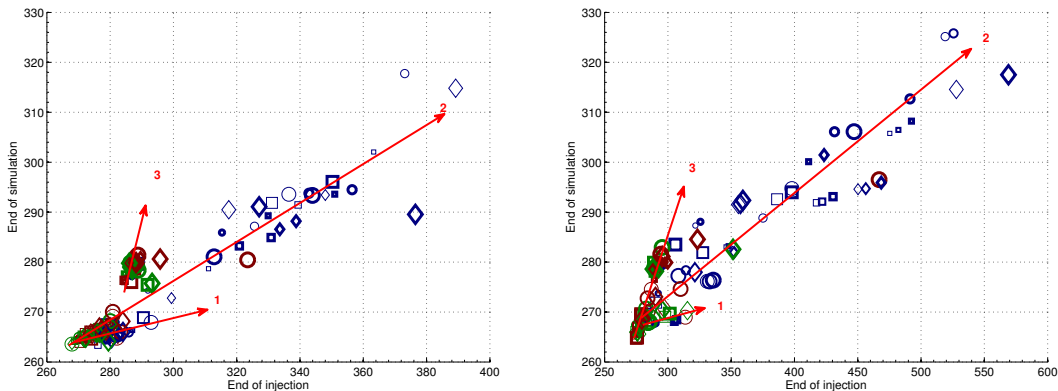


Figure 3: Cross-plot of average aquifer pressure at the end of simulation versus at the end of injection for linear (left) and quadratic (right) relative permeabilities.

displacement front for the quadratic case; compare the size of the two plumes in Figure 2. This means that the CO₂ plume will spread easier in the medium resulting in less flow through the boundary closest to the injector. Because of the lower mobility values in the quadratic case, more mass of CO₂ will be almost immobilized in the medium and the CO₂ plume will migrate very slowly compared with the linear case. Secondly, we observe higher pressures in the system during injection for quadratic permeabilities. The curvature of the quadratic curve gives lower mobility of CO₂ for small saturation values, and thence higher injection pressure is required to move the flow in the medium.

3.2 Pressure responses

The average aquifer pressure in general shows a sharp jump at the start of injection and a declining trend during injection and plume migration caused by pressure release through the open boundaries. (Specifying different boundary conditions would have resulted in different pressure trends). Figure 3 shows cross-plots of the average aquifer pressure at the end of injection and end of simulation for our two different choices of relative permeability functions. In both plots, one can recognize three different trends which have been indicated by three straight lines. The first trend, which has the lowest slope, represents cases with large pressure variation during injection and small range of pressure variation during the migration phase that follows after the end of injection. In these cases, the heterogeneity of the medium forms channels towards the open boundaries through which the injection pressure is released, resulting in low aquifer pressure at the end of simulation. The second trend, represents cases in which the heterogeneity affects injection, gravity segregation, and flow through open boundaries. In particular, we observe that most cases that have high injection pressure correspond to a low aggradation angle, for which low vertical permeability forces the injected CO₂ plume to move relatively slow in the lowest, poor-quality layers before migrating up towards the caprock. This increases the pressure in the domain during injection and keeps a higher pressure gradient to the open boundaries. In the third trend, the heterogeneity makes chambers and compartments in which the pressure increases during injection and then remains high. Cases with closed faults are of this class. The heterogeneity in these cases affects the gravity segregation process more than in the two other trends because of faults and a high level of barriers.

We also see the effect of curvature in the relative permeabilities by comparing the two plots. Higher range of pressure variations is observed during injection for the nonlinear relative permeability runs. Moreover, nonlinear relative permeability gives lower mobility which leads to higher pressure build-up during injection. This means that longer time is required for the pressure to be released through the open boundaries after injection and more cases therefore follow the second and third trend.

More details about the bottom-hole pressure will be given in a forthcoming paper, in which we also will discuss more realistic constraints on the injection operation.

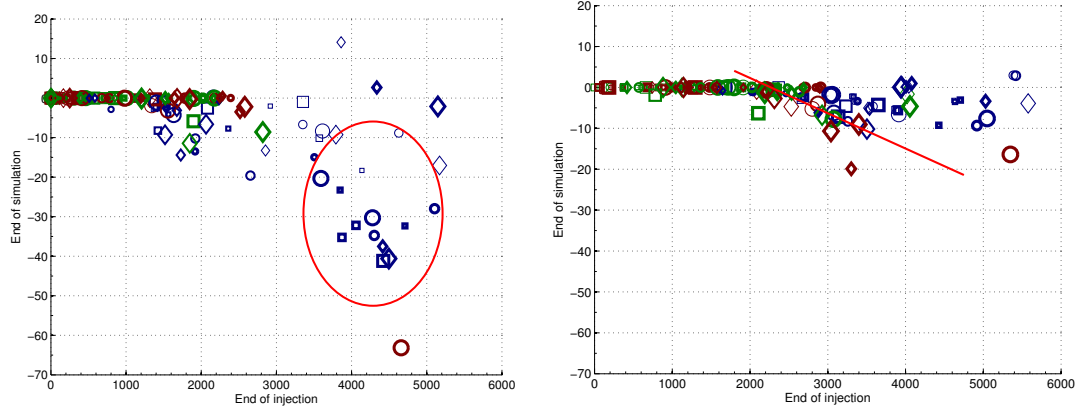


Figure 4: Cross-plot of CO₂ flux out over the down-dip boundary for linear (left) and quadratic (right) relative permeabilities. Positive values represent outward fluxes and negative values represent inward fluxes.

3.3 Plume migration

The direction in which the CO₂ plume moves in the medium will primarily impact the amount of residual (and structural) trapping, but as we will see later, also significantly change the risk for leakage through breaches and holes in the caprock. When evaluating the safety of a long-term storage operation, there are several potentially conflicting aspects that need to be considered with regard to plume migration. On one hand, we prefer the plume to spread out laterally to enhance residual trapping and mixing of CO₂ and brine, while on the other hand we want to confine the plume to the smallest volume possible to minimize the the risk of leakage and contamination into other aquifers, minimize the contact with potential leakage points and simplify monitoring operations. To investigate this aspect, we will study the sweep efficiency in local regions. On the other hand, if a big movable plume connects with a leakage pathway through the caprock, large volumes of CO₂ may escape, and for this reason, it may be better if the injected CO₂ splits into many small plumes. In our analysis, we will therefore also consider the number of plumes and their volumes.

3.3.1 Boundary fluxes

The sweep efficiency of the CO₂ plume, i.e., the percentage of the aquifer volume that has been in contact with CO₂, is positively correlated with the amount of residual trapping (and mixing of CO₂ and brine). Herein, we will consider the flux out of the open boundaries as an indirect measure of volumetric sweep efficiency. The model has open boundaries on three sides, which are modeled by imposing huge pore-volumes multipliers in the outer cells, while no-flow boundary conditions are imposed along the top faulted side. Using large pore-volume multipliers to represent an open boundary enables us to model flow both in and out of the domain, and this way, we can represent volumes of CO₂ leaving and later re-entering the aquifer. (In addition, this method will contribute to eliminate effects from Dirichlet type boundary conditions).

The lower boundary is closest to the injection point and hence the most likely place that injected CO₂ volumes will be lost. Figure 4 shows two cross-plots of the CO₂ across this boundary at the end of injection and the end of simulation. Towards the end of injection, most cases have positive flux values, which means that parts of the main plume connected to the injection point has been forced to leave the domain in the down-dip direction by the increased injection pressure. However, after injection stops, many cases have small negative fluxes, which means that a small volume of CO₂ reenters the domain. Once again, we observe that cases with low aggradation angle stand out from the rest. In these cases, the injected plume is almost entirely confined to the bottom of the model because of poor vertical communication. Hence, a large portion of the injected volume will be forced out of the domain in the down-dip direction. After the end of injection, gravity forces will gradually cause some of these lost volumes to move up-dip again and reenter the domain. We notice that cases with closed faults (shown in the red circle in the left plot of Figure 4) show a relatively higher return

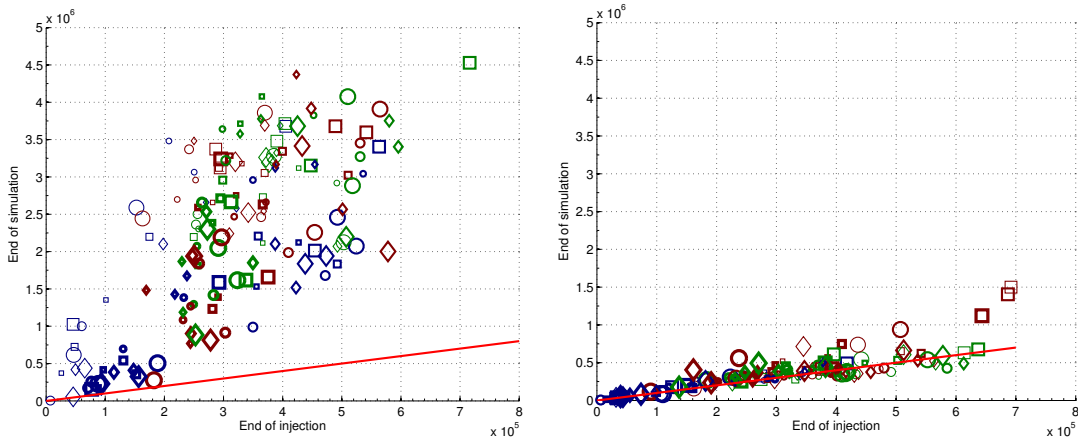


Figure 5: Residually trapped volumes for linear (left) and quadratic (right) relative permeabilities. Cases on the red lines have the same values at the end of injection and end of simulation.

flux for the linear relative permeability function. With nonlinear relative permeability function, some of the cases follow a linear trend (shown by the red line in the right-hand plot), in which the return flux is proportional to the outward flux.

3.3.2 Total mobile/residual CO₂

Residual trapping occurs when the CO₂ saturation is below the residual saturation value of 0.2. Although the residually trapped CO₂ is free to move in a molecular sense on the microscale, the corresponding bulk volume is considered immobile on the macro scale. To reduce the risk of leakage, it is therefore important to obtain an efficient volumetric sweep that will maximize the residual volumes and minimize the mobile volumes. Herein, we will define residually trapped volumes as volumes in which the CO₂ saturation is below the residual value of 0.2. Notice that with this definition, all mobile volumes (in which the saturation exceeds 0.2) will contain a residual portion of CO₂ that is not free to escape. This portion will eventually become residually trapped if the saturation of the mobile CO₂ decreases to the residual value.

Figure 5 shows cross-plots of the total residual volume at the end of injection and end of simulation. Drainage is the dominant flow process during injection. When injection ceases, the plume migration turns into a imbibition-dominated process which increases the residual trapping of CO₂. With linear relative permeability, the imbibition process takes place relatively fast, and the residual volume increases significantly from end of injection to end of simulation. Once again, low-aggradation cases form notable exception having small amounts of residual trapping. The reason is primarily that significant volumes have been lost over the down-dip boundary, and secondarily that the (vertical) sweep is limited because the CO₂ plume is confined to the lower layers of the reservoir during most of the simulation time.

With quadratic relative permeabilities, the migration process is significantly slower and many cases have almost the same residual volume at the end of injection and end of simulation. As already discussed, the curvature of the relative permeability function does not have a considerable influence on the flow paths (compare the streamline paths in Figure 2). Compared with the results in the left plot of Figure 5, we therefore ultimately expect a significant increase in residual trapping before the plume settles; this prognostication has been confirmed for a few (arbitrary selected) cases by computing the plume migration for more than ten thousand years. We also observe that in some cases the residual volumes *decrease* after injection ceases. This is caused by mobile CO₂ invading zones of residual CO₂, thereby turning residual volumes into mobile volumes according to the definition of residual trapping used herein. These cases are therefore likely to be influenced by hysteresis effects, which for simplicity have been disregarded in this study.

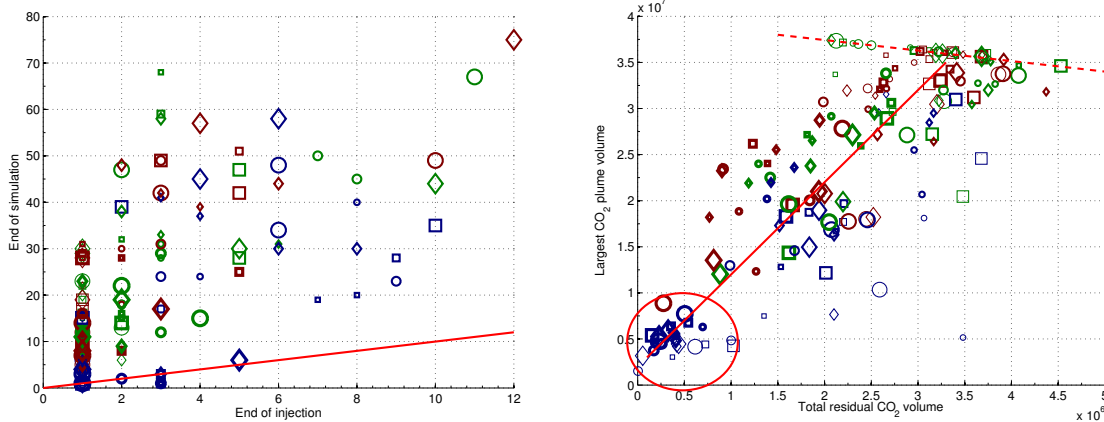


Figure 6: The cross-plot to the left shows the number of CO₂ plumes at the end of simulation versus the number of plumes at the end of injection for linear relative permeability function. The right plot shows the volume of the largest CO₂ plume versus the volume of residual CO₂ at the end of simulation.

3.3.3 Connected CO₂ volumes

In the next section, we will study the risk of leakage through the caprock. To this end, we will assume that all mobile CO₂ connected to a leakage point will escape through that point. Hence, it is preferable if the total mobile CO₂ volume is split into smaller plumes rather than forming a big mobile plume. Moreover, the surface area per volume increases by splitting the plume (assuming constant plume shape) and this helps residual trapping (and mixing of brine and CO₂).

During injection, the flow support from the well builds a connected mass of CO₂ shaping one or a few big plumes. When the injection ceases, the CO₂ starts distributing in the medium and plumes may split because of branches in the flow paths created by heterogeneity. The plot to the left in Figure 6 shows how the number of plumes increases significantly in most cases during the migration phase, except for a few low-aggradation cases for which the injected plumes stay intact or reform into a single plume.

The right plot in Figure 6 shows the volume of the largest CO₂ plume versus the residual trapping. Here, we see two major trends indicated by a solid and a dashed line. The solid line, having a positive slope, represents cases that lose CO₂ through the open boundaries, mainly through the one closest to the injection point. As a consequence, less CO₂ volume exists in the system and the size of the largest plume will be smaller. Hence, less volume will be swept while the plume migrates upward (if it does), which again means that less CO₂ is residually trapped. In particular, we notice the cases inside the ellipse which are the same cases that had large CO₂ volumes escaping through the down-dip boundary as shown in Figure 4. The dashed line with negative slope corresponds to cases for which almost all of the injected CO₂ stays inside the domain. These cases show a small range of variation for the largest plume size and are reflecting the effect of different heterogeneity features on the residual trapping process. Because equal volumes of CO₂ are injected in all cases, we notice that the bigger the largest plume is, the smaller the residual volume will be.

4 Analysis of Parameter Impact

The main purpose of the current study is to investigate how geological heterogeneity impacts the formation of a CO₂ plume during injection and during the early-stage migration after injection ceases. In this section, we will therefore perform a simple 'sensitivity analysis' that will tell us something of how the different geological parameters impact the flow responses discussed in the previous section. The five geological parameters impact the flow responses to different degrees; some parameters are more influential during injection, others take effect when the migration starts after injection has ceased, and some are influential both during injection and migration. Comparing the relative impact of the different parameters will indicate which of the parameters are most important to represent accurately when modeling a specific aquifer of the type considered herein.

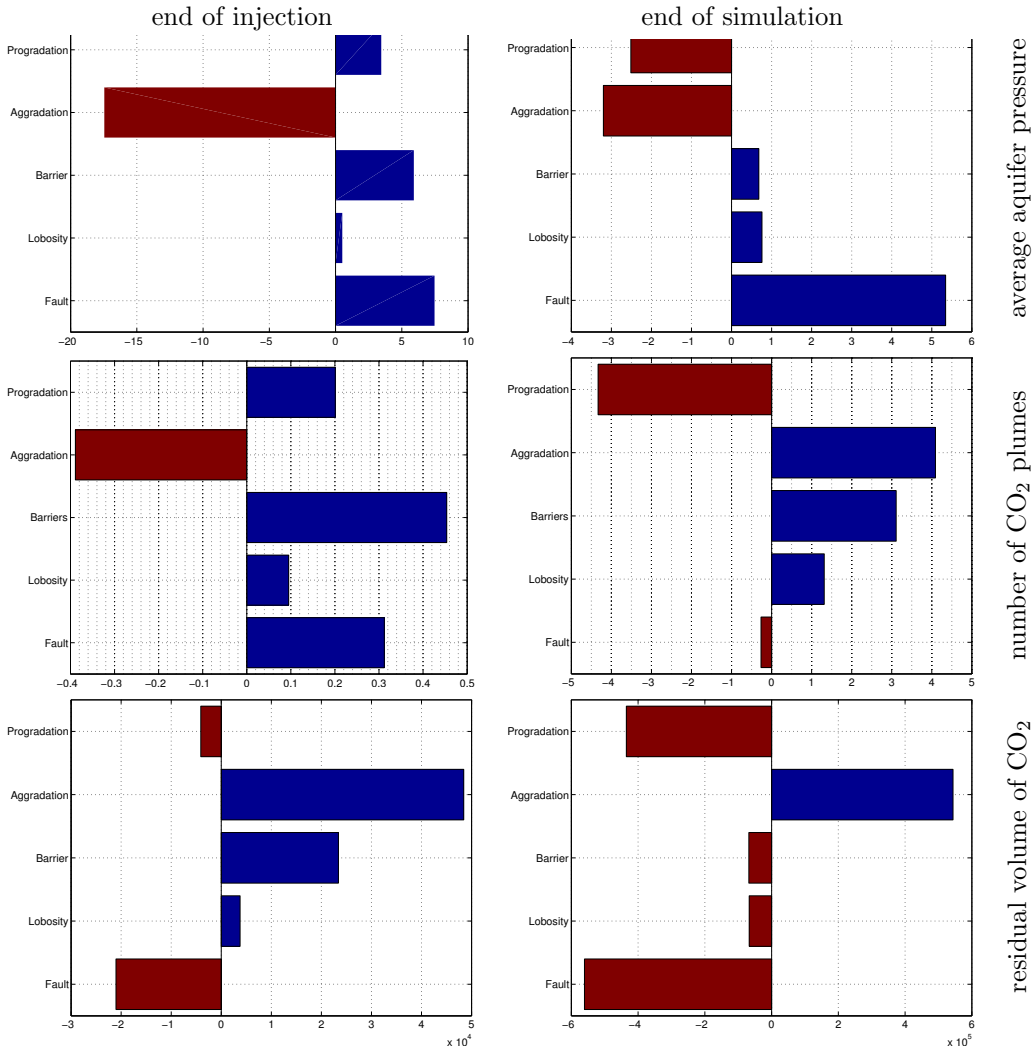


Figure 7: Sensitivities to different geological features at end of injection and end of simulation for the average aquifer pressure, number of CO₂ plumes, and residual volume of CO₂.

To quantify the relative impact of each geological parameter, we will define a normalized gradient for each feature. We will use barriers as an example to explain the analysis. There are three levels of barriers: low, medium and high. Suppose that we want to calculate the sensitivity of the number of plumes with respect to the level of coverage for the barrier sheets. We do this in two steps: first we average the number of plumes for cases of the same level of barriers. Having three levels of barrier, this results in three averaged plume numbers corresponding to each level of barriers. In the next step, we fit a line through these three points and calculate the inclination of this line which represents how the number of plumes increases if the barrier parameter increases one level. For other features like fault and lobosity, we follow the same procedure. We use three levels for each feature and fit a trend through these three points. For example, the first level of fault criteria relates to unfaulted cases, the second relates to open faults, and the third represents cases with closed faults.

Figure 7 shows the sensitivity for three different flow responses. In the upper row, we see that during injection the average aquifer pressure is most influenced by aggradation, while at the end of simulation the most influential feature is the fault specification. The lack of good vertical communication for low aggradation angles means that the CO₂ is confined to the lower (poor quality) layers and relatively high pressures must be imposed to inject the required amount of CO₂ into the aquifer. For higher angles, the CO₂ can flow more easily upward through channels with higher permeabilities and less pressure support is required. Hence, the negative gradient. After the injection ceases, the dominating force is gravity, the main flow direction is vertical, and the pressure is now mostly affected by faults. If the faults are closed, they will prevent the release of pressure through the open

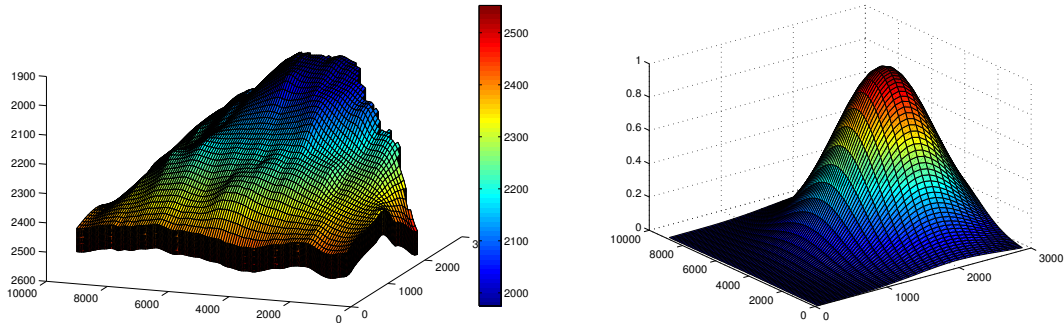


Figure 8: The left plot shows a sample grid geometry with depth values shown in meters. The right plot shows the Gaussian probability distribution for point leakage through the caprock. The distribution is centered at a point on the crest which is in the same slice as the injection point.

boundaries. We also observe that the effect of progradation switches from positive to negative after the injection is stopped: Injecting in the up-dip direction is easier than injecting down-dip, while a down-dip deposition opens up more conductive medium in front of the plume as it migrates towards the crest.

The second row in Figure 7 shows the sensitivity in the number of CO₂ plumes. During injection, the barriers coverage is the most influential parameter, because mud-draped surfaces enhance the lateral flow and force the plume to split rather than migrating towards and accumulating at the crest. Aggradation has a similar effect: the lower the angle is, the more the injected CO₂ spreads out laterally. At the end of simulation, progradation and aggradation are the dominant effects. In particular, higher aggradation angle improves the segregation across layers and thus increases the splitting of plumes through heterogeneities. The impact of the faults is more significant than the figure shows: open faults contribute to split plumes, while the unfaulted cases and the cases with closed faults introduce a small number of plumes. In average, the positive and negative contributions cancel out to almost zero. Finally, the bottom row in Figure 7 reports sensitivities for the total residual volume. Here, aggradation is the most influential parameter during injection and faults the most important parameter during the migration phase.

Similar analyzes have been conducted for other flow responses as well. Altogether, our sensitivity study shows that aggradation is the parameter that has most impact on the flow responses we have studied. Aggradation has either the largest or the second largest gradient during both injection and migration for almost all responses. The faulting has the second highest impact. Mostly effected by closed fault, the fault parameter influences the storage capacity and the extent to which a CO₂ plume accumulates under the caprock. Barriers play a dominating role for the splitting of plumes during injection, whereas the progradation affects the gravity segregation through conductive channels during the migration phase and the volume available to flow in the dip direction. Finally, lobosity has small impact compared to the other parameters and can therefore likely be ignored for the fluid responses considered above. However, lobosity has a considerable effect on the lateral movement and splitting of plumes during the migration period and may therefore have a more significant impact on the estimates of point leakage.

5 Leakage Risk

The SAIGUP study does not supply any information about the caprock and its geomechanical properties. We are therefore only able to conduct a conceptual study of the risk associated with point leakage through imperfections in the caprock. To this end, we assume that each point on the top surface has a prescribed probability for being a leakage point. As a simple example, we will assume that the probability for point leakage follows a standard 2D Gaussian distribution centered at a given point on the crest, see Figure 8. Moreover, we will assume that all mobile CO₂ (except for the residual portion) will escape through the caprock if a plume comes in contact with a leakage point. We have seen above that the heterogeneity and tilt of the medium will cause the injected CO₂ to be distributed

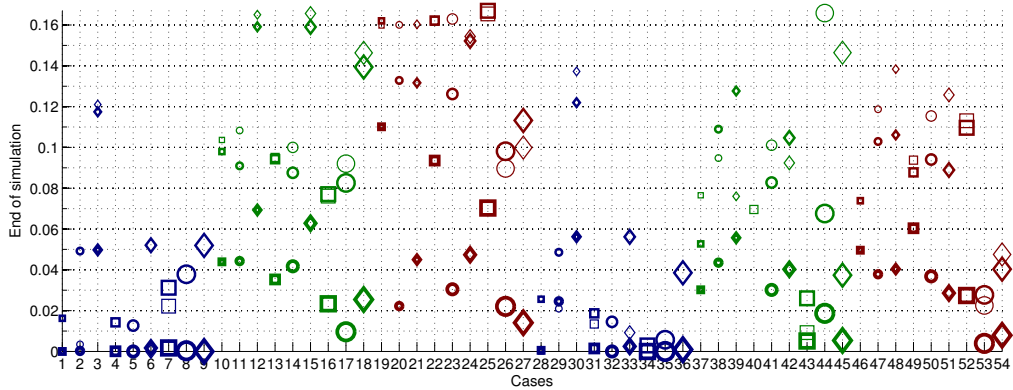


Figure 9: Leakage risk at end of simulation for linear relative permeabilities.

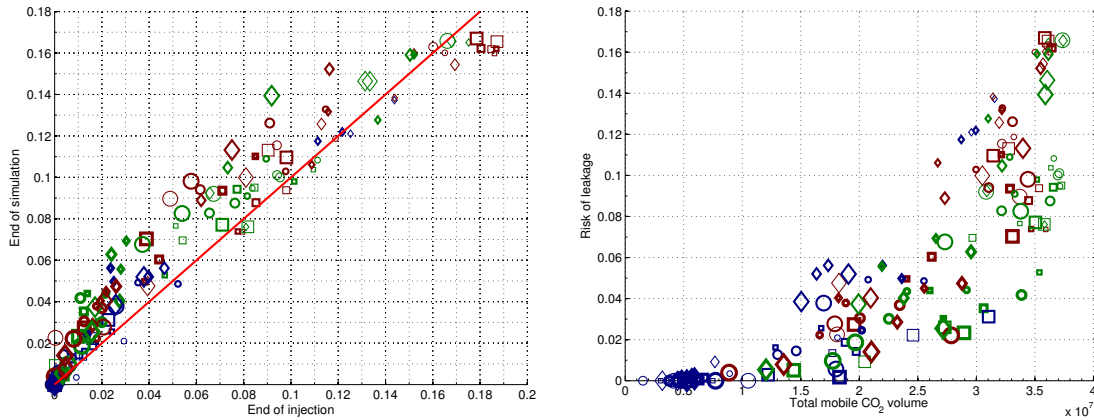


Figure 10: The left plot shows a cross-plot of leakage risk for linear relative permeability function. The right plot shows mobile CO₂ volume versus leakage risk at the end of simulation.

under the caprock as a number of plumes with variable sizes. For each cell along the top surface, we now define the risk as the probability of point leakage weighted by the size of the CO₂ plume that the cell is part of. We then sum the values for all the topmost cells, normalize this sum, and use the resulting single number as a measure of leakage risk. The worst possible case would be if all the injected CO₂ volume forms a mobile plume that contacts every point along the top surface; this gives a risk value equal to one. For all actual cases, however, the risk value will be less than one because not all of the CO₂ will be mobile (because of residual trapping and loss of volumes across the open boundaries), because the mobile volume may form more than one plume, or because not all the mobile volume has reached the top due to reduced vertical mobility.

Figure 9 shows the resulting leakage risks for all cases at the end of simulation computed using linear relative permeabilities. Similarly, the left plot in Figure 10 shows how the risk develops during the seventy year period from the end of injection to the end of simulation, whereas the right plot shows a cross-plot of the leakage risk versus the total volume of mobile CO₂. The plots lead to the rather obvious conclusion that improved vertical connection will increase the risk of leakage through possible imperfections in the caprock and that there is a positive correlation between the volume of mobile CO₂ in the system and leakage risk. However, we also observe that there are cases which have zero leakage risk. These are cases with low aggradation, for which the flow stays in the injected layers and moves laterally towards the open boundaries, resulting in a low amount of mobile CO₂ in the system. Furthermore, these cases have (almost) no cross-layered CO₂ movement, which means that (almost) no CO₂ reaches the top surface. In other words, the low-aggradation cases, which have seemed to be infeasible because of high injection pressure, larger lateral spread, and loss of volumes through the open boundaries in our discussion in the previous two sections, here appear as the most feasible with

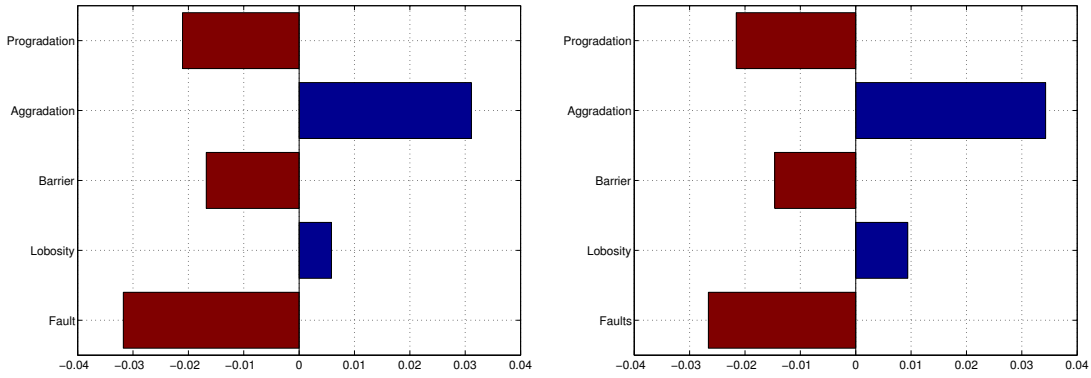


Figure 11: Sensitivity of the leakage risk with respect to the five geological parameters at the end of injection (left) and end of simulation (right).

respect to the chosen risk measure.

Figure 11 shows gradients for the leakage risk. Although less pronounced during injection time, the gravity force makes a major plume body attached to the crest both during the injection time and afterwards. Hence, we see that the leakage-risk sensitivity shows almost the same profile at end of injection and end of simulation. This can also be observed in Figure 10. The sensitivity is slightly less during injection compared to end of simulation, because more CO₂ will be below the caprock at end of simulation. This overtakes the effect of mobile volume reduction due to residual trapping process and the increase in the number of plumes at end of simulation, which both result in less risk of leakage.

Once again, aggradational angle and fault criteria are the two most influential features. Increasing the aggradational angle improves the vertical communication and contributes to increase the formation of CO₂ plumes below the caprock. Closed faults limit the movement of the plume and result in less accumulation below the caprock, whereas open faults generally increase the upward migration of plumes.

6 Conclusions

Herein, we have presented a study of how various geological parameters influence the injection and early-stage migration of CO₂ in progradational shallow-marine systems. One hundred and sixty equally probable realizations have been considered and several flow responses related to storage capacity and risk of point leakage have been calculated at the end of injection and after seventy years of gravity-dominated plume migration.

First of all, we have investigated the effect of relative permeability curvature by comparing the results of linear and quadratic relative permeability curves. The results show that linear relative permeabilities give significantly higher wave speeds that lead to earlier accumulation of CO₂ under the caprock, and will for this reason give conservative estimates of the plume migration and the risk associated with point leakage after a prescribed number of years.

Second, and more important, we have demonstrated and discussed how the heterogeneity induced by different geological parameters give large variations in flow responses. Each geological feature will influence the flow behavior and can result in local/global pressure build-up or pressure drop, enhance the flow direction, hinder the flow in the medium, or lead to loss of injected volumes over the open boundaries, and may induce different effects during the injection and plume migration. Specifically, we have demonstrated how variation in aggradational angle, fault criteria, and progradation direction significantly change the flow direction within the medium and hence impact the residual trapping and formation of movable CO₂ plumes under the caprock. Barriers are important during injection and must be modeled more carefully if the study focuses on injection operations.

Altogether, our study shows that geological heterogeneity has a major impact on the injection and formation of a CO₂ plume and the subsequent early-stage migration of this plume. A predictive study should therefore incorporate realistic estimates of geological uncertainty to provide reliable forecasts of operational risks and the long-term fate of injected CO₂.

References

- [1] M. Ashraf, K.-A. Lie, H. M. Nilsen, J. M. Nordbotten, and A. Skorstad. Impact of geological heterogeneity on early-stage CO₂ plume migration. In J. Carrera, editor, *Proceedings of the XVIII International Conference on Water Resources (CMWR 2010)*, Barcelona, Spain, 2010. CIMNE.
- [2] P. J. Cook, A. Rigg, and J. Bradshaw. Putting it back where it came from: Is geological disposal of carbon dioxide an option for australia. *Australian Petroleum Production and Exploration Association Journal*, 1, 2000.
- [3] S. P. Dutton, W. A. Flanders, and M. D. Barton. Reservoir characterization of a permian deep-water sandstone, East Ford field, Delaware basin, Texas. *AAPG Bulletin*, 87(4):609, 2003.
- [4] T. T. Eaton. On the importance of geological heterogeneity for flow simulation. *Sedimentary Geology*, 184(3-4):187–201, 2006.
- [5] B. Hitchon. *Aquifer disposal of carbon dioxide: hydrodynamic and mineral trapping: proof of concept*. Geoscience Pub., 1996.
- [6] J. A. Howell, A. Skorstad, A. MacDonald, A. Fordham, S. Flint, B. Fjellvoll, and T. Manzocchi. Sedimentological parameterization of shallow-marine reservoirs. *Petroleum Geoscience*, 14(1):17–34, 2008.
- [7] R. Juanes, E. J. Spiteri, F. M. Orr Jr, and M. J. Blunt. Impact of relative permeability hysteresis on geological CO₂ storage. *Water Resources Research*, 42:W12418, 2006.
- [8] T. Manzocchi, J. N. Carter, A. Skorstad, B. Fjellvoll, K. Stephen, J. A. Howell, J. D. Matthews, J. J. Walsh, M. Nepveu, C. Bos, J. Cole, P. Egberts, S. Flint, C. Hern, L. Holden, H. Hovland, H. Jackson, O. Kolbjørnsen, A. MacDonald, P. A. R. Nell, K. Onyeagoro, J. Strand, A. R. Syversveen, A. Tchistiakov, C. Yang, G. Yielding, and R. W. Zimmerman. Sensitivity of the impact of geological uncertainty on production from faulted and unfaulted shallow-marine oil reservoirs: objectives and methods. *Petroleum Geoscience*, 14(1):3–15, 2008.
- [9] J. D. Matthews, J. N. Carter, K. D. Stephen, R. W. Zimmerman, A. Skorstad, T. Manzocchi, and J. A. Howell. Assessing the effect of geological uncertainty on recovery estimates in shallow-marine reservoirs: the application of reservoir engineering to the saigup project. *Petroleum Geoscience*, 14(1):35–44, 2008.
- [10] J. M. Nordbotten, D. Kavetski, M. A. Celia, and S. Bachu. A semi-analytical model estimating leakage associated with CO₂ storage in large-scale multi-layered geological systems with multiple leaky wells. *Under Review at: Environmental Science and Technology*, 2008.
- [11] E. Spiteri, R. Juanes, M. Blunt, and F. Orr. Relative-permeability hysteresis: Trapping models and application to geological CO₂ sequestration. In *SPE Annual Technical Conference and Exhibition*, 2005.

Paper IV

3.4 Geological storage of CO₂: heterogeneity impact on pressure behavior

M. Ashraf

Submitted to *International Journal of Greenhouse Gas Control (IJGGC)*

Geological storage of CO₂: heterogeneity impact on pressure behavior

December 7, 2012

Contents

1	Introduction	2
2	Geological parameters	3
3	Injection scenario	5
4	Pressure analysis	6
4.1	Injection time	8
4.2	Well and aquifer pressure	9
4.3	Pressurized region	11
4.4	Build-up region	12
4.5	Farthest pulse	13
5	Discussion	14
6	Conclusion	16

Abstract

Due to the high rates of industrial CO₂ emission, it is an operational objective to maximize CO₂ injection rate into underground geological formations. Forcing the injection wells with high volumetric rates can result in an overpressurized system with possible breakings in the formation integrity, which increases the risk of CO₂ leakage.

The goal of this study is to investigate the injection pressure considerations that are needed to avoid uncontrolled development of fractures in the medium. Herein, we study how the geological heterogeneity influences the pressure behavior of a typical CO₂ injection operation. Five variable geological features are considered as input for sensitivity analysis. These features span a realistic geological space.

Two injection scenarios are examined. In the first scenario, CO₂ is injected at a constant rate and the pressure in the well and the domain is allowed to build up unlimitedly. In the second scenario, a pressure constraint is set on the well, and the injection rate is changed to keep the pressure below the limit. Model responses related to pressure build-up and propagation within the system are defined and demonstrated for a selected case. Results for all cases are presented and discussed accordingly. We conclude by ranking the most influential geological parameters.

1 Introduction

The increasing level of green-house gases in the atmosphere, and in particular carbon dioxide, is believed to cause global climate changes. The industrial emission rate is expected to increase over the next decade, without taking necessary preventive actions. For example, according to the Energy Information Administration (EIA), the US carbon dioxide emissions are forecast to reach 6.41 billion tonnes by 2030. The Kyoto protocol proposed an emission cut which requires 1.75 billion tonnes of annual carbon dioxide reduction [10].

Geological storage of CO₂ is a proposed solution to fight global climate change. Clear operational criteria and policies must be made for the process to avert unwanted consequences. Concerns connected to putting a large mass of CO₂ into underground geological formations are not limited to the spatial distribution of the injected fluid. The pressure signals imposed through the injection point can travel beyond the scale of the CO₂ invaded zones. Although geological barriers can hinder the pressure exchange between different regions, pressure can transfer through low-permeable rocks where the CO₂ is trapped by capillarity.

In addition to the depleted oil and gas fields, deep geological aquifers are practical targets for geological storage of CO₂. If injecting into brine aquifers, the pressure waves can push brine into connected fresh water aquifers and contaminate them. Brine displacement issues are discussed in [4] by defining open, closed, and semi-closed aquifer boundaries. Brine might also leak through abandoned wells into other zones. Cailly et al. [3] discuss well design considerations to prevent any leakage through wells.

Geomechanical deformations are important during injection period. They can lead to changes in effective permeability and porosity. It is possible that the pressure build-up around injection wells will crack the rock with uncontrolled fracture extensions to the structural sealing layers. Faults can be activated due to high pressure in the system, providing a

leakage path across layers. In addition to increased spatial CO₂ spread, an intensive induced fracture network can result in local earthquakes.

Pressure constraints must be considered for injection operations to limit the pressure buildup. However, this comes with the cost of injection rate reduction. Rock quality within the injection region has significant impact on pressure build up and therefore, geological uncertainty plays a considerable role in assessing the success and feasibility of the operation.

Any risk of breakings in the formation integrity must be assessed to define the appropriate preventive measures. We need to perform pressure sensitivity analysis to identify the influential parameters in the model. Uncertainty reduction in the influential parameters enhances the accuracy of pressure behavior prediction.

Geological uncertainty is a major issue in pressure analysis. Most of the pressure-related studies in the literature provide either deterministic case studies or generic preventive measures based on theoretical studies [9, 13, 6, 14, 12, 11]. It is important to include realistic geological descriptions in any study related to uncertainty. For example, permeability variation on the grid should be in the form of realizations of geological realistic formations. To the best of our knowledge, this is the first pressure study in the context of CO₂ storage that considers the geological uncertainty in the form of structural variables rather than engineering parameters, such as permeability and porosity.

Within oil recovery context, the impact of geological uncertainty is thoroughly investigated in the SAIGUP project for shallow-marine depositional systems [5, 7, 8]. In the SAIGUP study, variations of geological features are examined in a set of field development strategies via several injection/production patterns. The study concludes that geological uncertainty has a dramatic influence on the oil recovery estimates. A number of geological realizations from the SAIGUP are used in [1, 2] to investigate the impact of geological uncertainty on injection and early migration of CO₂. Certain structural features are considered for those studies and flow responses are defined to measure the storage capacity, the trapping efficiency, and the leakage risk and the sensitivity of these responses to variations in geological parameters is investigated. Large variation in responses are observed. Aggradation angle and barriers are recognized to be the most influential in the CO₂ flow behavior[1, 2]. The focus in [1, 2] is to measure the spatial CO₂ distribution sensitivity to the variation of geological description.

This study is complementing [1, 2], in the sense that we herein analyze the sensitivity of pressure to the same geological parameters. In addition to the injection scenario used in [1, 2], we examine a different injection scenario with more realistic well control for the injection operation. A detailed study is given for the pressure behavior during injection time.

2 Geological parameters

In the SAIGUP study, a large number of realistic realizations were generated based upon a parametrization of a set of carefully selected geological features and a detailed sensitivity analysis study is performed for field oil recovery over number of development scenarios. Both the sedimentological and structural geological parameters have shown to dominate the uncertainty in total oil production. Hence, more accurate geological description enhances the

quality of flow simulations.

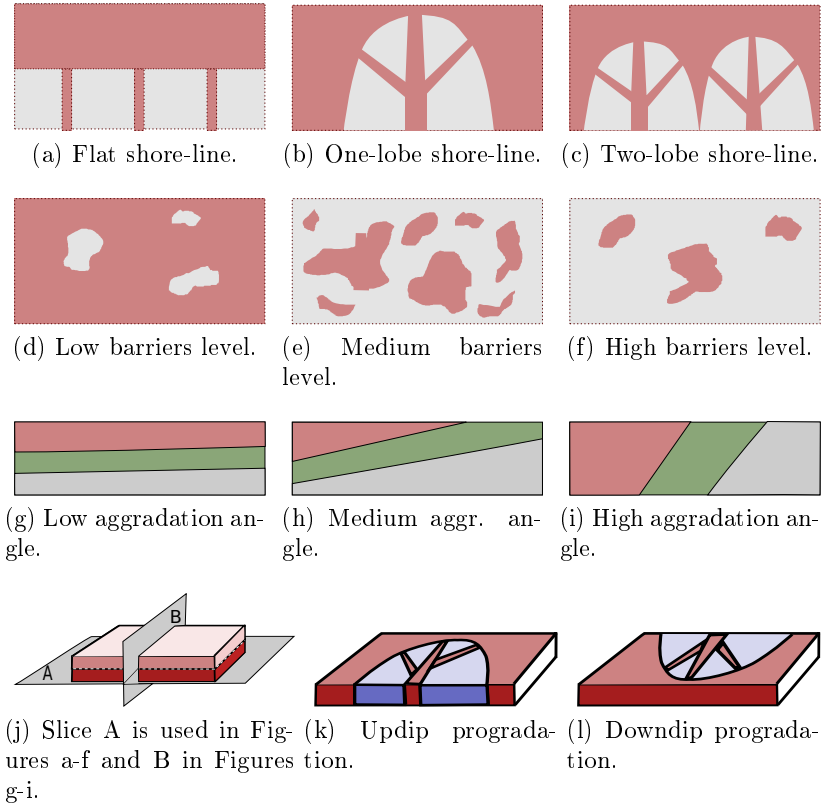


Figure 1: The studied geological features. a-c) Shoreline shape, gray is for poor quality rock and brown color resembles a good quality rock. d-f) Barriers level defined by transmissibility multiplier. Gray color is for zero and brown color shows one. g-i) Aggradational angle. k-l) Progradation direction.

Table 1: Marker codes used in the result plots. The code level corresponds to levels in Figure 1.

Code	Description	Code level	Feature level
Thickness	Fault	thin/medium/thick	unfaulted/open/close
Shape	Lobosity	square/circle/diamond	flat/one-lobe/two-lobe
Size	Barriers	small/medium/large	10% / 50% / 90%
Color	Aggradational	blue/green/red	low/medium/high
Case no. counting	Progradation	first half/second half	up-dip / down-dip

We have selected five geological parameters from the SAIGUP project to study the impact of heterogeneity on the pressure responses in a typical CO₂ injection problem. These parameters span realistic intervals for progradational shallow-marine depositional systems with limited tidal influence. The considered features with the grading levels in each one, are

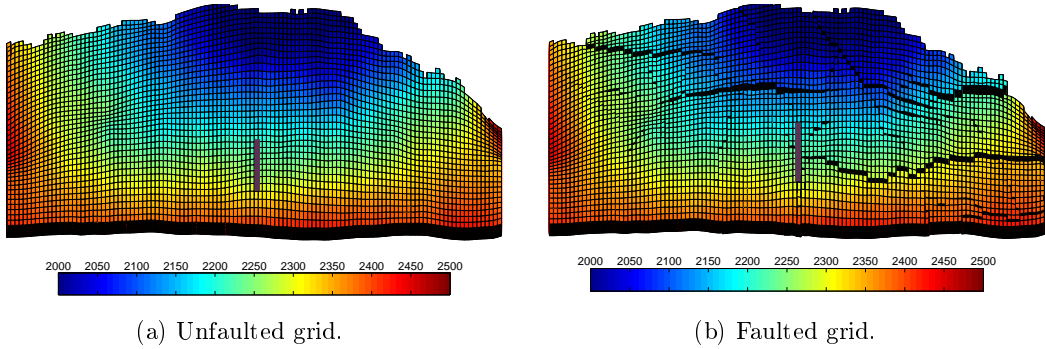


Figure 2: Models used in the study. Depth in meter is shown by color.

shown in Figure 1. In addition to the features shown in Figure 1, we also consider faulting levels: unfaulted, open faults, and close faults. In subsequent plots, each of these features are represented with codes such as shape, size and color which are explained in Table 1. For more details refer to [1].

3 Injection scenario

We define a CO₂ injection scenario to be implemented for all cases in which we use an injector down in the flank and hydrostatic boundary conditions on the sides, except the side near the crest (see Figure 2). No-flow boundary conditions are imposed on the top and bottom surfaces of the model. Model dimensions are: 9km × 3km × 80m. The well is completed only in the four layers in all cases. The idea is to inject as low as possible to increase the travel path and the volume swept by the plume. If the medium is homogeneous, following the injection we expect one big plume to be constructed and this plume to move up due to the gravity force until it accumulates under the structural trap beneath the cap-rock.

Slightly compressible supercritical CO₂ is considered and we seek to inject a volume of 40MM m³, which amounts to 20% of the total pore volume of the models. After the injection period, early plume migration is simulated in all of the studied cases and the simulation ends at 100 years. We use Corey-type quadratic functions for relative permeability, with end points 0.2 and 0.8 in both phases.

Low well injectivity can result in high pressure in the system. In this study, two injection strategies are implemented. In the first strategy (which is similar to the one used in [1]), the entire CO₂ volume is injected within 30 years at a constant volumetric rate. In the second strategy, we set an operational pressure constraint on the injector and continue injecting with appropriate rates to keep the pressure within the limit. We do some pressure response calculations to see the propagation of pressure pulses in the medium for both strategies.

In the pressure-constrained strategy, the injector operates with the priority of injecting a volumetric rate of 3650 m³/day. A pressure constraint of 400 bar is set on the injector. If the well bottom-hole pressure goes higher than that and violates this restriction (to maintain the target injection rate), the priority changes to keep the 400 bar by reducing the injection rate. The well continues operation switching between these priorities until a total CO₂ volume of

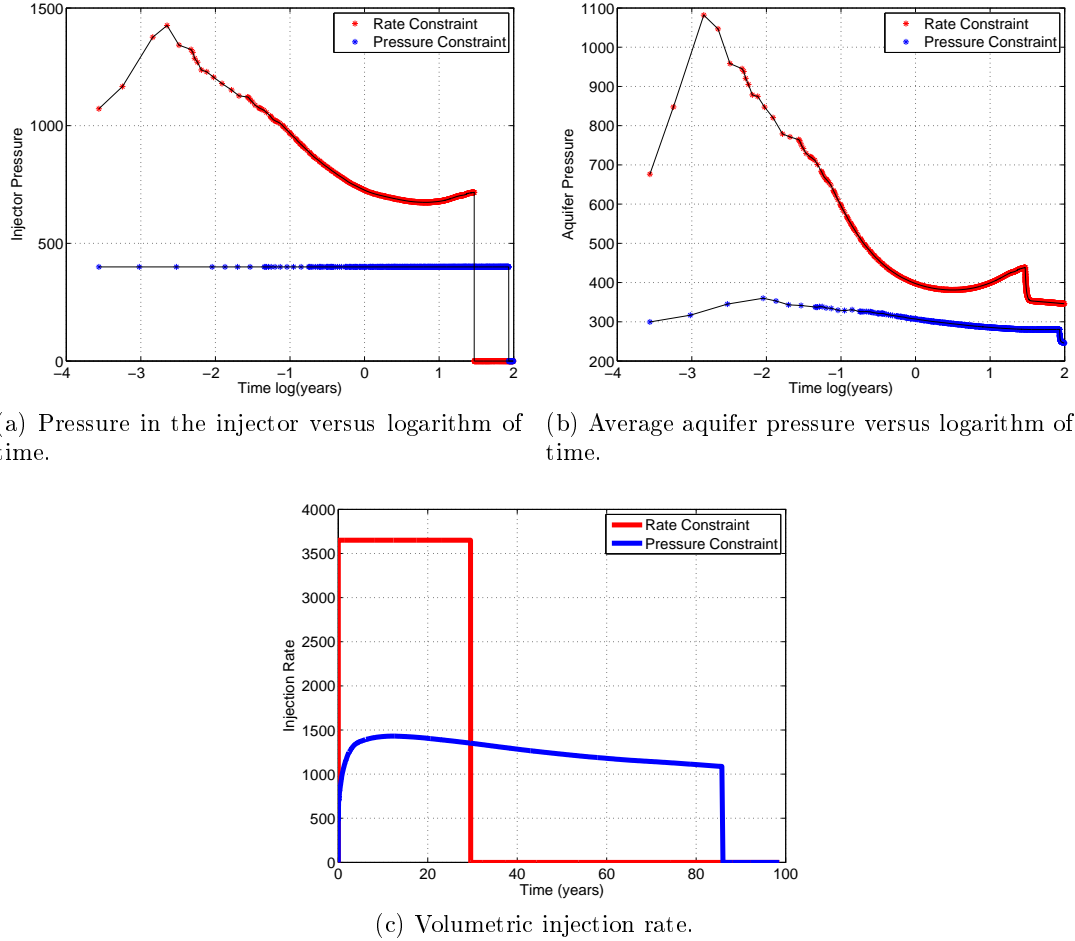


Figure 3: Aquifer and well pressure and injection rate in different injection scenarios shown for a test case.

40MM m³ is injected into the medium. As soon as the total injected volume reaches this number, the injector will be shut from the bore-hole and no injection happens for the rest of simulation time.

4 Pressure analysis

We start by discussing the pressure responses we will use in our study for one particular realization. Then we do the full analysis by considering all of the 160 specified realizations, which are made by combining the geological variable levels discussed earlier¹. Response plots are shown and discussed accordingly. Most of the reported results are chosen at 2.4 hours (0.1 day), i.e., at the beginning of injection. At that time, the system pressure response is higher compared to the later times when the pressure in the system drops to lower values

¹Combining all the features and levels makes 162 cases. However, two cases were missing in the original data set.

(Figure 3b). Also, upto this time the same amount of CO₂ is injected in all cases, which allows for a fair comparison between cases.

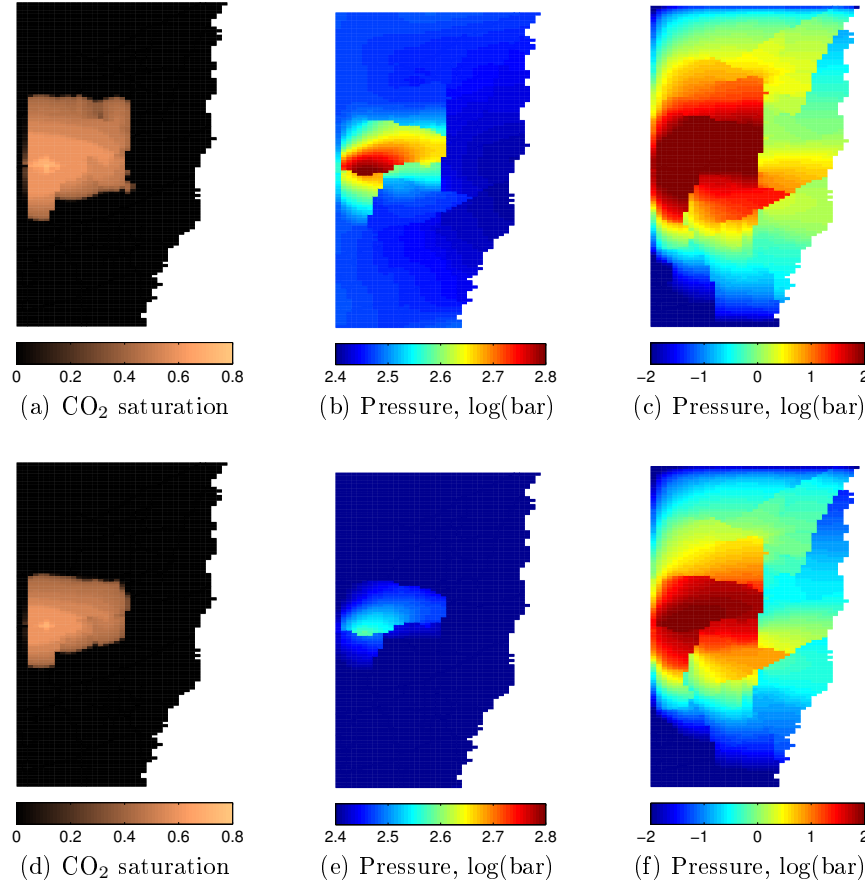


Figure 4: Responses at the middle of injection period (15 years). The first row corresponds to rate-constrained and the second row belongs to the pressure-constrained injection scenario. Figures c and f show the pressure build up from its initial value. Top view of last injection layer is shown in all figures.

Four types of responses are considered to be basis for the comparison between cases. One important question is how fast we can inject into a realization. To compare different cases, injection time is calculated considering a fixed total volume of injection in all models. Pressure behavior in the system is studied, by looking at aquifer average pressure and pressure drop across the well. An overpressure region is defined in which the volumetric spread of over-pressure locations in the model is measured. Finally, the farthest place from the injection point that a pressure build up has reached is reported for each realization to see the impact of heterogeneity and channellings on how the pressure wave travels through the medium.

Figure 4 shows the pressure and saturation responses for the two injection scenarios in a selected case. This case has one lobe, parallel rock-type stratigraphy (i.e., low aggradation angle), and up-dip progradation. It is faulted with almost open faults and has high barrier

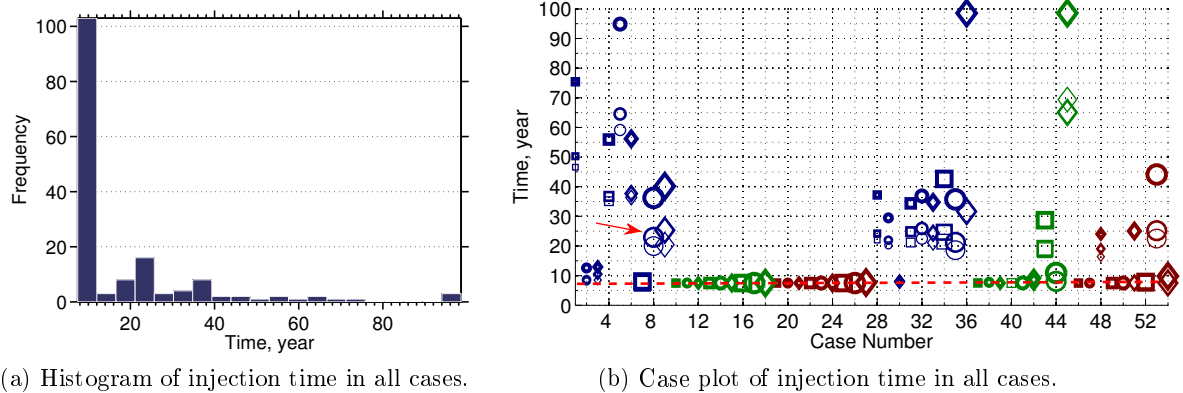


Figure 5: Time to inject quarter of the total specified CO₂ volume for all cases in the pressure-constrained scenario. The dashed red line in the right plot denotes the targeted injection time of 7.5 year, and the red arrow points to the case shown in Figure 4.

level. Responses for the rate constrained scenario are given in Figures 4a, 4b and 4c, and those for the pressure constrained scenario are given in Figures 4d, 4e and 4f.

The pressure build-up in Figures 4c and 4f tells about heterogeneity impact on maintaining the pressure locally rather than transferring it across the medium. Comparing Figures 4b and 4c with Figures 4e and 4f, we see that imposing a pressure constraint on the injector significantly reduces the pressure build-up in the medium (as should be expected). However, the pressure disturbance propagates widely through the system in both cases (Figures 4c and 4f), far beyond the CO₂ invaded zones in Figures 4a and 4d.

4.1 Injection time

In the pressure-constrained scenario, the less the injectivity of the well is, the longer it will take to inject into the medium, keeping the pressure below the critical limit. In some of the cases it takes longer than 100 years (i.e., longer than the considered total simulation time) to inject the specified CO₂ volume. To compare cases, we therefore calculate the time at which a quarter of the objective volume is injected. In all cases, this amount is injected within the total simulation time.

Figure 5 shows the injection time for all cases, using the pressure-constrained scenario. For many cases, the injector keeps the target rate, and thus, it completes the injection in 7.5 years (the dotted red line in the figure). The rest of the cases require longer injection time, due to the lower injectivity of the medium. This leads to pressure control in the injector, followed by a decrease in the injection rate.

Different codes used in the plot of Figure 5 are described in Table 1. Most of the cases with lower injection rates in the plot are colored blue, which translates to a low aggradational angle. Also cases with closed faults, denoted by thick markers, have (significantly) longer injection times.

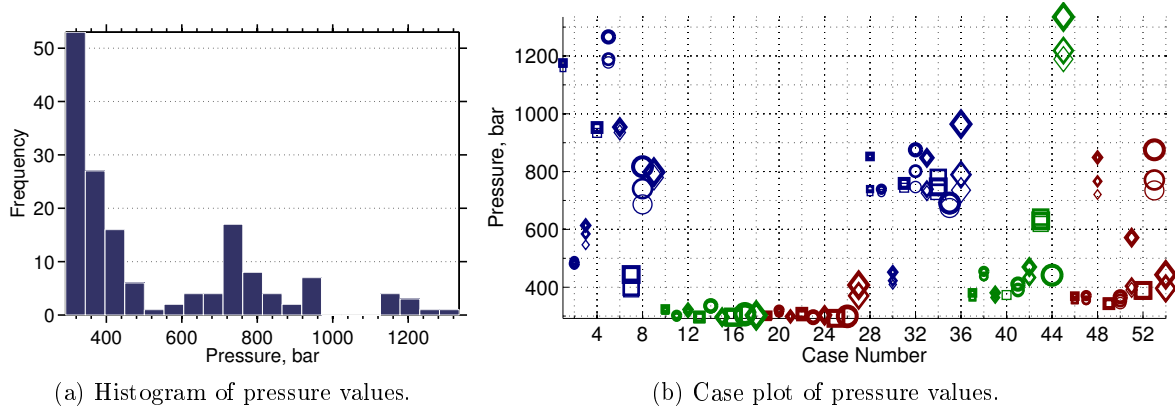


Figure 6: Average aquifer pressure for all cases in the rate-constrained scenario.

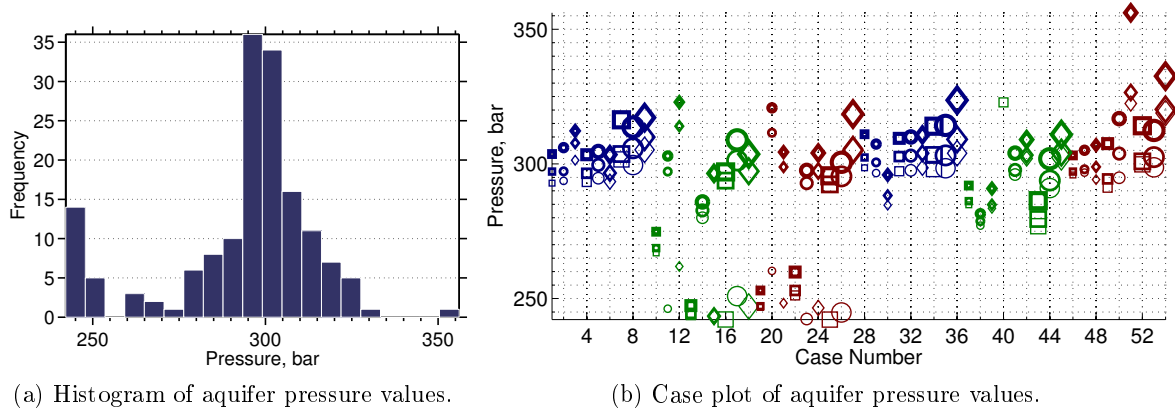


Figure 7: Aquifer average pressure for all cases in the pressure-constrained scenario.

time. Progradation effects are apparent on the higher aggradation cases: for some of the cases colored green and red in the second half of the plot in Figure 5, injection takes longer than the corresponding cases in the first half, which satisfy the targeted injection. This means that down-dip progradation, independent of aggradation angle level, can result in lower injectivity.

4.2 Well and aquifer pressure

To see the overpressure caused by different heterogeneities, we compare cases for their average pressure and well pressure drop. Histograms of average aquifer pressure are shown in Figures 6a and 7a for different injection scenarios and average aquifer pressure at 2.4 hours after the start of injection is plotted for all cases in Figures 6b and 7b. In the rate-constrained scenario, high ranges of average pressure are observed (Figure 6b). Effects of aggradation angle, progradation and faulting are visible in the plot. Three clusters can be identified in the histogram of Figure 6a with medium, high and extreme pressure values. In Figure 7a,

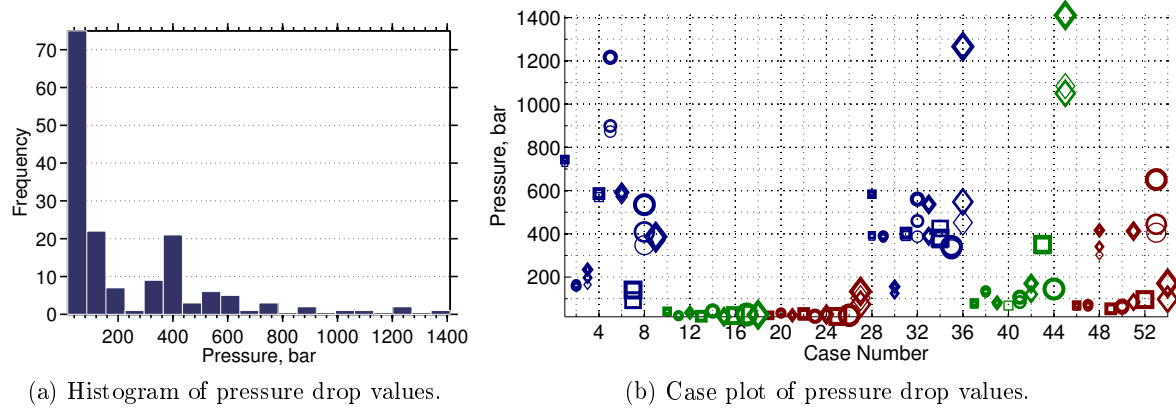


Figure 8: Average of injector pressure drop for all cases in the rate-constrained scenario.

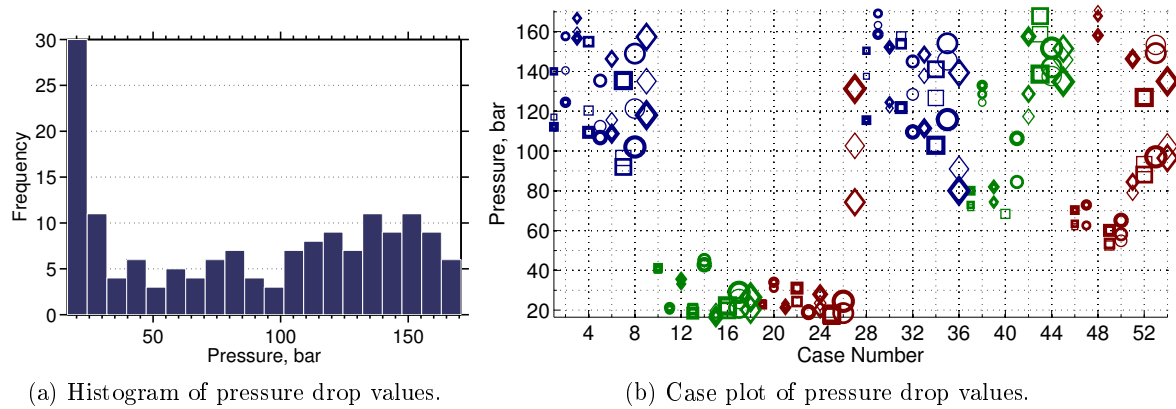


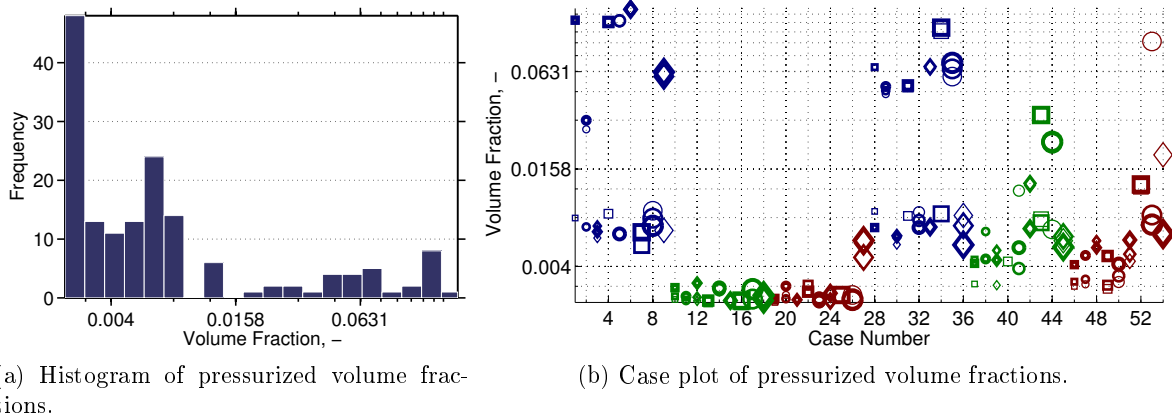
Figure 9: Average of injector pressure drop for all cases in the pressure-constrained scenario.

a small group of cases show lower pressures, while most of cases are distributed around the mean value (which reads 300 bar).

We define the average well pressure drop as the temporal average of the difference between the bottom-hole pressure and the average aquifer pressure.

Histograms of well pressure drop values are shown in Figures 8a and 9a. Higher values imply a poor injectivity of the medium. We see in Figure 8 that maintaining the target rate will in many cases require a huge pressure drop (up to 1400 bar in the worst cases) that would not be feasible nor possible to obtain. Pressure control on the injector reduces the range of pressure drop variation below 170 bar. The average injector pressure drop is plotted for all cases in Figures 8b and 9b.

Two regions can be identified in the medium, the region near the injection point; and the part of aquifer which is far from the injection point. The well-bore pressure is effected directly by heterogeneities in the near well-bore region, while the larger scale region influences the average aquifer pressure. Pressure drop variations in Figures 8a and 8b are influenced by the heterogeneity near the well-bore, where the reaction to injecting a fixed amount of CO₂



(a) Histogram of pressurized volume fractions.

(b) Case plot of pressurized volume fractions.

Figure 10: Pressurized volume fraction for all cases in the rate-constrained scenario.

starts by a local pressure build-up. Heterogeneity on the scale of aquifer plays a considerable role in the range of variations in Figures 9a and 9b. In the pressure-constrained scenario, local pressure is controlled by putting a constraint on the well. Hence, the pressure drop variations are controlled by the average aquifer pressure.

As we see in Figure 8b, low aggradation angle and down-dip progradations result in a poor injectivity and high pressure buildup in the injector. Vertical transmissibility drops dramatically for low aggradation angles [1]. This restricts the pressure transfer within the injection layer, and therefore the pressure builds up locally around the well. Moreover, in cases with down-dip progradation the low permeability rocks surrounding river branches near the injector result in a local pressure buildup.

A group of cases in Figure 9 have a relatively low pressure drop of less than 50 bar. These cases have a good injection quality, and the pressure is released through open boundaries easier than other cases. The rest of the cases show higher pressure drop because of the heterogeneities in the larger scale, far from the injector. These results are obtained for a fixed injection location to examine the heterogeneity impact on injectivity. Herein, we aim to honor the geological uncertainty. In practice, the injector must be drilled and completed in the best formation with highest possible injectivity.

Faults influence both local pressure build-up near the injector as well as the average aquifer pressure. Therefore, they have a visible trend in many cases in Figures 8b and 9b (for example, see the three cases denoted by red circles in the right end of Figure 8b). This is especially more apparent in cases with high level of barriers.

4.3 Pressurized region

Here, we study the overpressure distribution in the medium. An absolute pressure limit of 300 bar is set as threshold, such that all cells with a pressure higher than this value form a region that is called the pressurized region. The volumetric fraction of this region is defined by the ratio of pressurized volume to the total volume of all active cells in the model.

Histogram and case plot of the pressurized volume fraction at the start of injection are

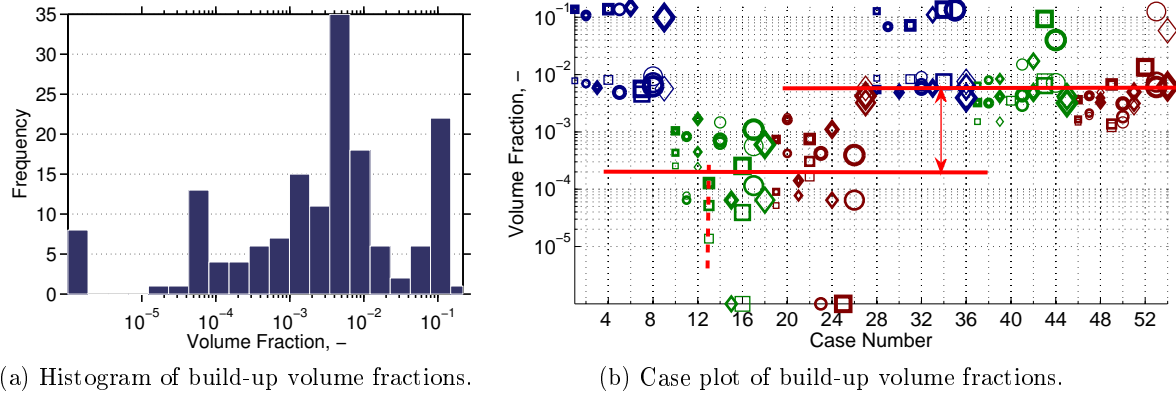


Figure 11: Build-up volume fraction for all cases in the rate-constrained scenario.

given in Figure 10. Here, we clearly see that low aggradation angle is very influential in the pressure buildup in the injection zone. A group of cases with low aggradation angle have a relatively large pressurized region in Figure 10b. However, also there are number of cases in Figure 10b that have a relatively low pressurized fraction. In these cases, the medium is conductive toward the open boundaries and the heterogeneity in the medium does not cause a major pressure buildup. Other observation in Figure 10b is the progradation effect; down-dip progradation, shows a rise in pressurized fraction for higher aggradation angles.

4.4 Build-up region

To study the pressure change, and how a pressure disturbance spreads through the medium, we use another metric. We calculate the pressure change by subtracting the initial pressure at each location from the current pressure. Different realizations are compared for the size of a region, which we call the buildup region, where the pressure increases from its initial value by 10 bar. The value 10 bar is chosen to make sure that the region has not reached the boundaries in any of the studied cases. The smaller the buildup region is, the less volume will be exposed to pressure change in the aquifer (Figure 11).

Higher pressure in the medium will obviously cause a larger buildup region. Impact of progradation on the pressure build-up is illustrated in Figure 11b. Up-dip progradation shows a relatively lower pressure buildup compared to down-dip progradation cases. We also see that aggradation dominates this effect, where cases with low aggradation angle show the same build-up pressure for both types of progradation directions (Note the blue colored markers that don't follow the lines in Figure 11b).

Several cases in Figure 11b show a trend for the fault parameter. The dashed line in the figure shows the trend of build-up pressure increase due to fault feature variations in three cases. Faulting changes the geometry of layers and puts different layers adjacent to each other. This enhances the connectivity in the medium. Local heterogeneities and closed

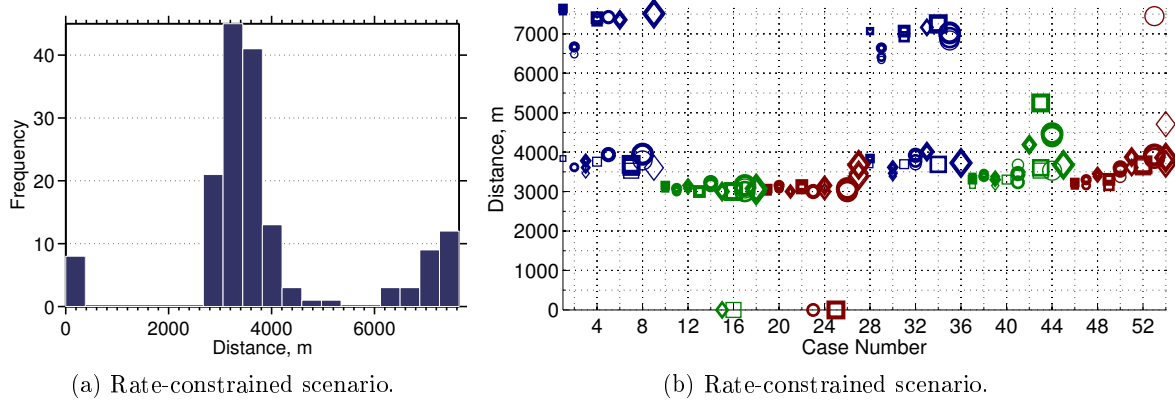


Figure 12: The farthest pulse of the pressure build-up distance from the injection point for all cases in the rate-constrained scenario.

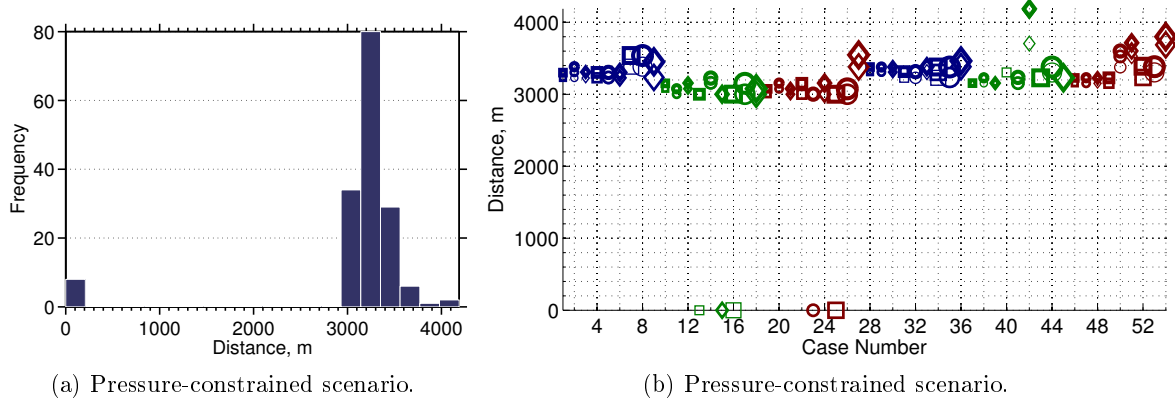


Figure 13: The farthest pulse of the pressure build-up distance from the injection point for all cases in the pressure-constrained scenario.

faults around the injector make a larger build-up region, because they cause higher pressure build-up in the domain. In these cases, the effect of heterogeneity of different scales, namely on the scale of near injector and far from injector, are combined causing a larger buildup fraction.

4.5 Farthest pulse

As discussed earlier, irregular geometries like faults and unconformities can lead to pressure spread in the domain. Looking at the volume fraction of pressurized and buildup regions helps in comparing cases for their pressure conductivity, but it does not show the extent of pressure spread in the medium. For that reason, we also look at the farthest cell from the injection point that falls within the buildup region defined earlier.

Figures 12 and 13 show the farthest pressure build-up distances from the injector in

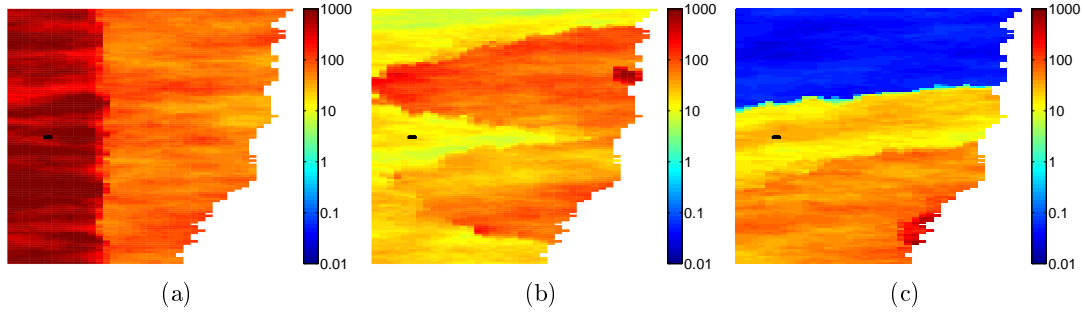


Figure 14: Permeability of three cases in unit millidarcies shown in color, and the Well location is illustrated with black color on each plot . Top view is shown in the plots.

different injection scenarios. In Figure 12a, three groups of cases can be identified: cases with zero distance of farthest pressure build-up pulse, cases with medium distances, and those with large distances from the injection point. Three specific cases are chosen as samples from each of the groups. In the first group, the pressure does not exceed the 10 bar threshold from its initial value in the medium. For these cases, the injector is placed in a permeable region and the medium is conductive towards open boundaries (Figure 14a). Hence, the imposed injection pressure does not build up, neither locally around the well nor globally in the aquifer scale. The second group in Figure 12a have a medium range of 3 – 4 km of distances from the injection point. Heterogeneity in these cases is not making a high pressure build-up around the injector and throughout the medium (Figure 14b).

In the third group, low permeability rocks in the injection layer cause a high pressure build-up around the injection point. If the injector zone is isolated by sealing heterogeneities, the pressure rises in a limited region. However, if the well is connected throughout the medium, and the heterogeneities in the aquifer scale contain relatively low permeability rocks, the pressure build up spreads wider in the aquifer. In Figure 14c, the injection point is located close to a low transmissibility rock. This rises the pressure level in the injector. Other parts of the aquifer are connected with poor quality rocks, resulting in a wide build-up region.

The farthest pulse distance ranges from 8 km to about 10 km in the extreme cases. By controlling the injection pressure, the maximum shrinks to less than 5 km (Figure 13a).

5 Discussion

So far, we reported the model responses that measure the pressure rise and pressure disturbance propagation in the domain. Pressurized volume fraction indicates the actual high pressures that may occur in an injection operation. Build-up volume fraction and farthest pulse are indicators of how the pressure disturbance is spread in the system. We are interested in limiting both the pressure increase and the area of well pressure influence in the aquifer.

In most of the results, aggradation angle, progradation direction and faults play a major role in the pressure behavior. For low aggradation angle, geological layers are made of rock types piled in a parallel stratigraphy. Thus, efficient vertical permeability is the harmonic

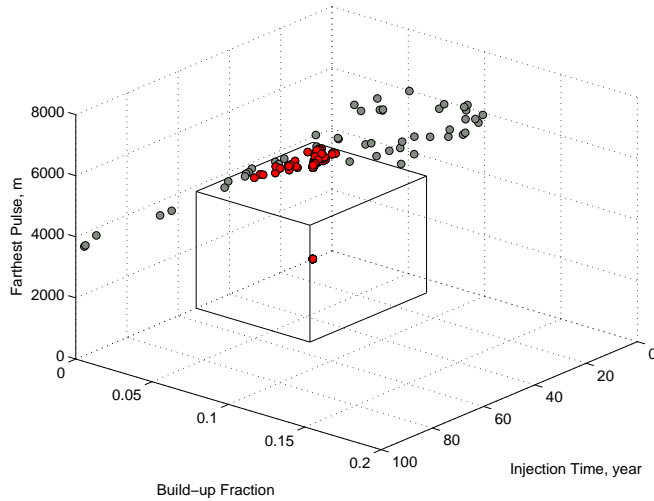


Figure 15: Pressure criteria implemented to filter the acceptable cases. Cases below the critical limits are plotted in red and cases exceeding the limits are plotted in gray.

average of these layers. If any of these layers contains a low permeability rock, this will result in a low vertical permeability. Injecting into a limited space sealed vertically, increases the pressure in the injection point.

Progradation direction can dominate the pressure behavior. It is very important to locate the injector in a high permeability zone is connected to other parts of the domain via permeable channels. Injecting into the river side of a shallow-marine depositional system, may end up into locating the injection point in a low quality rock between river branches joining the sea. This rises the pressure significantly near the injection point and can result in a high well-bore and aquifer pressure.

Structural deformations due to faulting process can increase the connectivity in the medium. If the transmissibility in the aquifer scale is high, the injection pressure releases through the open boundaries. However, if the injection area is surrounded by low quality medium, the pressure rises in the aquifer and the connectivity enhanced by fault geometries spread the build-up region in the domain. On the other hand, sealing faults result in high pressure within closed zones around the injection point. However, they may limit the pressure disturbance propagation in the domain.

From an operational perspective, pressure limits must be set to keep the operations within safe margins. One approach to study the safety of an operation could be setting critical limits on the pressure responses measured here. This limit is used to filter cases with desirable/acceptable pressure behavior. The critical margins are inferred from the realistic operational requirements. In our practice, we assume these margins to be 53 years for the injection time, 0.0787 for the pressurised volume fraction, 0.0745 for the build-up volume fraction, and 3822 m for the farthest pulse distance from the injection point. These values are picked from the middle points of range of variations in the results. By these assumptions, 49 cases out of total number of 160 cases exceed the critical limits.

Figure 15 shows the cases filtered by the pressure criteria. In Figure 15, the pressurized volume fraction is also considered in the filtration, though it is not shown in the plot axes.

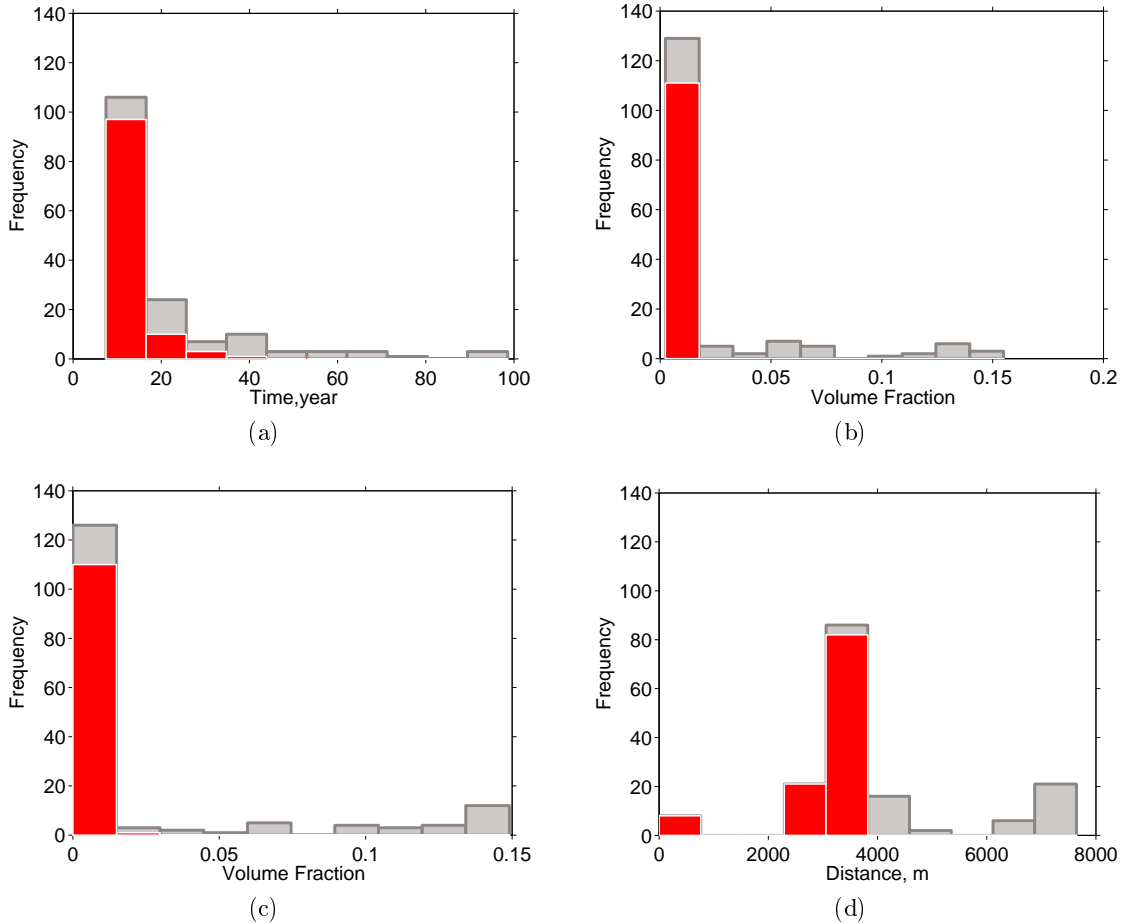


Figure 16: The histogram of filtered cases (colored in red) compared with the histogram of all cases for different pressure responses: a) Injection time, b) Pressurised volume fraction, c) Build-up volume fraction, and d) Farthest pulse distance from the injection point.

The plot shows that most of the cases that pass the filtering are concentrated in a region of low build-up fraction values. Figure 16 reports the histogram of filtered cases in comparison with the histogram of all studied cases for each response.

6 Conclusion

This work is a part of comprehensive sensitivity studies to assess the impact of geological heterogeneity on CO₂ injection and early migration. The aim of this study is to define preventing measures that can be used to avoid high pressures and the damages accompanied by them during the injection operations. Simulation responses related to the pressure behavior in the system are defined and calculated for two CO₂ injection scenarios. Geological variations in shallow-marine depositional systems are examined by using large number of realizations representing a spectrum of sedimentological and structural parameters. Operational critical values are considered for the defined preventive measures.

Most of the studied responses, show relatively a higher sensitivity to aggradation, progradation and faulting. Low aggradation angle keeps the flow restricted in a limited space. In cases with low rock quality in injection layers, pressure builds up in the well-bore. Injecting in down dip progradation, normally ends up in a higher pressure buildup and lower injectivity. In the down dip progradation, the majority of the region around injection point is made of low quality rock. Faults change the geometrical structure of the medium and they put different layers in contact. Pressure disturbance can leak through faults to larger distances from injection point. Closed faults can significantly reduce the injectivity quality.

The work-flow of pressure study demonstrated here can be used in a specific studies in the context of geological uncertainty. The work-flow can be used for other depositional systems and different values for operational limits can be used, which might lead to outcomes different than the results reported here.

References

- [1] M. Ashraf, K.A. Lie, Nilsen, and A. Skorstad. Impact of geological heterogeneity on early-stage CO₂ plume migration: Sensitivity analysis. In *ready for submission*, 2012.
- [2] M. Ashraf, K.A. Lie, H.M. Nilsen, J.M. Nordbotten, and A. Skorstad. Impact of geological heterogeneity on early-stage CO₂ plume migration. In *CMWR*, 2010.
- [3] B. Cailly, P. Le Thiez, P. Egermann, A. Audibert, S. Vidal-Gilbert, and X. Longaygue. Geological storage of CO₂: A state-of-the-art of injection processes and technologies. *Oil & Gas Science and Technology*, 60(3):517–525, 2005.
- [4] A. Cavanagh and N. Wildgust. Pressurization and brine displacement issues for deep saline formation CO₂ storage. *Energy Procedia*, 4:4814–4821, 2011.
- [5] J.A. Howell, A. Skorstad, A. MacDonald, A. Fordham, S. Flint, B. Fjellvoll, and T. Manzocchi. Sedimentological parameterization of shallow-marine reservoirs. *Petroleum Geoscience*, 14(1):17–34, 2008.
- [6] T. Le Guenan and J. Rohmer. Corrective measures based on pressure control strategies for CO₂ geological storage in deep aquifers. *International Journal of Greenhouse Gas Control*, 2010.
- [7] T. Manzocchi, J.N. Carter, A. Skorstad, B. Fjellvoll, K.D. Stephen, JA Howell, J.D. Matthews, J.J. Walsh, M. Nepveu, C. Bos, et al. Sensitivity of the impact of geological uncertainty on production from faulted and unfaulted shallow-marine oil reservoirs: objectives and methods. *Petroleum Geoscience*, 14(1):3–11, 2008.
- [8] J.D. Matthews, J.N. Carter, K.D. Stephen, R.W. Zimmerman, A. Skorstad, T. Manzocchi, and J.A. Howell. Assessing the effect of geological uncertainty on recovery estimates in shallow-marine reservoirs: the application of reservoir engineering to the SAIGUP project. *Petroleum Geoscience*, 14(1):35–44, 2008.

- [9] J.P. Nicot. Evaluation of large-scale CO₂ storage on fresh-water sections of aquifers: an example from the Texas Gulf Coast Basin. *International Journal of Greenhouse Gas Control*, 2(4):582–593, 2008.
- [10] C. Oldenburg. Comments on Economides and Ehlig-Economides,"Sequestering carbon dioxide in a closed underground volume" SPE 124430, October 2009. 2010.
- [11] J. Rutqvist, J. Birkholzer, F. Cappa, and C.-F. Tsang. Estimating maximum sustainable injection pressure during geological sequestration of CO₂ using coupled fluid flow and geomechanical fault-slip analysis. *Energy Conversion and Management*, 48(6):1798–1807, 2007.
- [12] J. Rutqvist and C.F. Tsang. A study of caprock hydromechanical changes associated with CO₂ injection into a brine formation. *Environmental Geology*, 42:296–305, 2002. 10.1007/s00254-001-0499-2.
- [13] L.G.H. van der Meer. Investigations regarding the storage of carbon dioxide in aquifers in the Netherlands. *Energy Conversion and Management*, 33(5-8):611–618, 1992.
- [14] L.G.H. van der Meer. The conditions limiting CO₂ storage in aquifers. *Energy Conversion and Management*, 34(9-11):959–966, 1993.

Paper V

3.5 Geological storage of CO₂: global sensitivity analysis and risk assessment using the arbitrary polynomial chaos expansion

M. Ashraf, S. Oladyshkin, W. Nowak

Submitted to the special issue of *International Journal of Greenhouse Gas Control (IJGGC)*

Geological storage of CO₂: global sensitivity analysis and risk assessment using the arbitrary polynomial chaos expansion

Meisam Ashraf^{a,b}, Sergey Oladyshkin^c, Wolfgang Nowak^c

^a*Department of Mathematics, University of Bergen, 5028 Bergen, Norway*

^b*SINTEF ICT, Department of Applied Mathematics P.O. Box 124 Blindern, N-0314 Oslo, Norway*

^c*SRC Simulation Technology, Institute for Modelling Hydraulic and Environmental Systems (LH2), University of Stuttgart, Pfaffenwaldring 61, 70569 Stuttgart, Germany.*

Abstract

Geological storage of CO₂ is a proposed interim solution for mitigating the climate change. The considerable costs and potential hazards of the technique require feasibility studies to assess all possible risks involved in the process. Modeling CO₂ storage requires working with large time and space scales, which in practice are accompanied by huge geological uncertainties.

The overall goal of this study is to demonstrate the application and feasibility of global sensitivity analysis with Sobol indices and probabilistic risk assessment via the very recent arbitrary polynomial chaos expansion (aPC) method. We model a typical CO₂ injection scenario implemented in realistic geological realizations. A number of uncertain parameters control the structural heterogeneities with assumed probability distributions. These parameters include the effect of barriers, the aggradation angle, fault transmissibility and regional groundwater effects. They represent realistic types of structural features that have not been analyzed before in this context and manner.

Within the aPC, a so-called response surface is representing how the model output changes with respect to the uncertain parameter values by multi-variate polynomials for all output quantities of interest. We choose the aPC, because the resulting response surface is significantly faster than the full original model, and so facilitates global sensitivity analysis and probabilistic risk assessment even for

Email addresses: meisam@resman.no (Meisam Ashraf),
Sergey.Oladyskin@iws.uni-stuttgart.de (Sergey Oladyshkin),
Wolfgang.Nowak@iws.uni-stuttgart.de (Wolfgang Nowak)

large problems.

Quantification of input parameter uncertainty is not the primary concern of this work, as it can change from one place to another. Therefore, no generalized conclusions on the reality of geological uncertainties can be drawn from this study.

Keywords:

CO₂ storage, Global sensitivity analysis, Probabilistic risk assessment, Uncertainty quantification, Arbitrary polynomial chaos, Sobol indices

1. Introduction

In the context of climate change mitigation, geological storage of CO₂ has been proposed as interim solution. The idea has been challenged during the last decades for its costs and potential hazards [1, 2]. A large number of studies has been performed in the industry and research communities to evaluate the safety and feasibility of CO₂ storage, addressing issues such as the status and barriers of CO₂ storage [3], screening and ranking of geological storage sites [4], large-scale impacts of CO₂ injection in deep saline aquifers [5], new solution methodologies for CO₂ leakage [6], the capture project [7], and leakage estimates [8]. Furthermore, many pilot projects have been installed, like In Salah [9], Ketzin [10], and Johansen [11]. A discussion on the experiences from the existing pilot projects is reported in [12].

Yet, there is a big demand for studies which demonstrate the appropriateness of the storage operation. Transparent scientific results are required to communicate the facts and evidences about feasibility and possible risks within public and industry. The large involved time and space scales, however, cause substantial computational issues in such studies (e.g., [13]), and the modeling procedure is accompanied by a huge extent of geological uncertainties (e.g., [14, 15, 16, 17]).

In an approach to quantify the impact of geological heterogeneity on model predictions of multiphase flow in geological formations, a large number of shallow marine depositional realizations has been generated and used in the sensitivity analysis of the impact of geological uncertainties on production forecasting (SAIGUP), see [18, 19, 20]. There, the impact of variable geological parameters has been quantified for oil recovery in different field development scenarios. The main general conclusion of that study is that realistic features of geological uncertainty in modeling (other than typical hydrological parameters) can lead to considerable uncertainties in prediction. Ashraf et al. [21, 22] used a number of SAIGUP realizations to study the impact of geological heterogeneity on the

injection and early migration of CO₂ in a shallow-marine aquifer with a complex, heterogeneous geological structure. That study transferred the significance of some of the geological structural features to the case of CO₂ injection.

In practice, modeling complicated physical phenomena in the subsurface requires stochastic approaches. Uncertainty can exist in different levels, from the formulation of dependency rules in the model to uncertainty about appropriate values for the model input parameters. Uncertainty coming from any source in the modeling procedure propagates through the model to the predicted responses. Ranking the important model parameters based on their influence on the model responses can support a better understanding of the system, and it can result in a better design of subsequent studies on the stochastic nature of the process. Hence, identifying and evaluating the sensitivities and uncertainties of model parameters and their impact on prediction uncertainties and projected risks is a significant task. Sensitivity analysis is known to be the right approach to identify the significance of uncertainty sources within the modeling process [23] and to improve the understanding of model behavior [24]. For example, the European Commission and the United States Environment Protection Agency recommend using sensitivity analysis in the context of extended compact assessment for policy making [25].

Uncertainty sources within the CO₂ storage problem can be classified in different types as geological, physical and operational uncertainties. This work is devoted to geological uncertainties. However the same procedure can be applied to extend the work for other types as well. Here, we use a set of SAIGUP realizations to perform a sensitivity analysis and to assess the risks caused by uncertainties in a choice of parameters that govern the geological structure of the featured shallow-marine deposit.

The goal of this study is to test and demonstrate the applicability of a recent set of methods to a realistic scenario. We choose a stochastic response surface method to project the model response to parameter changes onto high-dimensional polynomials via the arbitrary polynomial chaos expansion (aPC) [23, 26]. Highly similar ideas to the aPC have also been proposed in other scientific areas [27, 28, 29, 30]. As we review in Section 2, the involved orthogonal polynomial basis can be constructed for arbitrary probability distributions of the uncertain parameters. This data-driven approach provides fast convergence [23] in comparison to the classical polynomial chaos expansion (e.g., [31, 32, 33]). Moreover, it avoids the subjectivity of data treatment that would arise when being forced to fall back onto a limited number of theoretical distributions that can be tolerated with previous generalized versions of polynomial chaos expansions [34, 35]. The reduced

model represented by the response surface is significantly faster than the original complex one, and thus provides a promising starting point for global sensitivity analysis, uncertainty quantification, and probabilistic risk assessment.

In the current paper, we use global sensitivity analysis rather than a local one, because local analysis fails to cover the non-linear variation of model responses over the entire range of probability distributions of the input parameters. A practical approach in global sensitivity analysis is to work with the impact of uncertain parameters on prediction variances, because this shows a good success in nonlinear problems [36]. In the current study, we use Sobol indices [24] for sensitivity analysis, which are indeed working with variances. The fact that the aPC based response surface is based on orthonormal polynomials with exploitable known properties [37] substantially simplifies this analysis.

Finally, we perform risk analysis by applying a Monte-Carlo procedure to the response surface. The approximating polynomial is fast enough to be used for a large number of Monte-Carlo realizations. This makes it possible to cover the entire range of variations in the model input described by the assigned probability distributions, and thus provides accurate estimates for the risk in the system. We conclude with a discussion of the results.

The global sensitivity analysis and uncertainty quantification studies for CO₂ storage existing in the literature are concerned with classic hydrological uncertain parameters like porosity, pore volume and permeability as global constants (see for example [15, 26, 38]). To the best of our knowledge, the current study is the first one that implements the proposed mathematical analysis tools on realistic geological structural parameters at reservoir scale. The parameters we consider are the level of barriers presence, aggradation angle, fault transmissibility, and regional groundwater effects. The considered features are the structural and depositional features that dictate the distribution of hydrological parameters such as permeability and porosity, both in terms of value and spatial distribution. These are among the most uncertain geological parameters identified with the SAIGUP study (except the regional groundwater effect, which is specific to this study).

2. Response surface via arbitrary polynomial chaos expansion

Working with uncertain parameters in complex, non-linear and dynamic systems puts a high demand on stochastic tools to analyze the system and to propagate uncertainties through the system. Conceptually straightforward numerical Monte Carlo (MC) techniques are computationally demanding since the statistical accuracy of their predictions depends on the number of realizations used. The

Monte-Carlo estimation error (measured as standard deviation) for output statistics typically decreases only with the square root of the number of realizations used. Using a stochastic response surface is a promising approach in this respect.

Obviously, a response surface can be constructed in different ways, e.g. it can be constructed directly on a dense Cartesian grid of input parameters at extremely high computational efforts. In the current paper, we apply an alternative methodology which demands only a minimum number of model evaluations to construct the response surface. This approach is based on the theory of polynomial chaos expansion (PCE) introduced in [31]. Generally, all PCE techniques can be viewed as an efficient approximation to full-blown stochastic modeling (e.g., exhaustive MC). The basic idea is to represent the response of a model to changes in variables through a response surface that is defined with the help of an orthonormal polynomial basis in the parameter space. In simple words, the dependence of model output on all relevant input parameters is approximated by a high-dimensional polynomial. The resulting polynomials are functions of the model parameters. This projection can be interpreted as an advanced approach to statistical regression.

The PCE offers an efficient and accurate high-order way of including non-linear effects in stochastic analysis (e.g., [39, 40, 41]). One of the attractive features of PCE is the higher-order in uncertainty quantification, e.g., [32, 33, 42], as well as its computational speed when compared to other methods for uncertainty quantification performed on the full model, such as MC [43]. Due to its elegant reduction of models to polynomials, it allows performing many tasks analytically on the expansion coefficients. Alternatively, it allows performing excessive MC on the polynomials since they are vastly faster to evaluate than the original model.

Unfortunately, the original PCE concept [31] is optimal only for Gaussian distributed input parameters. To accommodate for a wide range of data distributions, a recent generalization of PCE is the arbitrary polynomial chaos (aPC [26]). Compared to earlier PCE techniques, the aPC adapts to arbitrary probability distribution shapes of input parameters and, in addition, can even work with unknown distribution shapes when only a few statistical moments can be inferred from limited data or from expert elicitation. The arbitrary distributions for the framework can be either discrete, continuous, or discretized continuous. They can be specified either analytically (as probability density/cumulative distribution functions), numerically as histogram or as raw data sets. This goes beyond the generalization of PCE in methods such as the generalized polynomial chaos (gPC) or the multi-element gPC (ME-gPC) [34, 35]. The aPC approach provides improved convergence in comparison to classical PCE techniques, when applied

to input distributions that fall outside the range of classical PCE. A more specific discussion and review of involved techniques will follow in Sections 2.1 to 2.3.

With an introduction to response methods via the aPC, we describe here the theoretical background that we use in our modeling procedure. The related techniques for sensitivity and risk analysis used in this work are explained in Sections 4 and 5.

2.1. Definitions and polynomial chaos expansion

Suppose that we approximate a problem by a functional Υ , which represents the model responses Γ for the input variables Θ :

$$\Gamma \approx \Upsilon(\Theta). \quad (1)$$

Like all PCE methods, the aPC is a stochastic approach to approximate the response surface. Considering the uncertainty in the input variables, the aPC constructs a set of polynomial basis function and expands the solution in this basis. Thus, the response vector Γ in Eq. (1) can be approximated by [23]:

$$\Gamma \approx \sum_{i=1}^{n_c} c_i \Pi_i(\Theta). \quad (2)$$

Here, n_c is the number of expansion terms, c_i are the expansion coefficients, and Π_i are the multi-dimensional polynomials for the variables $\Theta = [\theta_1, \dots, \theta_n]$, and n is the considered number of modeling parameters. If the model response $\Gamma(\Theta)$ depends on space and time, then so do the expansion coefficients c_i .

The number n_c of unknown coefficients c_i results from the number of possible polynomials with total degree equal to or less than d . This number depends on the degree d of the approximating polynomial, and the number of considered parameters n :

$$n_c = \frac{(d+n)!}{d!n!}. \quad (3)$$

2.2. Data-driven orthonormal basis

All polynomials Π_i in expansion (2) are orthogonal, i.e., they fulfill the following condition:

$$\int_{I \in \Omega} \Pi_l \Pi_m p(\Theta) d(\Theta) = \delta_{lm}, \quad (4)$$

where I is the support of Ω , δ is the Kronecker symbol, and $p(\Theta)$ is the probability density function for the input parameters. We obtain the orthonormal basis

with the moments-based method proposed in [23, 26]. Orthonormality has the advantage that many subsequent analysis steps are accessible to relatively simple analytical solutions.

Knowledge on variability never is so perfect such that we could express the probability of model parameter values in a unique distribution function. Available data are mostly scarce, and fitting a density function to observed frequencies is often biased by subjective choices of the modeler. Oladyshkin et al. [26] argued that, with aPC, it is possible to use available probabilistic information with no additional formal knowledge requirements for their probability distributions, only based on the statistical moments of the available data. They showed that, it is possible to calculate estimates for the mean, variance, and higher order moments of the model response $\Gamma(\Theta)$ even with incomplete information on the uncertainty of input data, provided in the form of only a few statistical moments up to some finite order.

2.3. Non-intrusive determination of the coefficients

The next task is to compute the coefficients c_i in Eq. 2. Generally, all PCE techniques can be sub-divided into intrusive [44, 45, 46] and non-intrusive [43, 47, 48, 49] approaches, i.e., methods that require or do not require modifications in the system of governing equations and corresponding changes in simulation codes. The challenge in choosing between the methods is to find a compromise between computational effort for model evaluations and a reasonable approximation of the physical processes by the interpolation.

For our study, we prefer the probabilistic collocation method (PCM: see [26, 43, 49]) from the group of non-intrusive approaches like sparse quadrature [50, 51, 52, 53]. In a simple sense, PCM can be interpreted as a smart (mathematically optimal) interpolation and extrapolation rule of model output between and beyond different input parameter sets. It is based on a minimal and optimally chosen set of model evaluations, each with a defined set of model parameters (called collocation points). For this reason, the collocation approach became more popular in the last years. Also, the collocation formulation does not require any knowledge of the initial model structure. It only requires knowledge on how to obtain the model output for a given set of input parameters, which allows treating the model like a “black-box”. The distinctive feature of non-intrusive approaches is that any simulation model can be considered a “black-box”, i.e. commercial software can be used without any modifications required.

According to [54], the optimal choice of collocation points corresponds to the roots of the polynomial of one degree higher ($d + 1$) than the order used in the

chaos expansion (d). This choice adapts the position of collocation points to the involved distribution shape, and is based on the theory of Gaussian integration (e.g., [55]). For one-dimensional problems (i.e., when analyzing only one uncertain model parameter), it allows exact numerical integrations of order $2d$ given $d + 1$ values of the function to be integrated.

For multi-parameter analysis, the number of available points from the corresponding Gaussian integration rule is $(d + 1)^n$, which is larger than the necessary number M of collocation points. The minimum value of M is equal to the number of coefficients n_c in Expansion (2), according to Eq. (3). The full tensor grid can be used only for low-order (1^{st} , 2^{nd}) analysis of few parameters. For higher-order analysis of many parameters, the tensor grid suffers from the curse of dimensionality (a full tensor grid in n dimensions requires $(d + 1)^n$ points, which rises exponentially in n) [56]. In that case, a smart choice of a sparse subset from the tensor grid becomes necessary. Then, PCM chooses the minimum required number of collocation points, equal to the number of coefficients n_c , from the full tensor grid according to their probability weight, i.e. according to their importance as specified by the available probability distribution of Θ . This simply means to select the collocation points from the most probable regions of the input parameter distribution (see [43]).

The weighted-residual method in the random space is defined as [49]:

$$\int (\Gamma - \sum_{i=1}^{n_c} c_i \Pi_i(\Theta)) w(\Theta) p(\Theta) d\tau = 0, \quad (5)$$

where $w(\Theta)$ is the weighting function and $p(\Theta)$ is the joint probability density function of Θ . Please note that choosing $w_i = \Pi_i$ in Eq. 5 results in the method discussed by [32] and [33]. In PCM, the weighting function is chosen as the delta function:

$$w(\Theta) = \delta(\Theta - \Theta_c). \quad (6)$$

Θ_c is the set of collocation points. Substituting from Eq. (6) into Eq. (5) gives the following:

$$\Gamma_c - \sum_{i=1}^{n_c} c_i \Pi(\Theta_c) = 0, \quad (7)$$

where Γ_c are the response values corresponding to the collocation values Θ_c . We solve Eq. (7) to find the coefficients c_i .

Hence, in total, n_c detailed runs are required to determine the n_c unknown coefficients. The roots of the data-driven polynomial basis (see Section 2.2) define

the positions of the collocation points specific to the distribution of input parameters at hand and, thus, indicate the optimal parameter sets for model evaluation, using all available information about the input parameters. In our study, we have $n = 4$ uncertain parameters and we use a polynomial of degree $d = 2$. This means that only $n_c = 15$ detailed runs are necessary to obtain the expansion coefficients and approximate the response surface.

3. CO₂ storage problem

Here, we describe the injection scenario for which we analyze sensitivities, uncertainties, and risks in Sections 4 and 5. The same flow responses are studied here as in [21, 22]. These are aquifer pressure, CO₂ mobile and residual volumes and leakage risk as described below. Then, we describe the uncertain parameters considered in the study followed by a discussion on the uncertain structural aspects of the considered geological settings.

3.1. Modeling scenario

A typical scenario of CO₂ injection is defined in which a volume of $40 \times 10^6 \text{ m}^3$ is injected via one well during an injection period of 30 years. This volume corresponds to 20% of the total aquifer pore volume. After stopping injection, simulation continues for 70 years to study the early migration of the CO₂ plume. For brevity, we omit the detailed model equations here and refer the interested reader to [23, 26].

In our scenario, we feature an aquifer system that is formed by shallow-marine deposits. There is one closed boundary on the top side of the model and the other sides are assumed to be open (Figure 1). All the open boundaries are modeled as Dirichlet boundaries, two of which with hydrostatic pressure distribution (the right and bottom boundaries in Figure 1). The remaining left boundary is also hydrostatic, but modified in order to account for the regional groundwater effect (see below).

The cells on the faces of the open boundaries are equipped with a very large pore volume multiplier, such that they numerically represent a much larger volume and effectively enlarge the domain. This helps to minimize the boundary effects of a computational domain that would otherwise be relatively small compared to the injected CO₂ volume (about 20% of the total pore volume, see above). The pore volume multiplier technique allows for a physically reasonable pressure build-up close to the boundary. Moreover, this allows the CO₂ that has left the domain to re-enter by gravity segregation after the injection has stopped.

A summary of the used parameter values is given in Table 1. The hydrological parameters like permeability and porosity vary within individual realizations due to the considered geological structure (see Figure 2 for the histograms of porosity and permeability in one selected realization). They also differ between the different realizations, as they are changed to represent different geological features. Although the geological realizations of this model vary in some geological features, but the same total pore volume, grid, and fault geometry is considered. The injection well is screened in the lower part of the model.

3.2. Analyzed model predictions

We seek to maximize the CO₂ storage volume and minimize the risk of leakage. These quantities are measured by various simulation outputs that are described in Table 2 and discussed in the following.

Aquifer pressure is considered as the spatial average of the pressure distribution in the domain, weighted by the pore volume of each rock type. Monitoring or predicting the pressure response is important to avoid over-pressurized injection operations.

Residual CO₂ volume is the volume of trapped CO₂ that is left in the small pores in an imbibition process. This volume is crucial for the long-term storage capacity of reservoirs.

Mobile CO₂ volume is the volume of CO₂ that can move in a continuous phase in the medium. It is considered as one of the important flow responses, because only mobile CO₂ volumes can lead to leakage through any failure in the sealing cap-rock or ill-plugged well.

Finally, we consider **leakage risk** through cap-rock failure. Cap-rock integrity is a major concern for the safety of CO₂ storage operations. An over-pressurized injection can lead to fractures that may extend up to the cap-rock, penetrate through the cap-rock, or activate pre-existing faults and fractures, and finally lead to CO₂ leakage. In addition, the capillary barrier effect of the cap-rock can be overcome by a local pressure build-up. Thus, the probability of cap-rock failure can depend on the geomechanical properties of the cap-rock and of the medium, on the topography of the cap-rock, and on the pressure build-up resulting from the CO₂ injection and migration. More details about failure mechanisms and failure criteria can be found in the literature (e.g., [57, 58, 59]). However, geomechanical modeling and knowledge about pre-existing features that can be activated during injection would be required to take these processes into account.

Here, we demonstrate how cap-rock integrity can be considered in the workflow of sensitivity analysis and uncertainty assessment in a simplified manner.

To avoid detailed studies of multiphase flow coupled with geomechanical simulations and fracture mechanics, we follow a pragmatic approach. The idea is to assign a spatial probability distribution of cap-rock failure over the area of the cap-rock layer, such that each point of the cap-rock has its own failure probability. In principle, this probability could be assigned in correspondence with the current pressure distribution and with geological features such as varying cap-rock thickness, material properties, faults and fractures. For the means of demonstration, we simply assign a spatial Gaussian function as a scenario assumption to provide the cap-rock failure probability for each point of the cap-rock (see Figure 3). Leakage risk is defined as the probability of leakage (due to cap-rock failure) times the amount of escaping CO₂ in case of leakage. Thus, we spatially integrate the product between cap-rock failure probability and the volume of mobile CO₂ below each point of the cap-rock over the entire area of the cap-rock.

3.3. Uncertain parameters

The most apparent uncertainty in CO₂ storage is the lack of geological knowledge. Large geological scales and diversity of rock properties make it impossible to obtain the whole descriptive picture for a study. A geological study will therefore be accompanied by huge levels of uncertainty. Many studies have shown the significance of geological heterogeneity on underground flow performance (e.g., [60, 61]). To obtain a descriptive image of a feature, like faults and depositional structure, such that uncertainty can be reduced, we must provide adequate data. The process of data collection from underground layers is very costly, therefore it is important to know the ranking of influence each feature has on the flow in order to optimize the cost of data acquisition in modeling.

From the geological parameters that are relevant for shallow-marine deposits used in [21, 22], we pick three parameters: the degree to which barriers may block horizontal and vertical flow, aggradation angle, and fault transmissibility. In addition to these, we consider the regional groundwater effect as an uncertain parameter in our study. Here, we give a brief description on each one, followed by the probabilities assigned to these parameters.

Barriers: During the formation of shallow-marine deposits, periodic floods result in a sheet of sandstone that dips, thins, and fines in a seaward direction. In the lower front, thin sheets of sandstone are inter-bedded with the mud-stones deposited from suspension. These mud-draped surfaces are potential significant barriers to both horizontal and vertical flow. In the SAIGUP realizations, these barriers were modeled by transmissibility multipliers in specific layers of the for-

mation. The position of the barriers is generated by creating an elliptic cone-shaped surface that follows the plan-view shoreline shape of the facies, characterized from real world data [18]. We define the degree of barrier presence by the areal percentage of zero-valued transmissibility multipliers. Figure 5 shows a medium level of barriers.

Aggradation angle: in shallow-marine systems, two main factors control the shape of the transition zone between river and basin: the amount of deposition supplied by the river and the accommodation space that the sea provides for these depositional masses. Deposition happens in a spectrum from larger grains depositing earlier on the land side, to fine deposits happening in the deep basin. If the river flux or sea level fluctuates, equilibrium changes into a new bedding shape based on the balance of these factors. In the SAIGUP study, progradational cases are considered, in which river flux increases and shifts the whole depositional system into the sea. The angle at which transitional deposits are stacked on each other because of this shifting is called the aggradation angle. Three levels of aggradation are shown in Figure 4: low, medium and high. The study reported in [21, 22] showed that aggradation can have a dramatic influence on the injection and migration process.

Fault transmissibility: Huge uncertainties can be involved when modeling the presence of faults. Faults are discrete objects that are modeled by changing the geometry of the simulation grid. The transmissibility for flow across faults changes during the process of faulting. This causes a spectrum of transmissibilities, from a sealing fault with no flow across it, to a fault that has not produced any barriers to the flow within its opening space.

Within a simulation grid, the influence of faults on the local and global flow behavior depends on a number of parameters including fault length, orientation, intensity and transmissibility. The well location with respect to the faults can change the overall behavior of injected CO₂ plume significantly. In the SAIGUP models, different levels of fault orientations, transmissibility, areal intensity, and well patterns are considered. For this study, we consider all fault modeling parameters at their medium level and consider to vary only the fault transmissibility. These variations, however, do not affect the definition of the no-flow boundary, which is motivated by the presence of an impermeable fault.

The used geology realizations contain compartmentalized fault systems comprising approximately equal densities of strike-parallel and strike-perpendicular faults based on a portion of the Gullfaks field [18, 62]. Figure 6 shows the fault pattern and location of the injector considered for the study.

It is shown in [63] that the transmissibility multiplier provides a numerically

more robust representation of faults within reservoir simulation than conventional permeability multipliers. We consider the fault transmissibility multipliers to range between zero and one. A multiplier value of one corresponds to a fault permeability equal to the harmonic average of cell permeabilities across the fault, i.e., to a fault without any influence on flow [63].

Regional groundwater effect: Geological modeling always comes with the uncertainty of how large the aquifer is and how it is connected to other underground aquifers. This is a direct consequence of the need to define boundary conditions to limit the computational domain, which cannot always coincide with meaningful physical boundaries in large-scale systems. However, connections to active external aquifers can be accounted for by adapting the values for the boundary conditions accordingly. Some connections might even change throughout the year, depending on rainfall. The flux across model boundaries might influence the CO₂ plume dynamics during and after injection. To simulate such effects, we changed the left boundary pressure by adding an uncertain additional pressure value Δp that varies between 0 and 100 bars.

As a scenario assumption, this pressure value is added at the start of injection, i.e., the pressure distribution is not at a steady state when the simulation starts, and this triggers a corresponding transient brine flow. We do so in order to analyze the effect of transient groundwater effects on the system. This may seem an arbitrary choice, but assuming a steady-state would also be arbitrary to some extent.

The overall process for sensitivity analysis, uncertainty propagation, and risk assessment starts by specifying probability information for the uncertain parameters. Next, one has to design and choose the simulation cases required to obtain the expansion coefficients in the approximating polynomial. However, in our study, we had access to the set of SAIGUP geological realizations and simulation results that had been designed without the considerations possible with the aPC. The computing time for each SAIGUP realization was about 2 hours on a 2.4GHz Intel Xeon CPU, and we decided to recycle these highly expensive simulations in our study. The large computing times are a key motivation to build a cheaper surrogate model for further analysis. Hence, we assume the histograms of uncertain parameters such that they result in collocation points that coincide with the SAIGUP designed values. Therefore, the histograms used in this study are almost uniform, as shown in Figure 7. In fact, these input distributions could also be handled with the gPC method already mentioned in the introduction, and would correspond to the use of Legendre polynomials. In our case, we use the aPC to avoid the step of modeling the input distributions as exactly uniform. Consequently, the polynomials resulting from the aPC approach are very close to Legendre polynomials.

The aPC, however, could be used for any type of histograms and so provides the freedom in other studies to adapt to arbitrary input statistics.

The main concern here is not a unique probability description of the input geological parameters, but rather we perform an uncertainty analysis practice, relying on a scenario assumption of probability distributions. Thus, no general geological conclusion is expected from this study, and results might change by feeding the work-flow with a different probability description.

4. Sensitivity analysis

In this section, we tackle global sensitivity analysis with Sobol indices based on the aPC technique, following the line of work on aPC by [23, 26, 37]. The big advantage of global aPC-based sensitivity analysis is that one can obtain global sensitivity information at computational costs that are hardly larger than those for local analysis. The reason is the following: local methods use infinitesimally small spacing between parameter sets for model evaluation to get numerical derivatives evaluated at a single point. The aPC-based method places the parameter sets for model evaluation at an optimized spacing in parameter space. This can be interpreted as fitting secants (or polynomials for non-linear analysis) to the model response. These secants (polynomials) approximate the model over the entire parameter space in a weighted least-square sense (compare with the best unbiased ensemble linearization approach described by [64]). This is more beneficial compared to computing a tangent or local second derivatives (compare FORM, SORM methods, e.g., [65]) that approximate the model well just around one point in the parameter space.

The system featured here is non-linear due to two reasons: First, the involved multi-phase flow equations [26] form a coupled system of non-linear partial differential equations, and second, these equations are non-linear in their coefficients. The latter is even more significant if parameters are spatially heterogeneous.

In the following, we briefly summarize the Sobol sensitivity indices technique for quantifying the relative importance of each individual input parameter in the final prediction. Then, we implement the method for our geological CO₂ storage problem, based on the aPC response surface.

The model responses featured here for global sensitivity analysis (this section) and for the probabilistic risk analysis (see Section 5) are listed in Table 2 and have been discussed in Section 3.1. In the sense of global sensitivity analysis [66], not only should the analysis technique be global, but also should the analyzed quantities be global. In the latter, global refers to the fact that they are relevant for the

engineer, are crucial in decision processes, etc. For example, an overall leakage risk is more informative in final decisions than the leakage rate at a specific point, and a total stored volume of CO₂ is more informative for volumetric efficiency considerations of the reservoir than the CO₂ saturation at individual points.

4.1. Sobol sensitivity indices

The method is well described in the literature [24, 36, 66, 67]. More recent works are concerned about expediting calculation pace by computing Sobol indices analytically from polynomial chaos expansions [26, 33, 37, 68, 69]. The idea behind the combination of PCE techniques with Sobol indices is to replace the analyzed system with an approximating function which leads to mathematical and numerical benefits in the sensitivity analysis.

Using polynomials for this approximation is convenient, because it is easy to analytically obtain the output variances from the statistics of the input variables of the polynomials. In our case, the solution is approximated by orthogonal polynomials with ascending polynomial degree. We expand the variance of model output into individual components originating from all possible combinations of input parameters. Assume that we break the system output into components as follows:

$$\Gamma = \Gamma_0 + \sum_i \Gamma_i + \sum_{i < j} \Gamma_{ij} + \dots \quad (8)$$

A single index (here: i) shows dependency to a specific input variable. More than one index (e.g.: i and j) shows interaction of two or more input variables. If we consider the input vector Θ to have n components θ_i for $i = 1, \dots, n$, then $\Gamma_i = f_i(\theta_i)$ and $\Gamma_{ij} = f_{ij}(\theta_i, \theta_j)$. In practice, we stop at a finite number of terms in Eq. (8). The first order sensitivity index, the so called Sobol index, is defined statistically as follows [66]:

$$S_i = \frac{V[E(\Gamma | \theta_i)]}{V(\Gamma)}, \quad (9)$$

where $E(\Gamma | \theta_i)$ is the conditional expectation of output Γ for a given value of θ_i and V is the variance operator. In plain words, S_i is the fraction of total variance $V(\Gamma)$ that can be explained by the parameter θ_i . Since θ_i can be fixed at any value in its uncertainty interval, each of those values produces a distinct expectation. In Eq. (9), the variance of those expectations is divided by the unconditional variance

of output (i.e., with no input variable fixed). For more than one index, a higher-order Sobol index can be defined as:

$$S_{ij} = \frac{V[E(\Gamma | \theta_i, \theta_j)] - V[E(\Gamma | \theta_i)] - V[E(\Gamma | \theta_j)]}{V(\Gamma)}. \quad (10)$$

Here, $V[E(\Gamma | \theta_i, \theta_j)]$ is the variance of output expectations after fixing θ_i and θ_j . This index represents the significance of variation in output generated from the joint uncertainty in several input variables, i.e., from the interaction of uncertain parameters. If we add all indices that contain a given variable θ_i , the sum is called the total Sobol index:

$$S_{Ti} = S_i + \sum_{j \neq i} S_{ij} + \sum_{j \neq i} \sum_{k \neq i} S_{ijk} + \dots \quad (11)$$

The total Sobol index is a sensitivity measure to rank parameters according to their influence on the model results. When this index is close to zero, the corresponding parameter has a negligible role in the variation of the system response. In that case, the uncertainty in that parameter does not introduce a considerable uncertainty in the response, and the parameter could be omitted from further analyses.

In practice, we evaluate the Sobol indices analytically from the expansion coefficients of the aPC as described by [37].

4.2. Sensitivity analysis

We calculate the total Sobol indices for the geological CO₂ storage problem that is described earlier. The results are based on an aPC expansion of order two that is obtained by fifteen detailed simulations. The choice of order two is supported by the results of [43], where the authors found in a similar CO₂ storage problem that second order may be the cheapest non-linear expansion, but still sufficiently accurate for this type of purpose. Recently, [37] provided the results of a numerical convergence analysis for aPC-based Sobol analysis. They report that increasing the expansion order beyond 2 introduces only small changes to the sensitivity values for their considered system, and does not change the ranking of the analyzed parameters anymore. A study similar to the current study without aPC needed one hundred and sixty runs to perform a sensitivity analysis with a different method [22]. The pattern of sensitivity reported here is similar to what is produced in that study, but at dramatically reduced costs.

4.3. Results

The flow behavior in the domain is influenced by the type and intensity of different heterogeneities. This influence can be traced in the CO₂ pressure and saturation distributions over time. During injection, viscous forces imposed by the injector dominate the force balance. Viscous forces act in the form of spatial pressure gradients in all directions. After 30 years, the injection stops, and gravity starts playing the major role in the flow dynamics, acting in the vertical direction [21, 22].

Barriers and aggradation angle have different impacts on the flow during each flow regime, i.e., injection or after injection. Low fault transmissibility hinders the flow and keeps the pressure in compartments. Geometry distortion in the geological layers because of the faulting processes plays a considerable role in the splitting of CO₂ plumes within the domain. Water flux from lateral boundaries due to the regional groundwater effect enhances the spread of CO₂ and leads the mass of CO₂ toward the other open boundaries.

Figure 8 shows the sensitivity of different responses to the uncertain parameters. Total Sobol indices are plotted at specific times. End of simulation refers to the year 100, i.e., 70 years after injection stops. This time duration is long enough for the flow to stabilize at a stationary condition for the majority of the model runs.

As already observed in [21, 22], the aggradation angle plays a significant role in the flow behavior. In cases with low aggradation angle, the stratigraphy of rock types is a pattern of parallel layering. For higher aggradation angles, rock-types are distributed between more modeling layers. The effective vertical permeability changes from the harmonic average (in Figure 9a) toward the arithmetic average (in Figure 9c), as the aggradation angle increases from 0 to 90 degrees. The harmonic average might be much smaller than the arithmetic average, in particular when there are vertically impermeable rock-types in the medium. The shallow marine depositional system contains some rock-types with almost zero transmissibility in the vertical direction. Therefore, a low aggradation angle can hinder the flow from traveling upward across layers in the domain and force it to stay trapped in some lower layers, as seen for many of the low aggradation angle realizations in our study. The relatively large sensitivities to the level of barrier presence is based on the same effects.

Our results show a relatively weak sensitivity of responses with respect to the water influx from one side of the model. This sensitivity is in particular low during injection, when the high pressure imposed from the well dominates the dynamics of flow in the medium (Figure 8a). The sensitivity patterns for the mobile and

residual CO₂ volume are similar in Figures 8b and 8c, because the mobile and residual CO₂ volume add up to the total injected CO₂ volume, with the exception of the CO₂ volume that has left the domain. Hence, they are highly dependent on each other.

More detailed results are shown in Figures 10a to 10d. Total Sobol indices are plotted for each response during the entire time interval. When the flow regime switches from injection to a gravity-dominated system, we observe a jump or sharp drop in some of the sensitivity plots (Figures 10a and 10c at 30 years).

The sensitivity of the aquifer pressure with respect to the presence of barriers jumps up, right after stopping the injection. This happens because barriers slow down the pressure release through open boundaries, resulting in local pressure build-ups.

The sensitivity of the residual CO₂ volume with respect to barriers presence drops soon after injection. This is reasonable since the residual trapped volume is more a function of lateral flow in the medium, compared to the vertical flow in the relatively small thickness of the aquifer.

5. Risk analysis

The risk R of a process is quantitatively defined as the extent of consequence C caused by the process, multiplied by the probability P of that consequence to happen:

$$R = P \times C. \quad (12)$$

The consequence can be defined by direct measures in the simulation responses, or it can be related to consequences caused in the environment outside the considered system. For example, in the case of CO₂ injection into deep aquifers, the amount of CO₂ which stays mobile and undissolved in the medium for a time after injection can be considered as a consequence, bearing the potential of leakage up to the surface if exposed to a geological leakage point. The consequence could also be defined by a criterion for external consequences, like the rate of climate change (either locally or globally) due to CO₂ leakage, the costs of pumping CO₂ that does not remain in the subsurface, or via the related costs for CO₂ emission certificates.

The other part is the probability of these consequences to happen. This depends on the stochastic behavior of the process which results in the respective outcomes.

We use the polynomial-based reduced model for risk analysis, because it is fast enough to perform a Monte-Carlo analysis with a large number (here: 10000)

of realizations on the polynomials. Thanks to the higher-order approximation via the aPC, the principal non-linear physical behavior of CO₂ storage is included in the analysis, and detailed probabilistic risk assessment becomes feasible. We analyze here the same quantities as in Section 4, i.e., average pressure, the volume of mobile or immobile CO₂, and leakage risk. For definitions, see Section 3.1.

5.1. Quantification of expected values in CO₂ storage

Average response values can be calculated analytically from the polynomial (e.g., [26]) or via the Monte-Carlo post-process as mentioned above. Figures 11a to 11d show some of the calculated expectations as functions of time. In Figure 11a, the mobile CO₂ volume increases linearly in the medium because of the constant injection rate during the first thirty years. After injection, the mobile volume of CO₂ is reduced due to the trapped volume in residual form and the migration of CO₂ across open boundaries.

Figure 11b shows the expected values for the volume of residually trapped CO₂ as a function of time. The plot shows the significance of imbibition during the plume migration period, when water replaces CO₂ that is moving upward because of gravity segregation. During injection, CO₂ invades the aquifer and drainage is dominant. Therefore, the expected residual CO₂ plot shows a smaller slope during injection than what it shows later in time.

When injection starts, a pressure pulse travels through the medium at a finite velocity because of the slight compressibility of brine. The initially built-up pressure releases through open boundaries over time and the average pressure drops in the aquifer (Figure 11c). Under realistic injection settings, an average (spatial and statistical) pressure rise of up to 400 bars (from 270 to 670 bars in the first simulation time step, not visible in Figure 11c) would be very unrealistic and would not be allowed to occur. This high pressure rise occurs because large pressure values have to be exceeded in the injection cell before CO₂ becomes mobile at saturations above the residual value.

Also, during early injection time, the pressure is larger than at the end of injection. There are a few realizations where the contributions from the external aquifer support, a dense barrier system close to 100% areal coverage, an adverse aggradation angle of the formation and extremely low fault transmissibilities interact to effectively block the CO₂ flow close to the well. This has strong effects on pressure when the rock at the injector position happens to be poorly permeable, leading to a very poor injectivity. An adapted CO₂ injection strategy would react by lowering the injection rate, by choosing a different injection position, or by even abandoning the entire site.

Based on the results of the current study, it is possible to identify such adverse combinations and guide site investigation strategies to pay attention to such situations. In a follow-up study (ready for submission), we are currently investigating an active injection strategy controlled by an upper allowable pressure limit.

However, the initial sharp pressure increase is released very quickly. This happens, when first parts of the CO₂ plume have found flow pathways into regions with better rock properties, providing the possibility to relax the pressure build-up, and also to let the CO₂ escape towards the boundaries.

The expected leakage risk is plotted in Figure 11d, and increases in value as the injected CO₂ travels upward and accumulates beneath the sealing cap-rock.

5.2. Results of CO₂ storage risk assessment

In this section, the probability distributions (rather than expected values) of system responses during and after injection are studied. Results from the MC analysis of the response surface are given as histograms of output values and also as cumulative distribution functions (CDF) for probabilities (Figures 12 and 13).

Figures 12a to 12c show the histograms of responses obtained from the Monte-Carlo process at the end of injection. A long tail is observed for lower residual and mobile CO₂ values in Figures 12b and 12c. The long tail means a large range of possible low values. Pressure shows a long tail for higher values. This means that even high critical values still have substantial probabilities to be exceeded, indicating that the possibility of geomechanical damage to sealing layers will have to receive a large attention. We observe an issue of mass conservation in Figure 12b, where a few realizations show more mobile CO₂ in the domain than the total injected volume (which is about 40×10^6 m²). This is a typical issue for a large class of statistical methods that interpolate or extrapolate simulation results in the parameter space, because their setup is not based on the mass conservation equation. In this specific case, the mass conservation issue is caused by approximating the response surface via polynomials, with vanishing residuals only at the collocation points. The polynomials are evaluated at many randomly chosen parameter sets drawn from the histograms shown in Figure 7, which do not coincide with the collocation points.

Finally, we report how the corresponding probabilities change over time in Figures 13a to 13c. High pressure buildup is considerable during the early injection time, and it is negligible after injection during plume migration (Figure 13a). An over-pressurized injection can induce fracturing in the medium, extending to the sealing layers. Any fractures caused in the structural traps can expose the mobile CO₂ to leakage paths. Therefore, higher pressure values can be interpreted

as high risk in early time. The injection scenario in this study is set to a fixed injection rate. To avoid risky pressures during the start of injection, the injector can be set on pressure control instead, by changing the injection rate in order to keep the injection pressure limited.

6. Conclusion

In this paper, we used the arbitrary polynomial chaos expansion (aPC) method in a sensitivity analysis and risk assessment process. The goal was to demonstrate the application and feasibility of aPC-based methods in the context of realistic CO₂ injection scenarios. We implemented this method for a typical CO₂ storage problem. Four uncertain parameters with assumed uncertainty distributions are considered. Injection and early migration of CO₂ is studied. The flow sensitivity to geological heterogeneity is evaluated and quantified using Sobol indices. Risk analysis is performed on the defined problem. Flow dynamics are discussed and corresponding interpretations and explanations of the sensitivity and risk results are provided.

The performance of the aPC method has been satisfactory. It is very fast, compared to other stochastic methods for low-parametric systems, and this speed-up allows us to perform an extensive Monte-Carlo process on the aPC-based response surface to calculate the probability of response values throughout simulation time. This study was a first-time application of the aPC to study a realistically complex type of geological structural uncertainty. Based on our assessment of aPC feasibility, we can strongly encourage the use of aPC for sensitivity and risk analysis in complex situations.

The results have shown that the most influential parameter for most of the responses is the aggradation angle of deposition layers of the considered shallow-marine aquifer. The least relevant parameter is the regional groundwater effect, especially during injection time. We re-iterate that the aim of this study was to demonstrate a practice of using arbitrary polynomial chaos expansion for the sensitivity and risk analysis of a typical CO₂ storage problem. Since, in general, the levels of involved input uncertainty are not unique, the physical and geological conclusions of this study are restricted to the probability assumptions taken here and should not be generalized to systems that are very different.

7. Acknowledgements

The authors would like to acknowledge the sponsors of the MatMora project defined in the University of Bergen in partnership with SINTEF-ICT and the Uni-

versity of Stuttgart, and the German Research Foundation (DFG) for financial support of the project within the Cluster of Excellence in Simulation Technology (EXC 310/1) at the University of Stuttgart. We would also like to thank the three anonymous reviewers for their constructive comments.

References

- [1] M. Lenzen, Global warming effect of leakage from CO₂ storage, *Critical Reviews in Environmental Science and Technology* 41 (24) (2011) 2169–2185.
- [2] P. Viebahn, J. Nitsch, M. Fischedick, A. Esken, D. Schüwer, N. Supersberger, U. Zuberbühler, O. Edenhofer, Comparison of carbon capture and storage with renewable energy technologies regarding structural, economic, and ecological aspects in Germany, *International Journal of Greenhouse Gas Control* 1 (1) (2007) 121–133.
- [3] S. Bachu, CO₂ storage in geological media: Role, means, status and barriers to deployment, *Progress in Energy and Combustion Science* 34 (2) (2008) 254–273.
- [4] S. Bachu, Screening and ranking of sedimentary basins for sequestration of CO₂ in geological media in response to climate change, *Environmental Geology* 44 (3) (2003) 277–289.
- [5] J. Birkholzer, Q. Zhou, C. Tsang, Large-scale impact of CO₂ storage in deep saline aquifers: A sensitivity study on pressure response in stratified systems, *International Journal of Greenhouse Gas Control* 3 (2) (2009) 181–194.
- [6] J. Nordbotten, M. Celia, S. Bachu, H. Dahle, Semianalytical solution for CO₂ leakage through an abandoned well, *Environmental Science & Technology* 39 (2) (2005) 602–611.
- [7] D. Thomas, Carbon Dioxide Capture for Storage in Deep Geologic Formations-Results from the CO₂ Capture Project, Vol. 1, Elsevier Science Ltd, 2005.
- [8] M. Celia, S. Bachu, J. Nordbotten, S. Gasda, H. Dahle, Quantitative estimation of CO₂ leakage from geological storage: Analytical models, numerical models and data needs, in: Proceedings of 7th International Conference on Greenhouse Gas Control Technologies.(GHGT-7), 2004.

- [9] F. Riddiford, I. Wright, C. Bishop, T. Espie, A. Tourqui, Monitoring geological storage the in salah gas CO₂ storage project, in: Proceedings of the 7th International Greenhouse Gas Technologies Conference, Vancouver, BC, 2004.
- [10] A. Förster, B. Norden, K. Zinck-Jørgensen, P. Frykman, J. Kulenkampff, E. Spangenberg, J. Erzinger, M. Zimmer, J. Kopp, G. Borm, et al., Baseline characterization of the CO2SINK geological storage site at Ketzin, Germany, *Environmental Geosciences* 13 (3) (2006) 145–161.
- [11] G. Eigestad, H. Dahle, B. Hellevang, F. Riis, W. Johansen, E. Øian, Geological modeling and simulation of CO₂ injection in the Johansen formation, *Computational Geosciences* 13 (4) (2009) 435–450.
- [12] K. Michael, A. Golab, V. Shulakova, J. Ennis-King, G. Allinson, S. Sharma, T. Aiken, Geological storage of CO₂ in saline aquifers—a review of the experience from existing storage operations, *International Journal of Greenhouse Gas Control* 4 (4) (2010) 659–667.
- [13] H. Class, A. Ebigo, R. Helmig, H. Dahle, J. Nordbotten, M. Celia, P. Audigane, M. Darcis, J. Ennis-King, Y. Fan, et al., A benchmark study on problems related to CO₂ storage in geologic formations, *Computational Geosciences* 13 (4) (2009) 409–434.
- [14] F. Walton, J. Tait, D. LeNeveu, M. Sheppard, Geological storage of CO₂: A statistical approach to assessing performance and risk, in: Proceedings of the 7th International Conference on Greenhouse Gas Control Technologies (GHGT-7), 2004.
- [15] S. Brennan, R. Burruss, M. Merrill, P. Freeman, L. Ruppert, A probabilistic assessment methodology for the evaluation of geologic carbon dioxide storage, *US Geological Survey Open-File Report* 1127 (2010) 31.
- [16] E. Wilson, T. Johnson, D. Keith, Regulating the ultimate sink: Managing the risks of geologic CO₂ storage, *Environmental Science and Technology* 37 (16) (2003) 3476–3483.
- [17] A. Hansson, M. Bryngelsson, Expert opinions on carbon dioxide capture and storage—a framing of uncertainties and possibilities, *Energy Policy* 37 (6) (2009) 2273–2282.

- [18] J. Howell, A. Skorstad, A. MacDonald, A. Fordham, S. Flint, B. Fjellvoll, T. Manzocchi, Sedimentological parameterization of shallow-marine reservoirs, *Petroleum Geoscience* 14 (1) (2008) 17–34.
- [19] T. Manzocchi, J. Carter, A. Skorstad, B. Fjellvoll, K. Stephen, J. Howell, J. Matthews, J. Walsh, M. Nepveu, C. Bos, et al., Sensitivity of the impact of geological uncertainty on production from faulted and unfaulted shallow-marine oil reservoirs: objectives and methods, *Petroleum Geoscience* 14 (1) (2008) 3–11.
- [20] J. Matthews, J. Carter, K. Stephen, R. Zimmerman, A. Skorstad, T. Manzocchi, J. Howell, Assessing the effect of geological uncertainty on recovery estimates in shallow-marine reservoirs: the application of reservoir engineering to the SAIGUP project, *Petroleum Geoscience* 14 (1) (2008) 35–44.
- [21] M. Ashraf, K. Lie, H. Nilsen, J. Nordbotten, A. Skorstad, Impact of geological heterogeneity on early-stage CO₂ plume migration, in: CMWR, 2010.
- [22] M. Ashraf, K.-A. Lie, H. M. Nilsen, A. Skorstad, Impact of geological heterogeneity on early-stage CO₂ plume migration: sensitivity study., in: Proceedings of ECMOR XII, 2010.
- [23] S. Oladyshkin, W. Nowak, Data-driven uncertainty quantification using the arbitrary polynomial chaos expansion, *Reliability Engineering & System Safety* 106 (2012) 179–190.
- [24] I. Sobol, Global sensitivity indices for nonlinear mathematical models and their Monte Carlo estimates, *Mathematics and Computers in Simulation* 55 (1-3) (2001) 271–280.
- [25] E. Commission, European Commission's Communication on Extended Impact Assessment, Brussels, Office for Official Publications of the European Communities, 2002.
- [26] S. Oladyshkin, H. Class, R. Helmig, W. Nowak, A concept for data-driven uncertainty quantification and its application to carbon dioxide storage in geological formations, *Advances in Water Resources* 34 (2011) 1508–1518.
doi:10.1016/j.advwatres.2011.08.005.

- [27] J. Witteveen, S. Sarkar, H. Bijl, Modeling physical uncertainties in dynamic stall induced fluid–structure interaction of turbine blades using arbitrary polynomial chaos, *Computers & Structures* 85 (11) (2007) 866–878.
- [28] J. Witteveen, H. Bijl, Modeling arbitrary uncertainties using Gram-Schmidt polynomial chaos, in: Proceedings of the 44th AIAA Aerospace Sciences Meeting and Exhibit, number AIAA-2006-0896, Reno, NV, Vol. 117, 2006.
- [29] R. Ghanem, A. Doostan, On the construction and analysis of stochastic models: characterization and propagation of the errors associated with limited data, *Journal of Computational Physics* 217 (1) (2006) 63–81.
- [30] C. Soize, R. Ghanem, Physical systems with random uncertainties: chaos representations with arbitrary probability measure, *SIAM Journal on Scientific Computing* 26 (2) (2004) 395–410.
- [31] N. Wiener, The homogeneous chaos, *American Journal of Mathematics* 60 (1938) 897–936.
- [32] R. G. Ghanem, P. D. Spanos, *Stochastic Finite Elements: A Spectral Approach*, Springer-Verlag, New York, 1991.
- [33] O. Le Maître, O. Knio, *Spectral methods for uncertainty quantification: with applications to computational fluid dynamics*, Springer, 2010.
- [34] X. Wan, G. Karniadakis, Multi-element generalized polynomial chaos for arbitrary probability measures, *SIAM Journal on Scientific Computing* 28 (3) (2007) 901–928.
- [35] D. Xiu, G. Karniadakis, The Wiener–Askey polynomial chaos for stochastic differential equations, *SIAM Journal on Scientific Computing* 24 (2) (2002) 619–644.
- [36] U. Reuter, M. Liebscher, Global sensitivity analysis in view of nonlinear structural behavior, in: Proceedings of the 7th LS-Dyna Forum, Bamberg, 2008.
- [37] S. Oladyshkin, F. P. J. de Barros, W. Nowak, Global sensitivity analysis: a flexible and efficient framework with an example from stochastic hydrogeology, *Advances in Water Resources* 37 (2012) 10–22.

- [38] A. Kovscek, Y. Wang, Geologic storage of carbon dioxide and enhanced oil recovery. i. uncertainty quantification employing a streamline based proxy for reservoir flow simulation, *Energy Conversion and Management* 46 (11) (2005) 1920–1940.
- [39] D. Zhang, Z. Lu, An efficient, high-order perturbation approach for flow in random media via Karhunen-Loeve and polynomial expansions, *Journal of Computational Physics* 194 (2004) 773–794.
- [40] J. Foo, G. Karniadakis, Multi-element probabilistic collocation method in high dimensions, *Journal of Computational Physics* 229 (5) (2010) 1536–1557.
- [41] N. Fajraoui, F. Ramasomanana, A. Younes, T. A. Mara, P. Ackermann, A. Guadagnini, Use of global sensitivity analysis and polynomial chaos expansion for interpretation of non-reactive transport experiments in laboratory-scale porous media, *Water Resources Research* (doi:10.1029/2010WR009639).
- [42] R. Ghanem, P. D. Spanos, Polynomial chaos in stochastic finite elements, *Journal of Applied Mechanics* 57 (1990) 197–202.
- [43] S. Oladyshkin, H. Class, R. Helmig, W. Nowak, An integrative approach to robust design and probabilistic risk assessment for CO₂ storage in geological formations, *Computational Geosciences* 15 (3) (2011) 565–577. doi:10.1007/s10596-011-9224-8.
- [44] R. Ghanem, P. Spanos, A stochastic Galerkin expansion for nonlinear random vibration analysis, *Probabilistic Engineering Mechanics* 8 (1993) 255–264.
- [45] G. Matthies, H., A. Keese., Galerkin methods for linear and nonlinear elliptic stochastic partial differential equations, *Computer Methods in Applied Mechanics and Engineering* 194 (2005) 1295–1331.
- [46] D. Xiu, G. E. Karniadakis, Modeling uncertainty in flow simulations via generalized polynomial chaos, *Journal of Computational Physics* 187 (2003) 137–167.

- [47] A. Keese, H. G. Matthies, Sparse quadrature as an alternative to MC for stochastic finite element techniques, *Proc. Appl. Math. Mech.* 3 (2003) 493–494.
- [48] S. Isukapalli, S., A. Roy, G. Georgopoulos, P., Stochastic response surface methods (srsms) for uncertainty propagation: Application to environmental and biological systems, *Risk Analysis* 18 (3) (1998) 351–363.
- [49] H. Li, D. Zhang, Probabilistic collocation method for flow in porous media: Comparisons with other stochastic methods, *Water Resources Research* 43 (2007) 44–48.
- [50] I. Babuška, F. Nobile, R. Tempone, A stochastic collocation method for elliptic partial differential equations with random input data, *SIAM Journal on Numerical Analysis* 45 (3) (2007) 1005–1034.
- [51] D. Xiu, J. Hesthaven, High-order collocation methods for differential equations with random inputs, *SIAM Journal on Scientific Computing* 27 (3) (2005) 1118–1139.
- [52] T. Gerstner, M. Griebel, Dimension–adaptive tensor–product quadrature, *Computing* 71 (1) (2003) 65–87.
- [53] V. Barthelmann, E. Novak, K. Ritter, High dimensional polynomial interpolation on sparse grids, *Advances in Computational Mathematics* 12 (4) (2000) 273–288.
- [54] J. Villadsen, M. L. Michelsen, Solution of differential equation models by polynomial approximation, Prentice-Hall, 1978.
- [55] M. Abramowitz, A. Stegun, I., *Handbook of Mathematical Functions with Formulas, Graphs, and Mathematical Tables*, New York: Dover, 1965.
- [56] F. Nobile, R. Tempone, C. Webster, A sparse grid stochastic collocation method for partial differential equations with random input data, *SIAM Journal on Numerical Analysis* 46 (5) (2008) 2309–2345.
- [57] P. Zweigel, L. Heill, Studies on the likelihood for caprock fracturing in the sleipner CO₂ injection case, Tech. rep., Sintef Petroleum Research Report (2003).

- [58] E. Aker, E. Skurtveit, L. Grande, F. Cuisiat, Ø. Johnsen, M. Soldal, B. Bohloli, Experimental methods for characterization of cap rock properties for CO₂ storage, *Multiphysical Testing of Soils and Shales* 303–308.
- [59] J. Rohmer, D. Seyed, Coupled large scale hydromechanical modelling for caprock failure risk assessment of co₂ storage in deep saline aquifers, *Oil & Gas Science and Technology–Revue de l’Institut Français du Pétrole* 65 (3) (2010) 503–517.
- [60] S. Dutton, W. Flanders, M. Barton, Reservoir characterization of a Permian deep-water sandstone, East Ford field, Delaware basin, Texas, *AAPG bulletin* 87 (4) (2003) 609–628.
- [61] T. Eaton, On the importance of geological heterogeneity for flow simulation, *Sedimentary Geology* 184 (3-4) (2006) 187–201.
- [62] T. Manzocchi, J. Matthews, J. Strand, J. Carter, A. Skorstad, J. Howell, K. Stephen, J. Walsh, A study of the structural controls on oil recovery from shallow-marine reservoirs, *Petroleum Geoscience* 14 (1) (2008) 55–70.
- [63] T. Manzocchi, J. Walsh, P. Nell, G. Yielding, Fault transmissibility multipliers for flow simulation models, *Petroleum Geoscience* 5 (1) (1999) 53–63.
- [64] W. Nowak, Best unbiased ensemble linearization and the quasi-linear Kalman ensemble generator, *Water Resources Research* 45 (W04431). doi:10.1029/2008WR007328.
- [65] S. Jang, Y., N. Sitar, D. Kiureghian, A., Reliability analysis of contaminant transport in saturated porous media., *Water Resources Research* 30 (8) (1994) 2435–2448.
- [66] A. Saltelli, *Global sensitivity analysis: the primer*, Wiley, 2007.
- [67] A. Saltelli, Global sensitivity analysis: an introduction, in: Proc. 4th International Conference on Sensitivity Analysis of Model Output, pp. 27–43.
- [68] T. Crestaux, O. Le MaíLtre, J. Martinez, Polynomial chaos expansion for sensitivity analysis, *Reliability Engineering & System Safety* 94 (7) (2009) 1161–1172.
- [69] B. Sudret, Global sensitivity analysis using polynomial chaos expansions, *Reliability Engineering & System Safety* 93 (7) (2008) 964–979.

Table 1: Aquifer model information.

Parameter	Value	Unit
Number of active cells in the model	78720	-
Resolution X,Y,Z	40 × 120 × 20	-
Scale X,Y,Z	3000 × 9000 × 80	m
Injection rate	3650	m ³ /day
Initial pressure	266.5	bar
Critical CO ₂ and water saturations	0.2	-
CO ₂ viscosity	0.04	cp
Water viscosity	0.4	cp
Rock compressibility	0.3e-6	1/bar

Table 2: Important model responses and their brief description. For more information, see [21, 22].

Response	Description
Aquifer pressure	Volume average of pressure, weighted by porosity
Mobile CO ₂	Volume of CO ₂ in places with saturation above critical value
Residual CO ₂	Volume of CO ₂ in places with saturation below critical value
Leakage risk	A risk value for the leakage through the cap-rock.

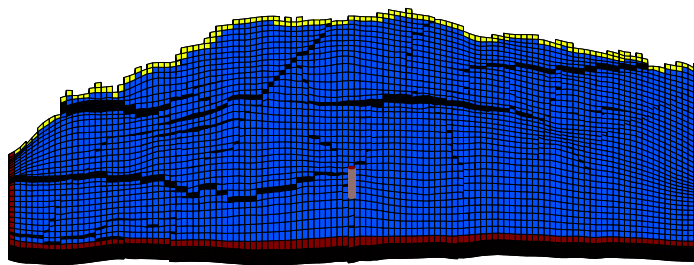


Figure 1: Boundary conditions and the well location in the designed injection scenario. Red color corresponds to the open boundaries and yellow color shows the closed side on the crest.

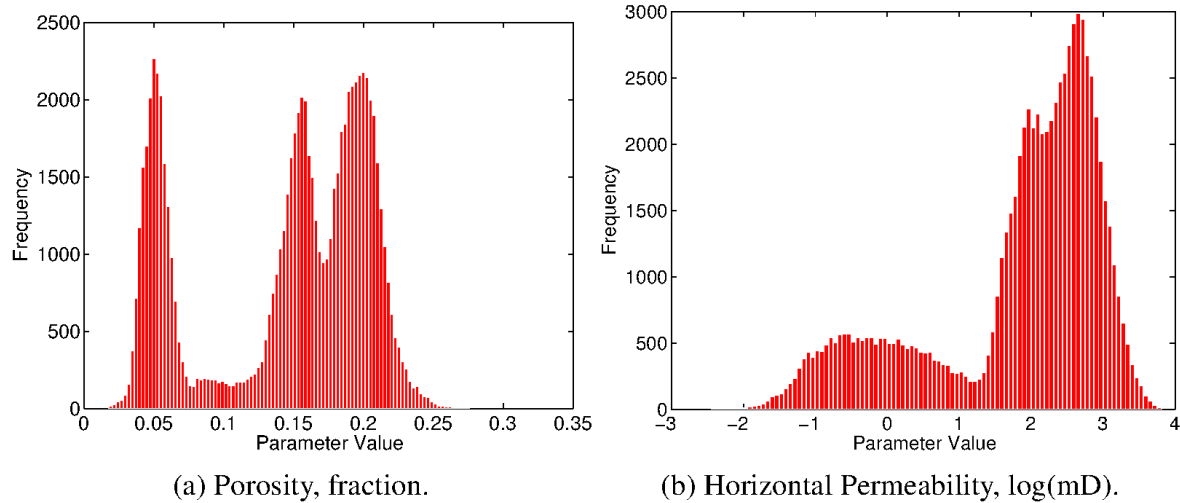


Figure 2: The histograms of hydrological parameters shown for a realization with low levels of heterogeneity. The vertical permeabilities are approximately one order of magnitude lower than the horizontal permeabilities.

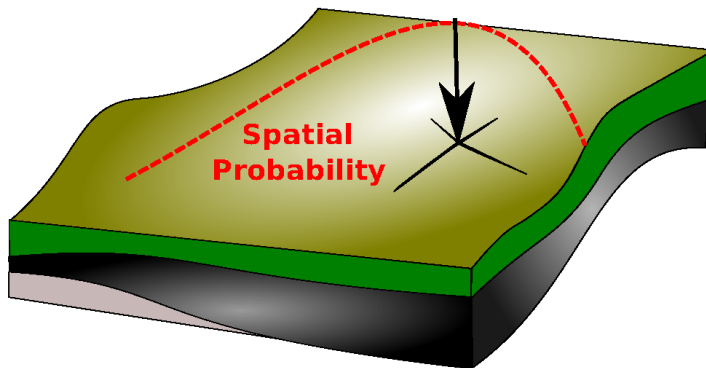


Figure 3: CO₂ leakage risk is computed as the product of a cap-rock failure probability and the amount of mobile CO₂ beneath the cap-rock, integrated over the entire surface area of the cap-rock. Here, we use a Gaussian function as simple scenario assumption for the cap-rock failure probability (indicated schematically by the color shading and the dashed red line with the black coordinate system).

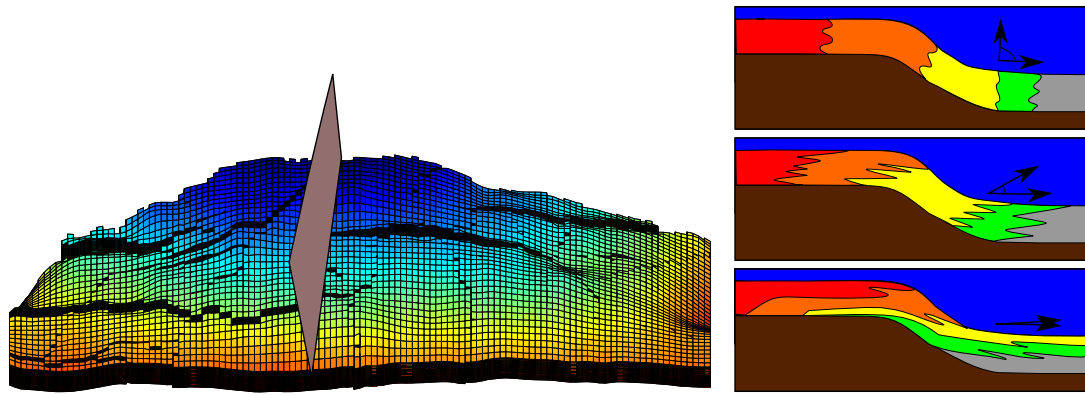


Figure 4: The river flows from left to right toward the sea on the model vertical section shown here (left figure). Aggradation angle is demonstrated in three levels (right figure); from top: low, medium and high aggradation angle. Between deposition and now, the entire system was rotated by tectonic effects such that the original river flow direction is oriented upward, not downward.

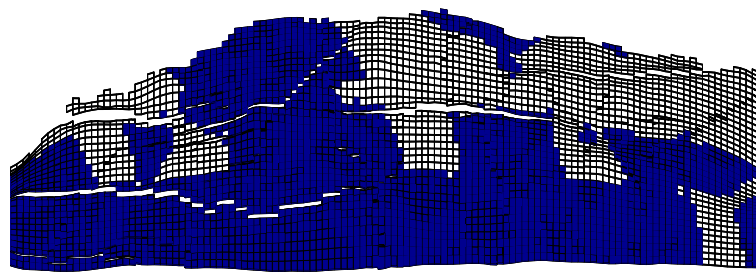


Figure 5: The figure shows 50% of zero transmissibility multipliers in a specific model layer representing a medium level of barriers. One layer of the model is shown in the figure.

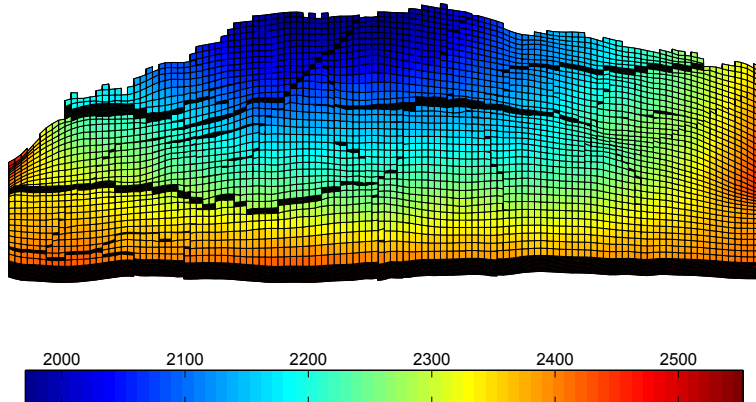


Figure 6: Fault orientation and intensity of the model used in the study. Depth in meter is shown by color on the grid.

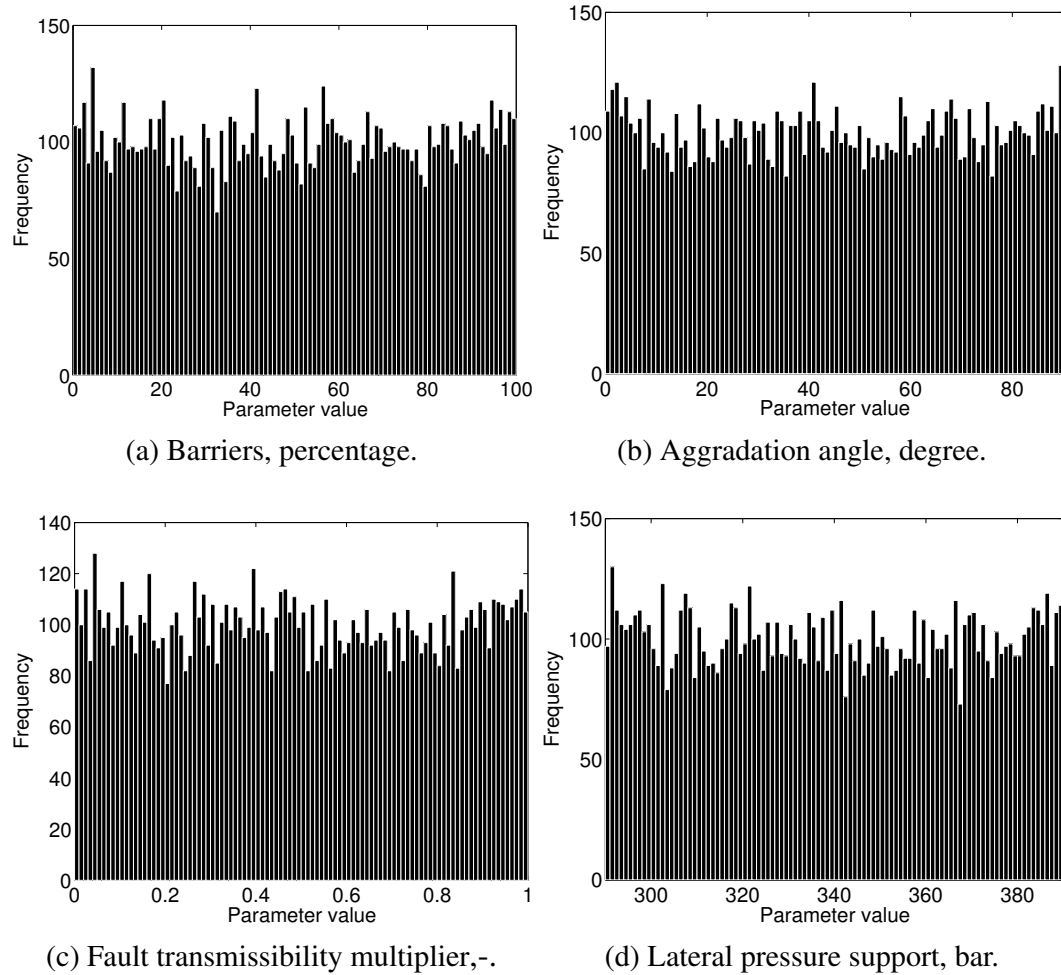


Figure 7: The histograms of geological variables used in this study are sampled from uniform distributions.

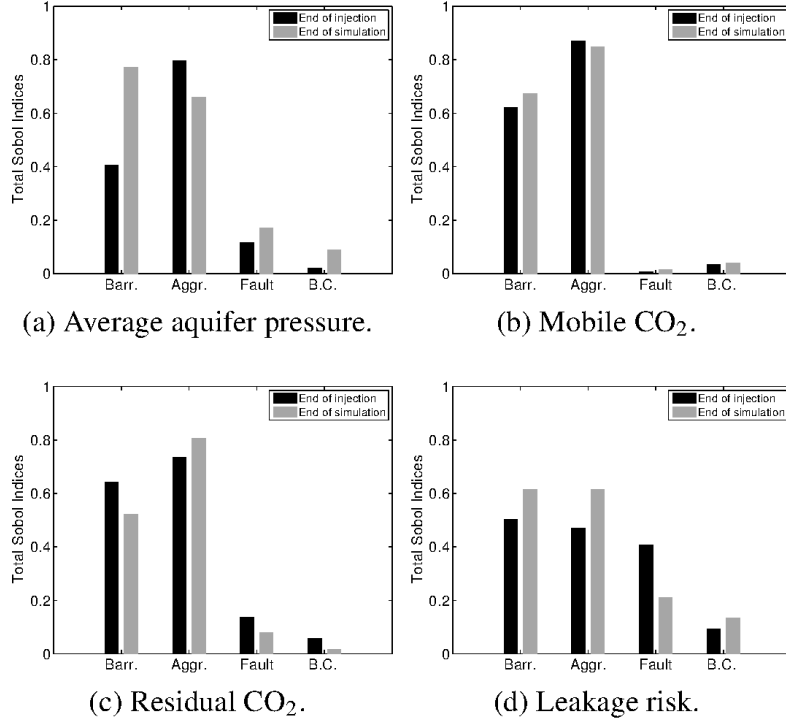


Figure 8: Sensitivity analysis for different responses (a: average aquifer pressure, b: mobile CO₂, c: residual CO₂, and d: leakage risk) with respect to the uncertain parameters. In the figures above, Barr. is for barriers, Aggr. for aggradation angle, Fault for fault transmissibility, and B.C. for regional groundwater effect.

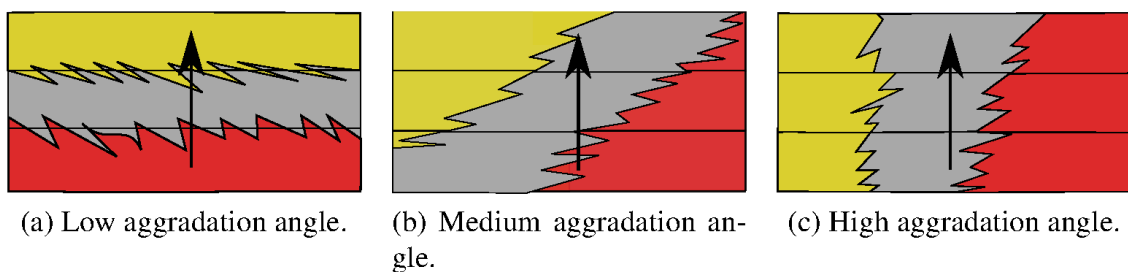


Figure 9: Illustration of how the aggradation angle affects the effective vertical conductivity.

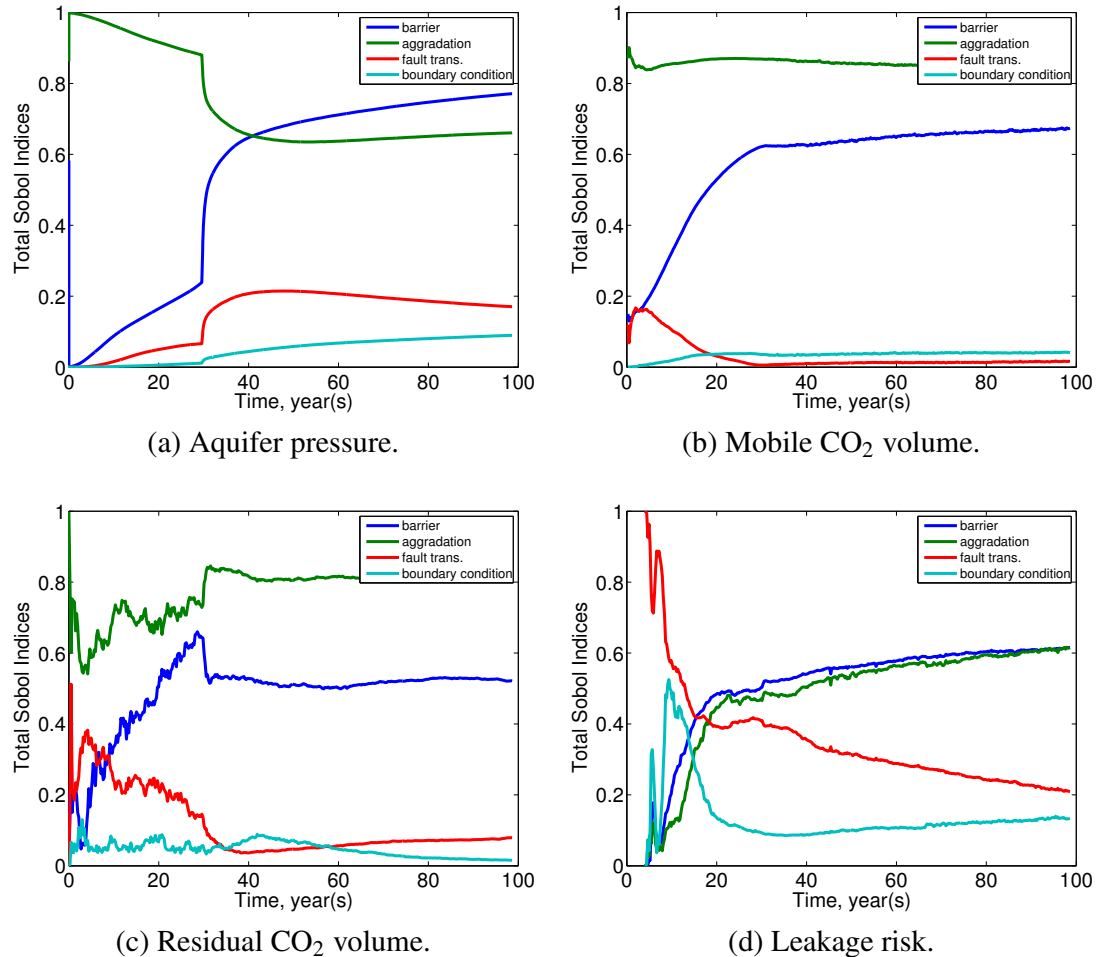


Figure 10: Sensitivities (expressed by total Sobol indices) plotted versus time for different responses.

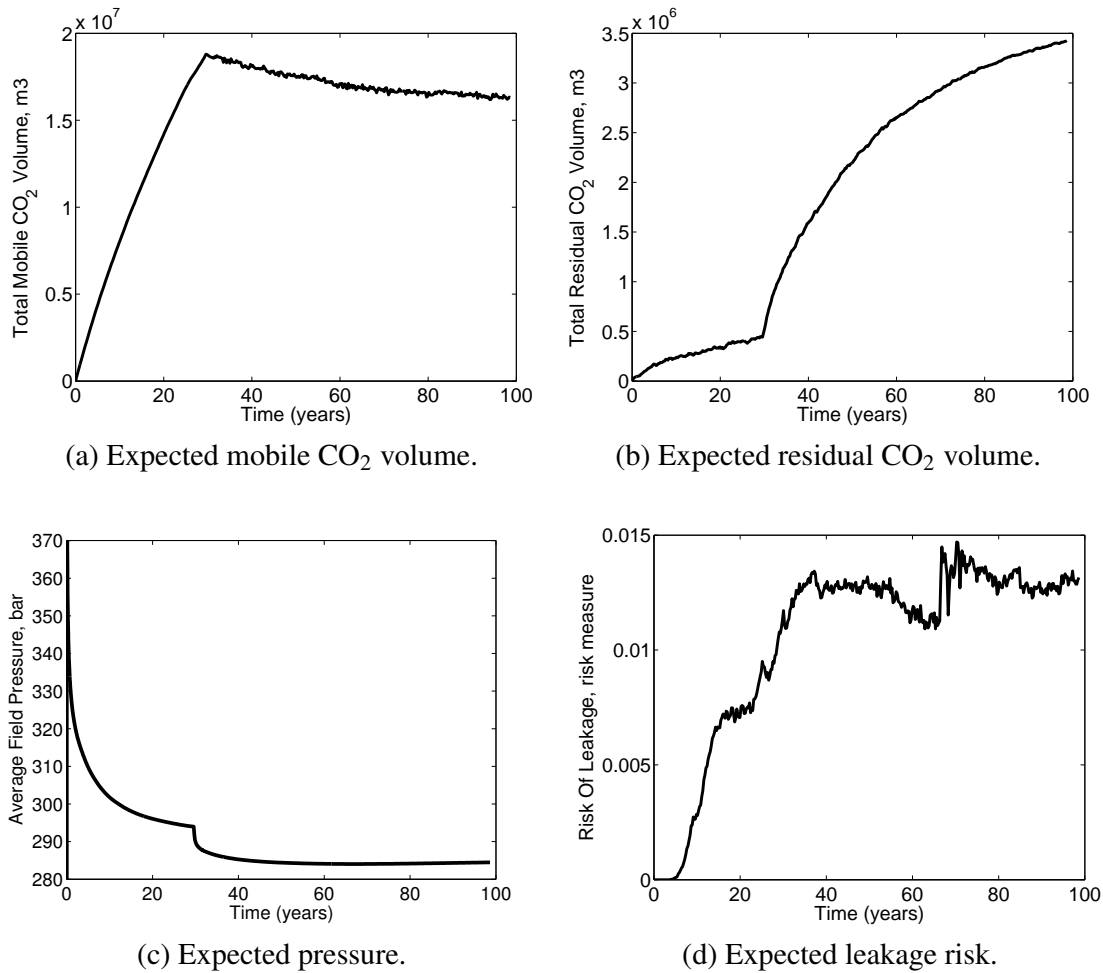


Figure 11: Expectation for response values versus time. The pressure value for initial time step in Figure c goes up to 670 bars.

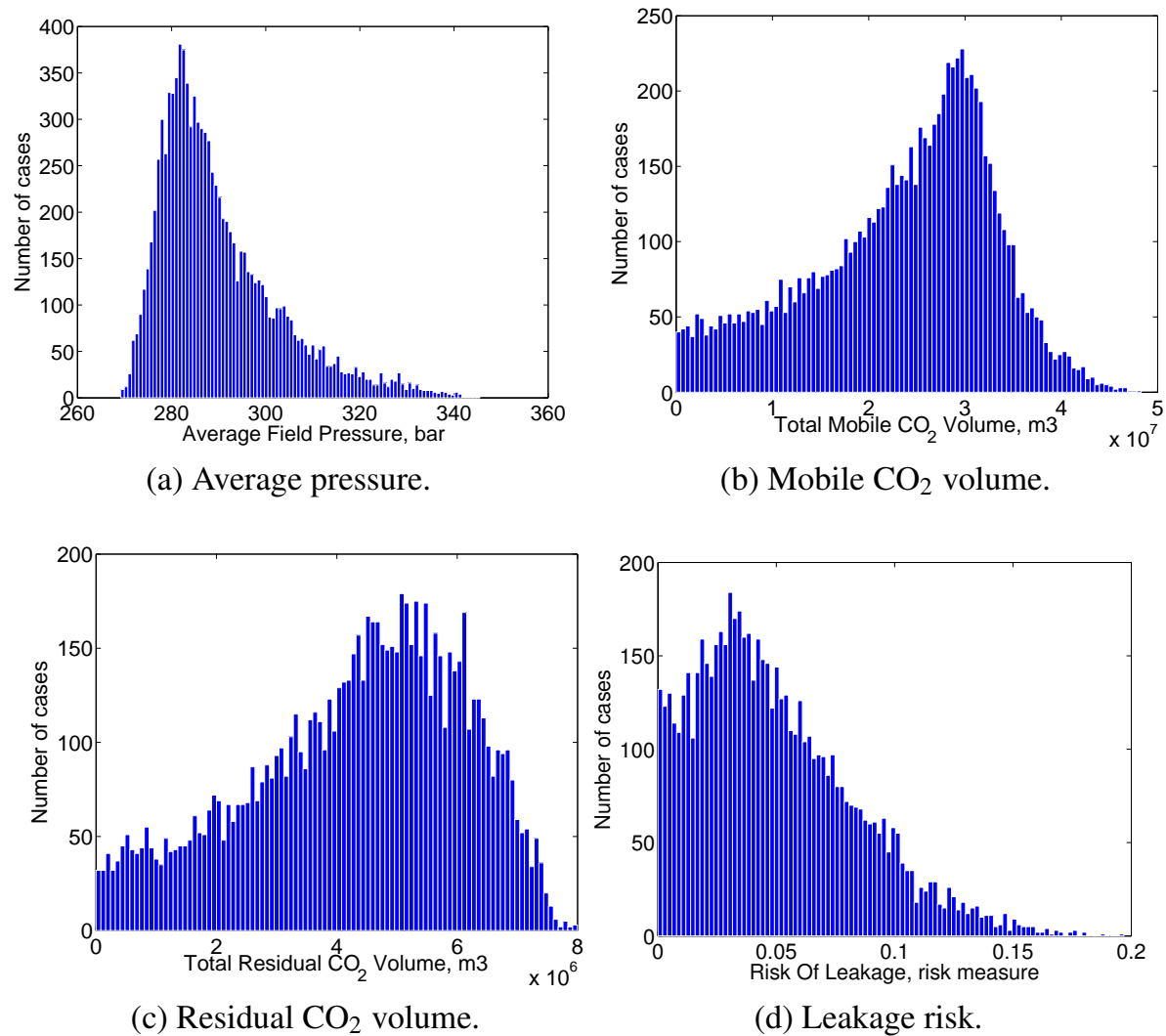


Figure 12: Histograms of selected response values.

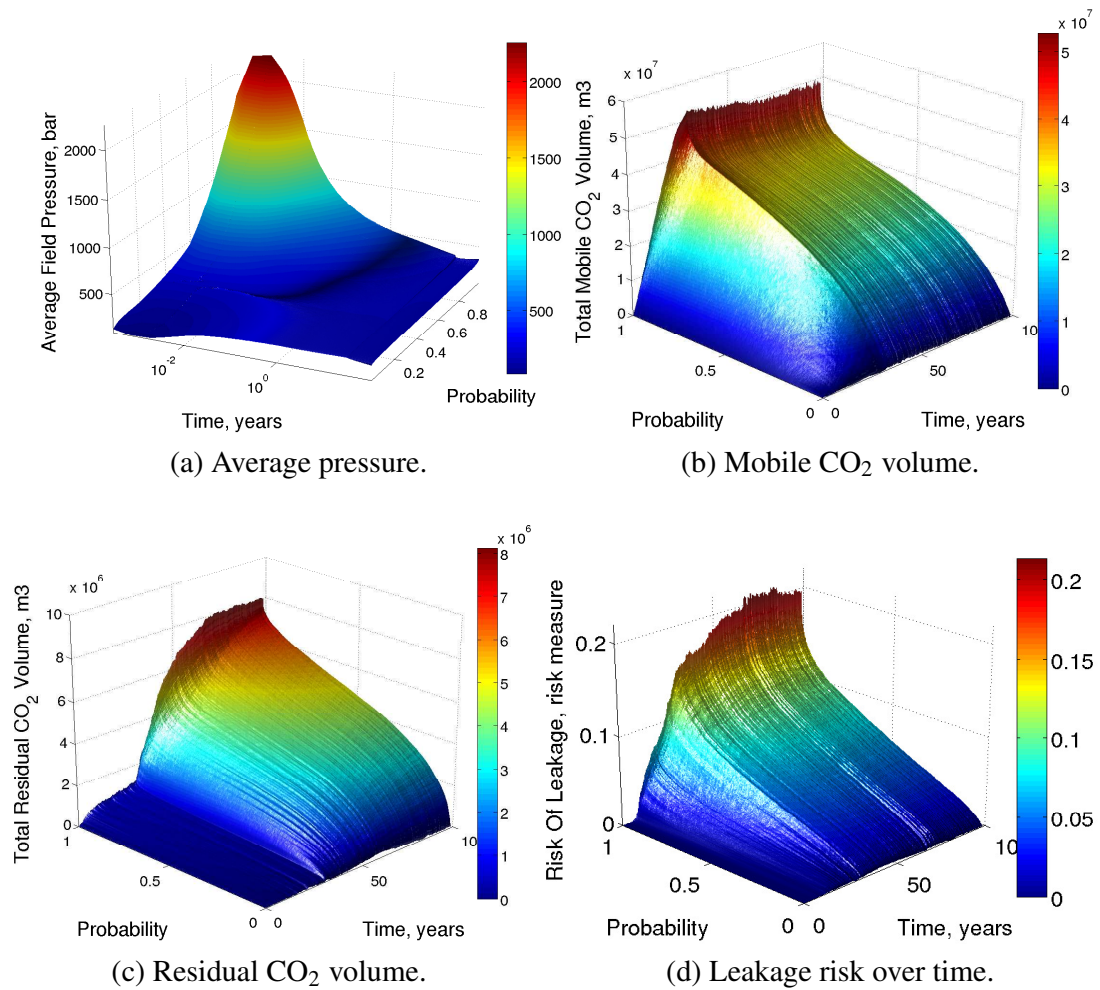


Figure 13: Evolution of the cumulative distribution function of different response values over time.

Bibliography

- [1] AAVATSMARK, I. Bevarelsesmetoder for hyperbolske differensialligninger. <http://www.mi.uib.no/~aavat/hyperbolsk.pdf>. 1.5.1
- [2] AAVATSMARK, I. Bevarelsesmetoder for elliptiske differensialligninger. <http://www.mi.uib.no/~aavat/elliptisk.pdf>, 2004. 1.5.1
- [3] ABRAMOWITZ, M., AND STEGUN, I., A. *Handbook of Mathematical Functions with Formulas, Graphs, and Mathematical Tables*. New York: Dover, 1965. 1.9.2
- [4] ALKAN, H., CINAR, Y., AND ÜLKER, E. Impact of capillary pressure, salinity and in situ conditions on co₂ injection into saline aquifers. *Transport in porous media* 84, 3 (2010), 799–819. 1.6.1
- [5] ALLEN, F., AND PUCKETT, D. Theoretical and experimental studies of rate-dependent two-phase immiscible flow. *SPE Production Engineering* 1, 1 (1986), 62–74. 1.6.1
- [6] ARWADE, S., MORADI, M., AND LOUGHJALAM, A. Variance decomposition and global sensitivity for structural systems. *Engineering Structures* 32, 1 (2010), 1–10. 1.9.3
- [7] BACHU, S. Sequestration of CO₂ in geological media: criteria and approach for site selection in response to climate change. *Energy Conversion and Management* 41, 9 (2000), 953–970. 1.1
- [8] BASHORE, W., ARAKTINGI, U., LEVY, M., AND SCHWELLER, W. The importance of the geological model for reservoir characterization using geostatistical techniques and the impact on subsequent fluid flow. In *SPE Annual Technical Conference and Exhibition* (1993). 1.1
- [9] BEAR, J. *Dynamics of fluids in porous media*. Dover publications, 1988. 1.5.1
- [10] BENSON LAB, S. U. Relative pereability explorer(rpe). <http://pangea.stanford.edu/research/bensonlab/relperm/index.html>. 1.5.2
- [11] BENTSEN, R. Effect of neglecting viscous coupling and dynamic capillary pressure on the one-dimensional flow of two immiscible phases through a porous medium. *SPE paper*, 026016 (1993). 1.6.1
- [12] BINNING, P., AND CELIA, M. Practical implementation of the fractional flow approach to multi-phase flow simulation. *Advances in water resources* 22, 5 (1999), 461–478. 1.5.2
- [13] BRADSHAW, J., AND COOK, P. Geological sequestration of carbon dioxide. *Environmental Geosciences* 8, 3 (2001), 149. 1.1
- [14] CAERS, J., AND ZHANG, T. Multiple-point geostatistics: a quantitative vehicle for integrating geologic analogs into multiple reservoir models. *AAPG* (2002). 1.4
- [15] CELIA, M., AND NORDBOTTEN, J. *Geological Storage of CO₂: Modeling Approaches for Large-Scale Simulation*. Wiley, 2011. 1.5.1, 1.1, 1.2, 1.7

- [16] CHEN, Z., BODVARSSON, G., AND WITHERSPOON, P. An integral equation formulation for two-phase flow and other nonlinear flow problems through porous media. In *SPE Annual Technical Conference and Exhibition* (1990). [1.6.1](#)
- [17] CLASS, H., EBIGBO, A., HELMIG, R., DAHLE, H., NORDBOTTEN, J., CELIA, M., AUDIGANE, P., DARCIS, M., ENNIS-KING, J., FAN, Y., ET AL. A benchmark study on problems related to CO₂ storage in geologic formations. *Computational Geosciences* 13, 4 (2009), 409–434. [1.7](#)
- [18] CRESTAUX, T., ET AL. Polynomial chaos expansion for sensitivity analysis. *Reliability Engineering & System Safety* 94, 7 (2009), 1161–1172. [1.9.3](#)
- [19] DONG, M., AND DULLIEN, F. Effect of capillary forces on immiscible displacement in porous media. In *SPE Annual Technical Conference and Exhibition* (1999). [1.6.1](#)
- [20] DUAN, Z., AND ZHANG, Z. Equation of state of the h₂o, co₂, and h₂o-co₂ systems up to 10 gpa and 2573.15 k: Molecular dynamics simulations with ab initio potential surface. *Geochimica et cosmochimica acta* 70, 9 (2006), 2311–2324. [1.5.2](#)
- [21] EATON, T. On the importance of geological heterogeneity for flow simulation. *Sedimentary Geology* 184, 3-4 (2006), 187–201. [1.1](#), [1.4](#)
- [22] ELENIUS, M., AND JOHANNSEN, K. On the time scales of nonlinear instability in miscible displacement porous media flow. *Computational Geosciences* (2012), 1–11. [1.6.2](#)
- [23] ELENIUS, M., NORDBOTTEN, J., AND KALISCH, H. Effects of a capillary transition zone on the stability of a diffusive boundary layer. [1.6.2](#)
- [24] ELENIUS, M., TCHELEPI, H., AND JOHANNSEN, K. CO₂ trapping in sloping aquifers: High resolution numerical simulations. In *XVIII International Conference on Water Resources, CIMNE, Barcelona* (2010). [1.6.2](#)
- [25] FAJRAOUI, N., RAMASOMANANA, F., YOUNES, A., MARA, T. A. AND ACKERER, P., AND GUADAGNINI, A. Use of global sensitivity analysis and polynomial chaos expansion for interpretation of non-reactive transport experiments in laboratory-scale porous media. *Water Resour. Res.*, doi:10.1029/2010WR009639 (2011). [1.9.2](#)
- [26] FARAJZADEH, R., AND BRUINING, J. An analytical method for predicting the performance of gravitationally-unstable flow in heterogeneous media. In *SPE EUROPEC/EAGE Annual Conference and Exhibition* (2011). [1.6.1](#)
- [27] FAYERS, F., AND SHELDON, J. The effect of capillary pressure and gravity on two-phase fluid flow in a porous medium. *Trans. AIME* 216 (1959), 147. [1.6.1](#)
- [28] FOO, J., AND KARNIADAKIS, G. Multi-element probabilistic collocation method in high dimensions. *Journal of Computational Physics* 229, 5 (2010), 1536–1557. [1.9.2](#)
- [29] FOUKAL, P., FRÖHLICH, C., SPRUIT, H., AND WIGLEY, T. Variations in solar luminosity and their effect on the earth's climate. *Nature* 443, 7108 (2006), 161–166. [1.2](#)
- [30] GHANEM, R., AND SPANOS, P. A stochastic galerkin expansion for nonlinear random vibration analysis. *Probabilistic Engineering Mechanics* 8 (1993), 255–264. [1.9.2](#)
- [31] GRAY, W., HERRERA, P., GASDA, S., AND DAHLE, H. Derivation of vertical equilibrium models for CO₂ migration from pore scale equations. *International Journal of Numerical Analysis and Modeling.* (2011). [1.7](#)

- [32] GREENWOOD, H. The compressibility of gaseous mixtures of carbon dioxide and water between 0 and 500 bars pressure and 450 and 800 centigrade. *Am. J. Sci* 267 (1969), 191–208. [1.5.2](#)
- [33] GUNTER, W., WIWEHAR, B., AND PERKINS, E. Aquifer disposal of co 2-rich greenhouse gases: extension of the time scale of experiment for co 2-sequestering reactions by geochemical modelling. *Mineralogy and Petrology* 59, 1 (1997), 121–140. [1.2](#), [1.6.2](#)
- [34] HADLEY, G., AND HANDY, L. A theoretical and experimental study of the steady state capillary end effect. In *Fall Meeting of the Petroleum Branch of AIME* (1956). [1.6.1](#)
- [35] HASSANZADEH, H., POOLADI-DARVISH, M., AND KEITH, D. Modelling of convective mixing in co storage. *Journal of Canadian Petroleum Technology* 44, 10 (2005). [1.6.2](#)
- [36] HITCHON, B., GUNTER, W., GENTZIS, T., AND BAILEY, R. Sedimentary basins and greenhouse gases: a serendipitous association. *Energy Conversion and Management* 40, 8 (1999), 825–843. [1.1](#)
- [37] HOUGHTON, J., ET AL. *Climate change 2001: the scientific basis*, vol. 881. Cambridge University Press Cambridge, 2001. [1.1](#)
- [38] HOWELL, J., SKORSTAD, A., MACDONALD, A., FORDHAM, A., FLINT, S., FJELLVOLL, B., AND MANZOCCHI, T. Sedimentological parameterization of shallow-marine reservoirs. *Petroleum Geoscience* 14, 1 (2008), 17–34. [1.4.2](#)
- [39] ISUKAPALLI, S., S., ROY, A., AND GEORGOPoulos, P., G. Stochastic response surface methods (srsm) for uncertainty propagation: Application to environmental and biological systems. *Risk Analysis* 18, 3 (1998), 351–363. [1.9.2](#)
- [40] JANG, Y., S., SITAR, N., AND KIUREGHIAN, A., D. Reliability analysis of contaminant transport in saturated porous media. *Water Resources Research* 30, 8 (1994), 2435–2448. [1.9.3](#)
- [41] KEESE, A., AND MATTHIES, H. G. Sparse quadrature as an alternative to mc for stochastic finite element techniques. *Proc. Appl. Math. Mech.* 3 (2003), 493–494. [1.9.2](#)
- [42] LI, H., AND ZHANG, D. Probabilistic collocation method for flow in porous media: Comparisons with other stochastic methods. *Water Resources Research* 43 (2007), 44–48. [1.9.2](#)
- [43] LIE, K., KROGSTAD, S., LIGAARDEN, I., NATVIG, J., NILSEN, H., AND SKAFLESTAD, B. Open-source matlab implementation of consistent discretisations on complex grids. *Computational Geosciences* (2011), 1–26. [1.10](#)
- [44] LIE, K., LIGAARDEN, I., AND NILSEN, H. Accurate discretization of vertically-averaged models of CO₂ plume migration. *ECMOR XII–12th European Conference on the Mathematics of Oil Recovery, EAGE, Oxford, UK*. [1.7](#)
- [45] LIGAARDEN, I., AND NILSEN, H. Numerical aspects of using vertical equilibrium models for simulating CO₂ sequestration. In *Proceedings of ECMOR XII–12th European Conference on the Mathematics of Oil Recovery, EAGE, Oxford, UK* (2010). [1.7](#)
- [46] MANZOCCHI, T., CARTER, J., SKORSTAD, A., FJELLVOLL, B., STEPHEN, K., HOWELL, J., MATTHEWS, J., WALSH, J., NEPVEU, M., BOS, C., ET AL. Sensitivity of the impact of geological uncertainty on production from faulted and unfaulted shallow-marine oil reservoirs: objectives and methods. *Petroleum Geoscience* 14, 1 (2008), 3–11. [1.4.2](#)
- [47] MATEMATICS, S. A. Matlab reservoir simulation toolbox. <http://www.sintef.no/MRST>. [1.10](#)

- [48] MATTHEWS, J., CARTER, J., STEPHEN, K., ZIMMERMAN, R., SKORSTAD, A., MANZOCCHI, T., AND HOWELL, J. Assessing the effect of geological uncertainty on recovery estimates in shallow-marine reservoirs: the application of reservoir engineering to the SAIGUP project. *Petroleum Geoscience* 14, 1 (2008), 35–44. [1.4.2](#)
- [49] MATTHIES, H., G., AND KEESE., A. Galerkin methods for linear and nonlinear elliptic stochastic partial differential equations. *Comp. Meth. Appl. Mech. Engrg.* 194 (2005), 1295–1331. [1.9.2](#)
- [50] MELICK, J., GARDNER, M., AND ULAND, M. Incorporating geologic heterogeneity in 3d basin-scale models for CO₂ sequestration: Examples from the powder river basin, ne wyoming and se montana. In *SPE International Conference on CO₂ Capture, Storage, and Utilization* (2009). [1.1](#)
- [51] MILLIKEN, W., LEVY, M., STREBELLE, S., AND ZHANG, Y. The effect of geologic parameters and uncertainties on subsurface flow: deepwater depositional systems. In *SPE Western Regional and Pacific Section AAPG Joint Meeting* (2008). [1.1](#)
- [52] MØLL NILSEN, H., HERRERA, P., ASHRAF, M., LIGAARDEN, I., IDING, M., HERMANRUD, C., LIE, K., NORDBOTTEN, J., DAHLE, H., AND KEILEGAVLEN, E. Field-case simulation of CO₂ plume migration using vertical-equilibrium models. *Energy Procedia* 4 (2011), 3801–3808. [1.7](#), [1.7](#)
- [53] MORRIS, M., D. Morris factorial sampling plans for preliminary computational experiments. *Technometrics*, 33 (1991), 161–174. [1.9.3](#)
- [54] MUSKAT, M. *The Flow of Homogeneous Fluids Through Porous Media*. 1937. [1.5.1](#)
- [55] NILSEN, H., SYVERSVEEN, A., LIE, K., TVERANGER, J., AND NORDBOTTEN, J. Impact of top-surface morphology on co₂ storage capacity. *International Journal of Greenhouse Gas Control* 11 (2012), 221–235. [2.2](#)
- [56] NORDBOTTEN, J., CELIA, M., AND BACHU, S. Injection and storage of co 2 in deep saline aquifers: Analytical solution for co 2 plume evolution during injection. *Transport in Porous Media* 58, 3 (2005), 339–360. [1.6.1](#)
- [57] OLADYSHKIN, S., CLASS, H., HELMIG, R., AND NOWAK, W. A concept for data-driven uncertainty quantification and its application to carbon dioxide storage in geological formations. *Advances in Water Resources* 34 (2011), 1508–1518, doi: [10.1016/j.advwatres.2011.08.005](https://doi.org/10.1016/j.advwatres.2011.08.005). [1.9.2](#), [1.9.2](#), [1.9.3](#)
- [58] OLADYSHKIN, S., CLASS, H., HELMIG, R., AND NOWAK, W. An integrative approach to robust design and probabilistic risk assessment for CO₂ storage in geological formations. *Computational Geosciences* 15, 3 (2011), 565–577, doi: [10.1007/s10596-011-9224-8](https://doi.org/10.1007/s10596-011-9224-8). [1.9.2](#), [1.9.2](#)
- [59] OLADYSHKIN, S., DE BARROS, F. P. J., AND NOWAK, W. Global sensitivity analysis: a flexible and efficient framework with an example from stochastic hydrogeology. *Advances in Water Resources In Press* (2011). [1.9.3](#)
- [60] RAPOPORT, L., AND LEAS, W. Properties of linear waterfloods. *Trans. AIME* 198, 1953 (1953), 139–148. [1.6.1](#)
- [61] REUTER, U., AND LIEBSCHER, M. Global sensitivity analysis in view of nonlinear structural behavior. In *Proceedings of the 7th LS-Dyna Forum, Bamberg* (2008). [1.9.1](#), [1.9.3](#)
- [62] ROSADO-VAZQUEZ, F., RANGEL-GERMAN, E., AND RODRIGUEZ-DE LA GARZA, F. Analysis of capillary, gravity and viscous forces effects in oil/water displacement. In *International Oil Conference and Exhibition in Mexico* (2007). [1.6.1](#)

- [63] SAHIMI, M. *Flow and transport in porous media and fractured rock: From classical methods to modern approaches*. Wiley-VCH, 2011. [1.5.1](#)
- [64] SALTELLI, A. Global sensitivity analysis: an introduction. In *Proc. 4th International Conference on Sensitivity Analysis of Model Output*, pp. 27–43. [1.9.1](#)
- [65] SALTELLI, A. *Global sensitivity analysis: the primer*. Wiley, 2007. [1.9.3](#), [1.9.3](#)
- [66] SYVERSVEEN, A., NILSEN, H., LIE, K., TVERANGER, J., AND ABRAHAMSEN, P. A study on how top-surface morphology influences the storage capacity of co₂ in saline aquifers. *Geostatistics Oslo 2012* (2012), 481–492. [1.7](#), [1.8.2](#), [2.2](#)
- [67] VILLADSEN, J., AND MICHELSEN, M. L. *Solution of differential equation models by polynomial approximation*. Prentice-Hall, 1978. [1.9.2](#)
- [68] XIU, D., AND KARNIADAKIS, G. E. Modeling uncertainty in flow simulations via generalized polynomial chaos. *Journal of Computational Physics* 187 (2003), 137–167. [1.9.2](#)
- [69] YANG, W. An analytical solution to two-phase flow in porous media and its application to water coning. *SPE Reservoir Eng. J.*, 1 38 (1992). [1.6.1](#)
- [70] YORTSOS, Y., AND FOKAS, A. An analytical solution for linear waterflood including the effects of capillary pressure. *Old SPE Journal* 23, 1 (1983), 115–124. [1.6.1](#), [1.6.1](#)
- [71] ZHANG, D., AND LU, Z. An efficient, high-order perturbation approach for flow in random media via karhunen-loeve and polynomial expansions. *Journal of Computational Physics* 194 (2004), 773–794. [1.9.2](#)